AD-A109 856 OHIO STATE UNIV COLUMBUS DEPT OF GEODETIC SCIENCE A--ETC F/G 8/5
SIMULATION STUDIES ON THE COMPUTATION OF THE GRAVITY VECTOR IN --ETC(U)
JUN 81 K E KATSAMBALOS F19628-79-C-0027
UNCLASSIFIED 314 AFGL-TR-81-0187 NL

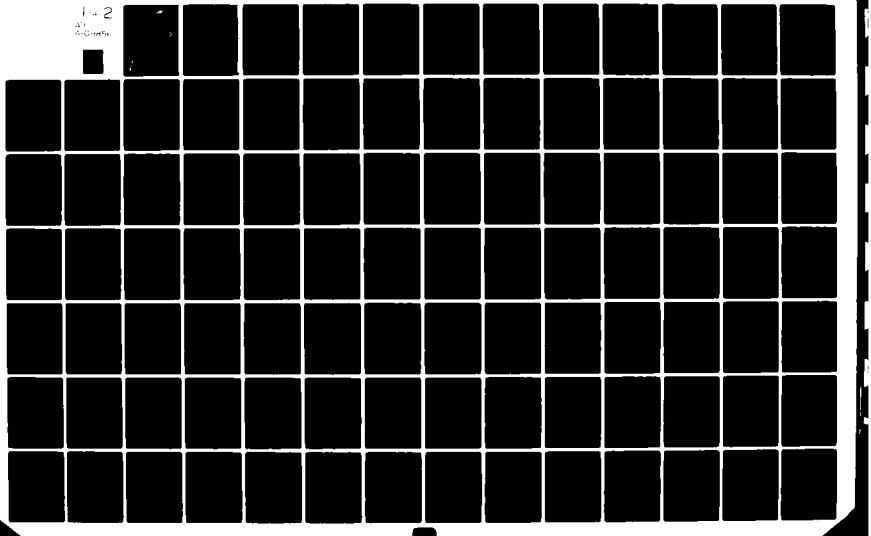

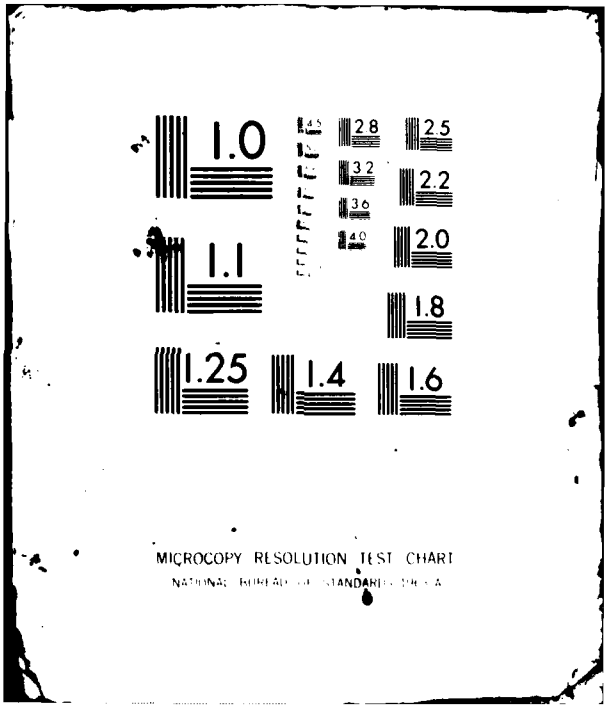
1.0
1.1
1.25
1.4
1.6
1.8
2.0
2.2
2.5
2.8
3.2
3.6
4.0
MICROCOPY RESOLUTION TEST CHART
NATIONAL BUREAU OF STANDARDS-1963-A

AFGL-TR-81-0187

LEVEL II

SIMULATION STUDIES ON THE COMPUTATION OF THE GRAVITY VECTOR IN SPACE FROM SURFACE DATA CONSIDERING THE TOPOGRAPHY OF THE EARTH

Kostas E. Katsambalos

The Ohio State University
Research Foundation
Columbus, Ohio 43210

June, 1981

Scientific Report No. 8

AIR FORCE GEOPHYSICS LABORATORY
AIR FORCE SYSTEMS COMMAND
UNITED STATES AIR FORCE
HANSCOM AFB, MASSACHUSETTS 01731

Unclassified

SECURITY CLASSIFICATION OF THIS PAGE (When Data Entered)

REPORT DOCUMENTATION PAGE	READ INSTRUCTIONS BEFORE COMPLETING FORM
1. REPORT NUMBER: AFGL-TR-81-0187	2. GOVT ACCESSION NO.: AD-A109 856
	3. RECIPIENT'S CATALOG NUMBER:
4. TITLE (and Subtitle): SIMULATION STUDIES ON THE COMPUTATION OF THE GRAVITY VECTOR IN SPACE FROM SURFACE DATA CONSIDERING THE TOPOGRAPHY OF THE EARTH	5. TYPE OF REPORT & PERIOD COVERED: Scientific Report No. 8
	6. PERFORMING ORG. REPORT NUMBER: Dept. of Geodetic Sci. #314
7. AUTHOR(s): Kostas E. Katsambalos	8. CONTRACT OR GRANT NUMBER(s): F19628-79-C-0027
9. PERFORMING ORGANIZATION NAME AND ADDRESS: The Ohio State University Research Foundation Columbus, Ohio 43210	10. PROGRAM ELEMENT, PROJECT, TASK AREA & WORK UNIT NUMBERS: 61102F 2309G1AW
11. CONTROLLING OFFICE NAME AND ADDRESS: Air Force Geophysics Laboratory Hanscom AFB, Massachusetts 01730 Contract Monitor: Bela Szabo/LW	12. REPORT DATE: June, 1981
	13. NUMBER OF PAGES: 136
14. MONITORING AGENCY NAME & ADDRESS (if different from Controlling Office)	15. SECURITY CLASS. (of this report): Unclassified
	15a. DECLASSIFICATION/DOWNGRADING SCHEDULE

16. DISTRIBUTION STATEMENT (of this Report)

A - Approved for public release; distribution unlimited

17. DISTRIBUTION STATEMENT (of the abstract entered in Block 20, if different from Report)

18. SUPPLEMENTARY NOTES

19. KEY WORDS (Continue on reverse side if necessary and identify by block number)

geodesy, gravity

20. ABSTRACT (Continue on reverse side if necessary and identify by block number)

Three approaches are investigated for the computation of the components of the gravity vector in space considering the topography of the earth: a numerical integration approach based on the application of Green's third identity, the Discrete Dirac approach, and the Least-Squares Collocation approach. Under a spherical approximation, the surface of the earth is assumed to be known through the elevations of its points above a reference sphere. The first technique requires as data gravity disturbances

DD FORM 1 JAN 73 1473 EDITION OF 1 NOV 65 IS OBSOLETE

Unclassified

SECURITY CLASSIFICATION OF THIS PAGE (When Data Entered)

and disturbing potentials on the earth's surface, while the other two techniques require as data surface gravity anomalies. Two point masses located on the axes of symmetry of two simple terrain models (a cone and a sphere), generate on their surfaces the synthetic data needed for the simulations. The agreement between the rigorously computed vectors (from the models), and those from the three techniques, is analyzed in terms of factors such as the inclination of the model's surface, data density, altitude of the space point etc. The application of the Dirac approach is questionable due to its limited accuracy for large data spacing. The Green's approach is recommended for computations above 10 km altitude, while the Collocation approach is suitable for computations at points between the earth's surface and the 10 km level. Comparison of these techniques with the classical approach (the Direct Integration Method), indicate that the consideration of the topography improved significantly the accuracy of the computations.

Foreword

This report was prepared by Kostas Katsambalos, Graduate Research Associate, Department of Geodetic Science, The Ohio State University, under Air Force Contract No. F19628-79-C-0027, The Ohio State University Research Foundation Project No. 711664, Project Supervisor Richard H. Rapp. The contract covering this research is administered by the Air Force Geophysics Laboratory, Hanscom Air Force Base, Massachusetts, with Mr. Bela Szabo, Contract Monitor.

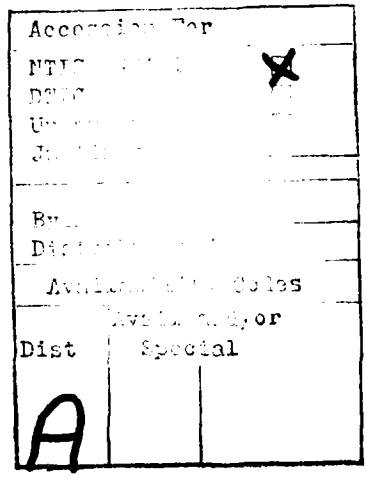

TABLE OF CONTENTS

LIST OF TABLES

LIST OF FIGURES

Chapter 1

INTRODUCTION

There are three Boundary-Value Problems (BVP) of potential theory (Moritz, 1964, p.1; Heiskanen and Moritz, 1967, p.36):

1. First BVP (Dirichlet's problem): Given an arbitrary function on a surface S, determine a function V which is harmonic either inside or outside S, and which assumes on S the values of the prescribed function.

2. Second BVP (Neumann's problem): Given the normal derivative $\partial V/\partial n$ of a function on a surface S, determine the function V which is harmonic either inside or outside S, whose normal derivative assumes the prescribed boundary values on S.

3. Third BVP: Determine a function V which is harmonic either inside or outside a given surface S, and is such that the linear combination $hV + k\partial V/\partial n$ assumes prescribed values on S.

It is clear that in all three problems, the surface S is assumed to be known (i.e. the locations of points on the surface are determined in a specified coordinate system), and only the harmonic function V is to be determined from the various data on S. The geodetic BVP may be defined as the determination of the physical surface of the earth, if the gravity vector $\vec{g}$ and the gravity potential W are given on it (Moritz, 1965, p.36). This problem calls for the determination of the surface of:

(a) the geoid (Stokes' problem) using gravity data reduced from the physical surface of the earth to the surface of the geoid, or
(b) the telluroid (Molodensky's problem) from gravity data given on the physical surface of the earth.

Since the surface (geoid or telluroid) is the unknown, the geodetic BVP is not directly related to any of the three problems of potential theory mentioned above. What makes the solution of the geodetic BVP possible as a 3rd BVP, is the fact that certain restrictions are enforced (Moritz, 1964, p.2), namely:

(a) the geoid is an equipotential surface of the gravity field of the earth (Stokes' approach), and
(b) in addition to the gravity $\vec{g}$, the potential difference $\Delta W = W - W_0$ at every surface point is determined from

levelling combined with gravity observations (Molodensky's approach), W_0 being the potential of the geoid.

The definitions above will help us later in determining the kind of BVP we need to solve in the present study. Let us now state the problem.

Certain geodetic applications, such as aircraft inertial navigation systems, and the computation of rocket trajectories, or components of the gravity disturbance vector, require the calculation of the gravity vector components at a certain altitude in space, from data collected on the physical surface of the earth. Zero-order solutions to this problem (i.e. solutions ignoring the topography of the earth and/or the surface inclinations) can be found in the literature (cf. Hirvonen and Moritz, 1963; Heiskanen and Moritz, 1967; Mueller, 1966). These methods are:

1. The Direct Integration method, which is based on the generalized Stokes' formula;

2. The Coating method (see also in (Orlin, 1959));

3. The Upward Continuation method, which is based on the Poisson's integral equation (Shebalin, 1979).

Apart from these three methods, which are considered as the classical approaches, there are also other techniques. However not all of them yield the three components of the gravity disturbance vector. Some of them are applied for the computation of the gravity anomaly (Δg) only, and some others for the computaion of the disturbing potential (T) alone. These methods are:

4. The Stokes' formula in combination with the use of Poisson's integral theorem (L. de Witte, 1969);

5. The Green's third identity (Moritz, 1965; B. Witte, 1969; Koch, 1967-b, 1968-a);

6. A Bjerhammar-type of solution, based on the reduction of gravity data on a defined sphere internal to the surface of the earth, and then application of the Poisson's integral for the upward continuation of the gravity data to a space point (Bjerhammar, 1978; Moritz, 1965, p.54; Sjöberg, 1978);

7. Polynomical modeling of the anomalous gravity field, for the upward continuation of gravity data (Paul and Nagy, 1972);

8. Series expansion of the external anomalous potential (Petrovskaya, 1979);

9. The Finite Element method (Richardson and Hopkins, 1978; Junkins and Saunders, 1977);

10. Geopotential Modeling by the so-called point-masses technique (Needham, 1970):

11. The method of Least-Squares Collocation, or a combination of Collocation with integral equations (Lachapelle, 1977; Tscherning and Forsberg, 1978; Forsberg and Tscherning, 1980):

12. The Initial-Value method (Nakiboglou and Lim 1979).

For the computation of the gravity vector $\vec{g}$ at a space point P, we first need to evaluate the components of the gravity disturbance vector $\vec{\delta}$ at this point (Heiskanen and Moritz 1967, p.227). Since $\vec{\delta}$ = grad T (more details will follow in the next chapter), the problem is equivalent to the estimation of the partial derivatives of the disturbing potential T at the same space point P. A first-order solution, linear in elevation (h) of the earth's topography is discussed in (Moritz, 1965. part 2), but only the expression for the gravity anomaly at P is derived following a planar approximation.

In this study we develop a method for the computation of the three components of the gravity disturbance vector at space points, using data on the physical surface of the earth. The topography of the earth is not neglected, and the need to know the deflection of the vertical is avoided. Only surface gravimetry, elevation data, and (possibly) a geopotential model will be used. Green's third identity is the starting point for this approach (Chapters 2, 3, and 4).

The development of another method, based on the Bjerhammar's discrete (Dirac) approach for the upward continuation of gravity data is also investigated (Chapters 5, and 6). The two methods are then compared to each other.

Finally, the applicability of least-squares collocation is examined, and the results of the three approaches are compared with respect to factors such as the inclination of the terrain, the altitude of the space point, the density of the surface data, etc. (Chapter 7).

In order to avoid the random and the systematic errors which exist in real data, we decided to test the accuracy of the three approaches through a simulation study, by substituting for the topography of the earth a number of simple terrain models (Chapter 3). The exact vectors computed from these models can then be compared to the computed ones from the three approaches, using the synthetic data on the model's surface. Such simulation with terrain models, but for different applications have been made in the past too. For example the effect of the topography on the external gravity anomalies is discussed by Moritz (1965), and the computation of the first derivatives of the disturbing

potential on the earth's surface by Green's formula is described by Koch (1967-b, 1968-a).

Due to the fact that throughout this study the surface of the earth is assumed to be known, the problem of the determination of the gravity disturbance bector is closer to the BVP as defined in potential theory, than to the geodetic BVP. Koch and Pope (1972) called this problem "the geodetic BVP using the known surface of the earth", and they have stated theorems on its uniqueness and existence. The three methods which will be described in the following chapters, require as data (in addition to the information which defines the surface), surface gravity anomalies (Δg), or disturbing potentials (T) and gravity disturbances (δg) as boundary values. These three quantities are related to each other through the fundamental equation of physical geodesy (Heiskanen and Moritz, 1967, p.88):

$$\Delta g = - \frac{\partial T}{\partial r} - \frac{2\,T}{r} = \delta g - \frac{2\,T}{r}$$

If the boundary values are gravity anomalies (linear combination of T and $\partial T/\partial r$), our problem is equivalent to the 3rd BVP above, since the components of $\vec{\gamma} = \text{grad}\,T$ are the partial derivatives of T . However, if the boundary values are gravity disturbances and disturbing potentials (not their linear combination), our problem is none of the three BVP of potential theory as they are defined in the beginning of this chapter.

The Direct Integration, the Coating, and the Upward Continuation methods which were mentioned above, were referred to as the classical approaches, because the topography of the earth is neglected, and the data required for their application must be reduced on the surface of the sphere which approximates the geoid. These classical approaches are extensively discussed in (Heiskanen and Moritz, 1967, chapter 6). The Green's, the Dirac, and the collocation approaches which will be discussed in this paper, will be referred to as the improved techniques, since the earth's topography is not neglected, and the required data is boundary values on the earth's surface, with no need to apply gravity reductions from this surface to the geoid.

In chapter 8, these improved techniques are compared to the classical approach (the Direct Integration method). It will be shown that the results from the improved techniques agree to the exact values (computed from the model) better than the results from the classical approach do. This clearly indicates that these techniques offer an improved solution for the computation of the gravity vector in space, without neglecting the topography of the earth.

Chapter 2.

THE APPLICATION OF GREEN'S THIRD IDENTITY

2.1 Introduction

If W is the gravity potential of the earth, and U is is the normal gravity potential of an equipotential ellipsoid, then the earth's gravity vector, and the normal gravity vector are defined as (Heiskanen and Moritz, 1967, p.85):

$$\vec{g} = \text{grad } W = \left(\frac{\partial W}{\partial X}, \frac{\partial W}{\partial Y}, \frac{\partial W}{\partial Z}\right)$$
$$\vec{\gamma} = \text{grad } U = \left(\frac{\partial U}{\partial X}, \frac{\partial U}{\partial Y}, \frac{\partial U}{\partial Z}\right) \qquad (2.1)$$

(X, Y, Z) is a cartesian geocentric coordinate system, whose origin is at the center of mass of the earth; the Z-axis coincides with the earth's mean rotational axis, and the X, Y, axes form a right-handed system with the Z-axis, such that the X-axis lies in the Greenwich meridian plane.

The gravity disturbance vector at any point P is defined as the difference between $\vec{g}$ and $\vec{\gamma}$:

$$\vec{\delta}_P = \vec{g}_P - \vec{\gamma}_P \qquad (2.2)$$

Let $\vec{m}$ be the unit vector normal to the equipotential surface $W = W_P$ of the earth's gravity field at P , and $\vec{\ell}$ be the unit vector normal to the equipotential surface $U = U_P$ of the normal gravity field at P . Then

$$\vec{\delta} = \vec{g} - \vec{\gamma} = \text{grad } W - \text{grad } U = \text{grad } (W - U)$$
$$= \text{grad } T = \left(\frac{\partial T}{\partial X}, \frac{\partial T}{\partial Y}, \frac{\partial T}{\partial Z}\right) \qquad (2.3)$$

T being the disturbing potential at P . If we consider only the magnitudes of the vectors $\vec{g}$ and $\vec{\gamma}$, then the gravity disturbance δg_P at P is :

$$\delta g_P = g_P - \gamma_P = -\left(\frac{\partial W}{\partial m} - \frac{\partial U}{\partial \ell}\right)_P \doteq -\left(\frac{\partial W}{\partial m} - \frac{\partial U}{\partial m}\right)_P = -\left(\frac{\partial T}{\partial m}\right)_P \qquad (2.4)$$

This equation shows that if we ignore the difference in the direction of $\vec{m}$ and $\vec{\ell}$, or in other words the tilt of the surfaces W_P and U_P with respect to each other, then the normal component of the gravity disturbance vector is identical to the difference $g_P - \gamma_P$. The error of

such an approximation is of the order of the square of the deflection of the vertical (Molodensky, et al., 1962, p.79).

The gravity vector $\vec{g}$ can be computed at any space point P, provided that we are able to estimate the gravity disturbance vector $\vec{\delta}$, because the computation of the normal gravity vector $\vec{\gamma}$ does not present any practical or theoretical difficulty (Heiskanen and Moritz,1967, chapter 6), provided that the altitude of P is known. Therefore, if we evaluate the three components:

$$\frac{\partial T}{\partial X}, \frac{\partial T}{\partial Y}, \frac{\partial T}{\partial Z}$$

of the gravity disturbance vector $\vec{\delta}$, the gravity vector $\vec{g}$ will then be:

$$\vec{g} = \vec{\delta} + \vec{\gamma} = \left(\frac{\partial T}{\partial X}, \frac{\partial T}{\partial Y}, \frac{\partial T}{\partial Z}\right) + \left(\frac{\partial U}{\partial X}, \frac{\partial U}{\partial Y}, \frac{\partial U}{\partial Z}\right) \qquad (2.5)$$

2.2 Green's Third Identity

If υ denotes the exterior space of an arbitrary surface S, then, Green's third identity is an integral equation of the form (Heiskanen and Moritz, 1967, p.12):

$$\iiint_{\upsilon} \frac{1}{\ell} \Delta V \, d\upsilon = -pV - \iint_{S} \left\{\frac{1}{\ell} \frac{\partial V}{\partial n} - V \frac{\partial}{\partial n}\left(\frac{1}{\ell}\right)\right\} dS \qquad (2.6)$$

where:

V a continuous and finite function in the space outside S which vanishes at infinity.

υ the exterior space of the surface S.

n outer normal to the surface S.

ℓ the distance from the space point to the surface element dS.

$$p = \begin{cases} 4\pi, & \text{if the identity is applied to a point outside S.} \\ 2\pi, & \text{.. .. .. on S.} \\ 0, & \text{.. .. .. inside S.} \end{cases}$$

If V happens to be a harmonic function in the space outside S, by definition it satisfies Laplace's equation ($\Delta V = 0$), and therefore, the left-hand side of (2.6) is identical to zero. Furthermore, if the mass of the atmosphere is neglected, the disturbing potential $T = W - U$ is a harmonic function (Heiskanen and Moritz, 1967, p.86):

$$\Delta T = \frac{\partial^2 T}{\partial X^2} + \frac{\partial^2 T}{\partial Y^2} + \frac{\partial^2 T}{\partial Z^2} = 0 \qquad (2.7)$$

The partial derivatives of T in a cartesian coordinate system are harmonic functions too, because they satisfy

Laplace's equation:

$$\frac{\partial^2}{\partial X^2}\left(\frac{\partial T}{\partial X}\right) + \frac{\partial^2}{\partial Y^2}\left(\frac{\partial T}{\partial X}\right) + \frac{\partial^2}{\partial Z^2}\left(\frac{\partial T}{\partial X}\right) = \frac{\partial}{\partial X}\Delta T = 0 \qquad (2.8)$$

and similarly for $\frac{\partial T}{\partial Y}$ and $\frac{\partial T}{\partial Z}$. If we now apply Green's identity to the disturbing potential T for the exterior of the earth's surface ($p = 4\pi$), the following very important equation of physical geodesy is obtained (ibid., p.12):

$$T_P = \frac{1}{4\pi} \iint_S \left\{ T \frac{\partial}{\partial n}\left(\frac{1}{\ell}\right) - \frac{1}{\ell}\frac{\partial T}{\partial n} \right\} dS \qquad (2.9)$$

S being the physical surface of the earth, T the disturbing potential at the surface element dS, ℓ is the distance from the space point P to dS, and T_P is the disturbing potential at P. Green's third identity can also be applied to the derivatives:

$$\frac{\partial T}{\partial X}, \quad \frac{\partial T}{\partial Y}, \quad \frac{\partial T}{\partial Z}$$

of the disturbing potential in a cartesian coordinate system:

$$\left(\frac{\partial T}{\partial X}\right)_P = \frac{1}{4\pi} \iint_S \left\{ \frac{\partial T}{\partial X} \frac{\partial}{\partial n}\left(\frac{1}{\ell}\right) - \frac{1}{\ell}\frac{\partial}{\partial n}\left(\frac{\partial T}{\partial X}\right) \right\} dS$$

$$\left(\frac{\partial T}{\partial Y}\right)_P = \frac{1}{4\pi} \iint_S \left\{ \frac{T}{\partial Y} \frac{\partial}{\partial n}\left(\frac{1}{\ell}\right) - \frac{1}{\ell}\frac{\partial}{\partial n}\left(\frac{\partial T}{\partial Y}\right) \right\} dS \qquad (2.10)$$

$$\left(\frac{\partial T}{\partial Z}\right)_P = \frac{1}{4\pi} \iint_S \left\{ \frac{\partial T}{\partial Z} \frac{\partial}{\partial n}\left(\frac{1}{\ell}\right) - \frac{1}{\ell}\frac{\partial}{\partial n}\left(\frac{\partial T}{\partial Z}\right) \right\} dS$$

An initial attempt to use these three equations for the computation of the gravity disturbance vector, resulted in very complicated expressions the practical use of which was questionable. More specifically, the deflections of the vertical on the surface S were needed, as well as their partial derivatives in a local cartesian coordinate system. Therefore, we decided to proceed by differentiating (2.9) directly in a cartesian coordinate system.

Instead of using (2.9) in its present form, certain authors have used another form (Molodensky, et al., 1962, p.45; Koch, 1967-b, p.29; Koch, 1968-a, p.11):

$$T_P = \frac{1}{4\pi} \iint_S \left\{ (T - T(P_0)) \frac{\partial}{\partial n}\left(\frac{1}{\ell}\right) - \frac{1}{\ell}\frac{\partial T}{\partial n} \right\} dS \qquad (2.9')$$

where $T(P_0)$ is the disturbing potential at the projection P_0 of P onto the surface S. As Molodensky (et al., ibid) explained, this second form of (2.9) is an artifact that does not affect the rigour of the equation. $T(P_0)$ is a constant, and the integral

$$\iint_S \frac{\partial}{\partial n}\left(\frac{1}{\ell}\right) dS = 0$$

is equal to zero, if we integrate over the whole surface. However, if the integration is taken over a limited area around P_0 - say within a 5° or 10° cap - , the term

$$- \iint T(P_0) \frac{\partial}{\partial n}\left(\frac{1}{\ell}\right) dS$$

is not equal to zero, and therefore will cause errors in the computation of T_p. In our derivation for the components of the gravity disturbance vector in space, we decided to use the original form (equation 2.9), because as we will se later, a limited amount of data is used, and not a global data set.

Let us now derive the equations for the derivatives of T under a spherical approximation (Moritz, 1966, p.25). This does not mean that the topography of the earth is not considered, or neglected. It means that the given heights above a reference ellipsoid, are taken as heights above a mean-earth sphere of radius R, by neglecting the flattening of the ellipsoid. The effect of this spherical approximation on the disturbing potential is estimated to be of the order of 0.003 T (Moritz, 1980, p.15). Let Q be an arbitrary point on the earth's surface S, and P the point in space where the derivatives of T are to be computed. (see figure 2.1). Let us also define the following two coordinate systems:

a. A right-handed cartesian coordinate system $(\bar{X}, \bar{Y}, \bar{Z})$ located at the space point P. The $\bar{Z}$-axis is in the direction from the geocenter O to P, the $\bar{X}$-axis points to the north, and the $\bar{Y}$-axis points to the west.

b. A right-handed cartesian coordinate system (x,y,z) located at the variable surface point Q (topocentric system). The z-axis points up, the x-axis to the north, and the y-axis to the west.

If we differentiate (2.9) with respect to $\bar{X}$, $\bar{Y}$, $\bar{Z}$, we obtain:

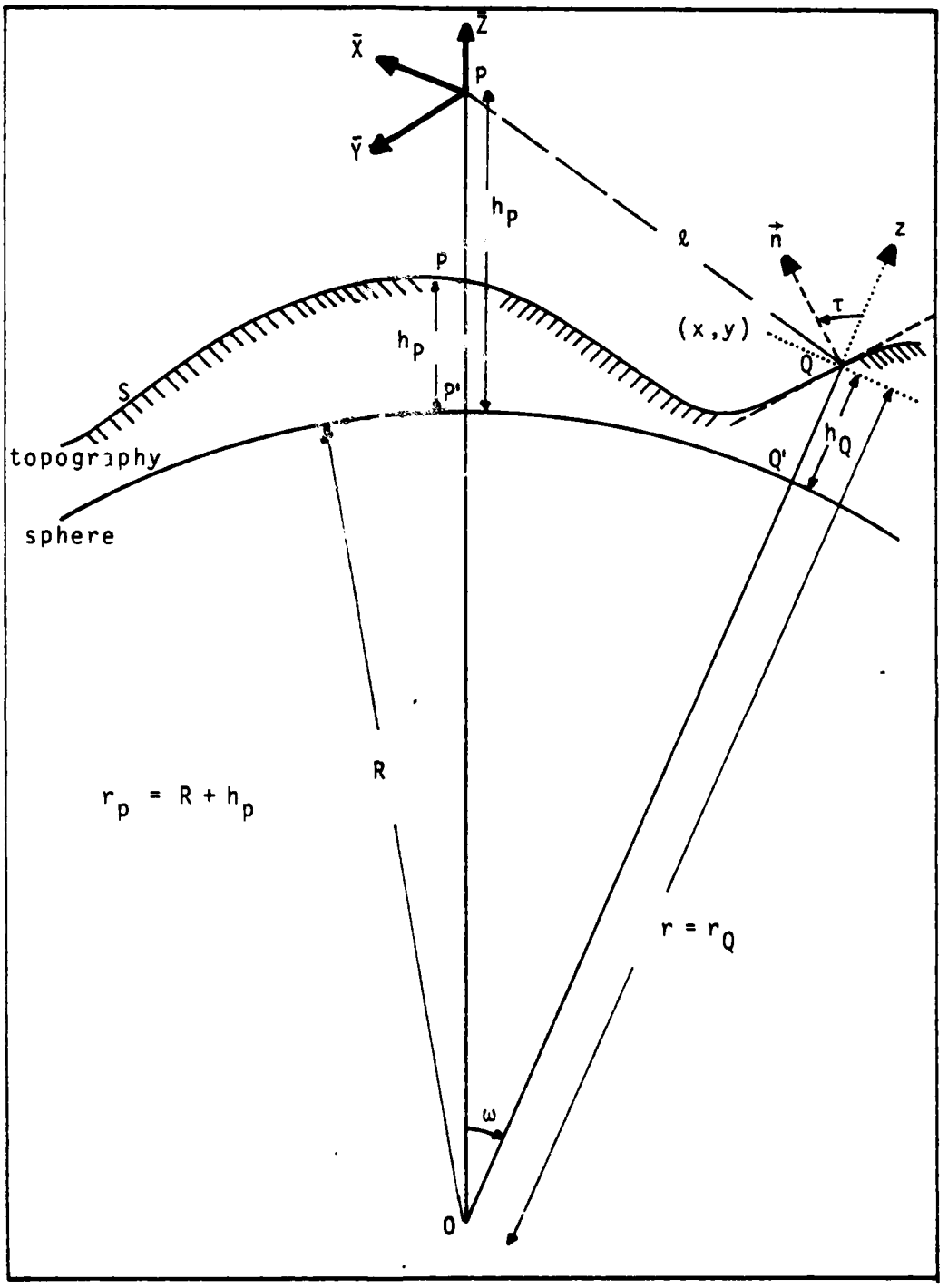

Figure 2.1: Geometric Configuration for the Green's Approach.

$$\left(\frac{\partial T}{\partial \bar{X}}\right)_P = \frac{1}{4\pi} \iint_S \left\{T \frac{\partial}{\partial \bar{X}} \left(\frac{\partial}{\partial n}\left(\frac{1}{\ell}\right)\right) - \frac{\partial}{\partial \bar{X}}\left(\frac{1}{\ell}\right) \frac{\partial T}{\partial n}\right\} dS$$

$$\left(\frac{\partial T}{\partial \bar{Y}}\right)_P - \frac{1}{4\pi} \iint_S \left\{T \frac{\partial}{\partial \bar{Y}} \left(\frac{\partial}{\partial n}\left(\frac{1}{\ell}\right)\right) - \frac{\partial}{\partial \bar{Y}}\left(\frac{1}{\ell}\right) \frac{\partial T}{\partial n}\right\} dS \quad (2.11)$$

$$\left(\frac{\partial T}{\partial \bar{Z}}\right)_P - \frac{1}{4\pi} \iint_S \left\{T \frac{\partial}{\partial \bar{Z}} \left(\frac{\partial}{\partial n}\left(\frac{1}{\ell}\right)\right) - \frac{\partial}{\partial \bar{Z}}\left(\frac{1}{\ell}\right) \frac{\partial T}{\partial n}\right\} dS$$

As it will be shown in the next section, the term $\partial T/\partial n$ is a function of the deflection of the vertical components (ξ,η). Hence, (2.11) have the same difficulties as (2.10) if applied. For this reason, equation (2.9) for T will be modified following the Molodensky's technique (Molodensky, et al., 1962), which has also been used in (Moritz, 1965, 1966). The theory behind these developments is outlined in the next two sections.

2.3 Moritz's approach

For a differentiable scalar function F, the gradient of F is written in terms of its components as:

$$\text{grad } F = \nabla F = \left(\frac{\partial F}{\partial x}, \frac{\partial F}{\partial y}, \frac{\partial F}{\partial z}\right) \quad (2.12)$$

where (x,y,z) is a coordinate system with arbitrary location and orientation. The component of grad F in the direction of a unit vector $\vec{n}$ is the dot product:

$$\frac{\partial F}{\partial n} = \vec{n} \cdot \text{grad } F \quad (2.13)$$

Physically, this product is the rate of change of the scalar F at the point (x,y,z) in the direction of the vector $\vec{n} = (n_1, n_2, n_3)$. Directly from (2.13) we get:

$$\frac{\partial F}{\partial n} = n_1 \frac{\partial F}{\partial x} + n_2 \frac{\partial F}{\partial y} + n_3 \frac{\partial F}{\partial z} \quad (2.14)$$

If F is the disturbing potential T, the term $\partial F/\partial n$ is actually the term appearing in (2.11). In this section, we follow Moritz's approach for its evaluation (Moritz, 1964). Let (x,y,z) be the local cartesian coordinate system, as defined in the previous section, located at the arbitrary surface point Q. In this system, the earth's topography can be represented as

$$S(x, y, z) = 0 \quad (2.15)$$

or by the explicit form $z = h(x,y)$, which yields:

$$S(x\ ,\ y\ ,\ h(x,\ y)) = 0 \tag{2.16}$$

Differentiating (2.16) with respect to x and y we obtain:

$$\frac{dS}{dx} = \frac{\partial S}{\partial x} + \frac{\partial S}{\partial z}\frac{\partial h}{\partial x} = 0$$

$$\frac{dS}{dy} = \frac{\partial S}{\partial y} + \frac{\partial S}{\partial z}\frac{\partial h}{\partial y} = 0 \tag{2.17}$$

If $\vec{n}$ is the unit vector perpendicular to the surface $S(x,y,z) = 0$ at a point (x,y,z), its components are proportional to the components of the vector grad S :

$$\begin{aligned}\text{grad } S &= \left(\frac{\partial S}{\partial x}\ ,\ \frac{\partial S}{\partial y}\ ,\ \frac{\partial S}{\partial z}\right)\\ &= \left(-\frac{\partial S}{\partial z}\frac{\partial h}{\partial x}\ ,\ -\frac{\partial S}{\partial z}\frac{\partial h}{\partial y}\ ,\ \frac{\partial S}{\partial z}\right)\\ &= \frac{\partial S}{\partial z}\left(-\frac{\partial h}{\partial x}\ ,\ -\frac{\partial h}{\partial y}\ ,\ 1\right)\end{aligned} \tag{2.18}$$

Therefore, the unit vector $\vec{n}$ can be written as:

$$\vec{n} = \frac{\left(-\frac{\partial h}{\partial x}\ ,\ -\frac{\partial h}{\partial y}\ ,\ 1\right)}{\sqrt{\left(-\frac{\partial h}{\partial x}\right)^2 + \left(-\frac{\partial h}{\partial y}\right)^2 + 1}} \tag{2.19}$$

If β is the angle of maximum inclination at a particular surface point Q , then

$$\cos\beta = \vec{n}_0 \cdot \vec{n} \tag{2.20}$$

where $\vec{n}$ is the unit vector normal to S at Q , and $\vec{n}_0$ is the unit vector along the z-axis:

$$\vec{n}_0 = (0\ ,\ 0\ ,\ 1) \tag{2.21}$$

$$\vec{n} = (n_1\ ,\ n_2\ ,\ n_3) = \left(n_1\ ,\ n_2\ ,\ \frac{1}{\sqrt{\left(\frac{\partial h}{\partial x}\right)^2 + \left(\frac{\partial h}{\partial y}\right)^2 + 1}}\right) \tag{2.22}$$

Let

$$\frac{\partial h}{\partial x} = \tan \tau_x$$

and

$$\frac{\partial h}{\partial y} = \tan \tau_y \qquad (2.23)$$

Here τ_x and τ_y are the components of the topographic inclination in the x and y directions respectively. We obtain from (2.20):

$$\cos\beta = n_3 \;\therefore\; \cos\beta = \frac{1}{\sqrt{\tan^2 \tau_x + \tan^2 \tau_y + 1}} \qquad (2.24)$$

and from well-known trigonometric identities:

$$\tan^2\beta = \tan^2 \tau_x + \tan^2 \tau_y \qquad (2.25)$$

Therefore, the unit vector $\vec{n}$ in (2.19) can be expressed as:

$$\vec{n} = \cos\beta\,(-\tan \tau_x\,,\; -\tan \tau_y\,,\; 1) \qquad (2.26)$$

and finally, (2.14) yields:

$$\frac{\partial F}{\partial n} = \left[\frac{\partial F}{\partial h} - \left(\frac{\partial F}{\partial x}\tan \tau_x + \frac{\partial F}{\partial y}\tan \tau_y\right)\right]\cos\beta \qquad (2.27)$$

Equation (2.27) was first derived by Moritz (1964, p.20), and it was applied to the disturbing potential $T(\approx F)$, in which case:

$$\frac{\partial T}{\partial x} = -\gamma\xi \qquad (2.28\text{-a})$$

$$\frac{\partial T}{\partial y} = +\gamma\eta \qquad (2.28\text{-b})$$

$$\frac{\partial T}{\partial z} = \frac{\partial T}{\partial h} \approx -\delta g \qquad (2.28\text{-c})$$

The plus sign in (2.28-b) is due to the fact that in the present study the local (x,y,z) - system is a right-handed cartesian system, with the y-axis pointing to the west, instead to the east as it is usually done in the literature (cf. Heiskanen and Moritz, 1967, p.112; Moritz, 1980, p.14). ξ, and η are the components of the deflection of the vertical, and δg is the normal component of the

gravity disturbance vector. The normal gravity at Q is denoted by γ . Equations (2.28) and (2.27) yield:

$$\frac{\partial T}{\partial n} = -[\delta g + \gamma(-\xi \tan \tau_x + \eta \tan \tau_y)] \cos \beta \qquad (2.29)$$

As we mentioned below equation (2.11), by substituting (2.29) into (2.11), the unknown deflection of the vertical components appear in the integrals. A technique which is independent of these components has been developed by Molodensky, et al. (1962), and it is outlined in the next section.

2.4 Molodensky's Approach

The basic idea behind this development is to modify the integral equation (2.9) for the disturbing potential in such a way, that the term $\partial T/\partial n$ does not appear any more as a function of the components of the deflection of the vertical.

Let us denote by $\partial T/\partial x$, $\partial T/\partial y$, the derivatives of T along the horizontal plane (x,y) at the surface point Q , and by $\partial_2 T/\partial x$, $\partial_2 T/\partial y$, the derivatives of T along the surface S (cf. Molodensky, et al., 1962, p.84; Moritz, 1964, p.21). These two sets of partial derivatives are related to each other through the following equations:

$$\frac{\partial_2 T}{\partial x} = \frac{\partial T}{\partial x}\frac{\partial x}{\partial x} + \frac{\partial T}{\partial y}\frac{\partial y}{\partial x} + \frac{\partial T}{\partial z}\frac{\partial z}{\partial x}$$

$$\frac{\partial_2 T}{\partial y} = \frac{\partial T}{\partial x}\frac{\partial x}{\partial y} + \frac{\partial T}{\partial y}\frac{\partial y}{\partial y} + \frac{\partial T}{\partial z}\frac{\partial z}{\partial y}$$

which, if combined with (2.23) and (2.28-c), yield:

$$\frac{\partial_2 T}{\partial x} = \frac{\partial T}{\partial x} + \frac{\partial T}{\partial z}\frac{\partial z}{\partial x} = \frac{\partial T}{\partial x} - \delta g \tan \tau_x$$

$$\frac{\partial_2 T}{\partial y} = \frac{\partial T}{\partial y} + \frac{\partial T}{\partial z}\frac{\partial z}{\partial y} = \frac{\partial T}{\partial y} - \delta g \tan \tau_y \qquad (2.30)$$

or

$$\frac{\partial T}{\partial x} = \frac{\partial_2 T}{\partial x} + \delta g \tan \tau_x$$

$$\frac{\partial T}{\partial y} = \frac{\partial_2 T}{\partial y} + \delta g \tan \tau_y \qquad (2.31)$$

We can not substitute (2.31) and (2.24) into (2.27) for $T = F$, in order to obtain:

$$\frac{\partial T}{\partial n} = -\frac{\delta g}{\cos\beta} - \cos\beta \left(\frac{\partial_2 T}{\partial x} \tan \tau_x + \frac{\partial_2 T}{\partial y} \tan \tau_y\right) \tag{2.32}$$

This leads to the following equation (see also in Moritz, 1964, p.22):

$$\frac{\partial T}{\partial n} = -\frac{\delta g}{\cos\beta} - \cos\beta \, \bar{D}\,(T, h) \tag{2.33}$$

where

$$\bar{D}(T,h) = \frac{\partial_2 T}{\partial x} \tan \tau_x + \frac{\partial_2 T}{\partial y} \tan \tau_y \tag{2.34}$$

is a special case of the operator:

$$\bar{D}(U,V) = \frac{\partial_2 U}{\partial x}\frac{\partial V}{\partial x} + \frac{\partial_2 U}{\partial y}\frac{\partial_2 V}{\partial y} \tag{2.35}$$

Instead of substituting (2.33) into (2.11) as we did with the Moritz's approach, we will proceed as follows. First, (2.33) is multiplied by $1/\ell$ to obtain:

$$\frac{1}{\ell}\frac{\partial T}{\partial n} = -\left(\frac{\delta g}{\ell\cos\beta} + \frac{\cos\beta}{\ell}\bar{D}\,(T,h)\right) \tag{2.36}$$

and from the definition of the operator $\bar{D}$ (Moritz, 1966, p.18) we get:

$$\frac{1}{\ell}\bar{D}\,(T,h) = \bar{D}\left(\frac{T}{\ell},h\right) - T\,\bar{D}\left(\frac{1}{\ell},h\right) \tag{2.37}$$

If now (2.36) is substituted into the integral equation for the disturbing potential, (2.9) yields:

$$T_p = \frac{1}{4\pi}\iint_S \left\{ T\frac{\partial}{\partial n}\left(\frac{1}{\ell}\right) + \frac{\delta g}{\ell\cos\beta} + \frac{\cos\beta}{\ell}\bar{D}\,(T,h)\right\} dS \tag{2.38}$$

and then (2.37) into (2.38) results in:

$$T_p = \frac{1}{4\pi}\iint_S \left\{T\frac{\partial}{\partial n}\left(\frac{1}{\ell}\right) + \frac{\delta g}{\ell\cos\beta} + \cos\beta\left[\bar{D}\left(\frac{T}{\ell},h\right) - T\bar{D}\left(\frac{1}{\ell},h\right)\right]\right\} dS \tag{2.39}$$

Our goal is to differentiate (2.39) with respect to $\bar{X}$, $\bar{Y}$, and $\bar{Z}$, but it is still necessary to simplify the expression for the operator $\bar{D}$ in terms of known quantities. We start from Molodensky's identity (Molodensky,et al., 1962, p.85)

$$\iint_S \bar{D}(U,V)\cos\beta\, dS = -\iint_S U\Delta_2 V \cos\beta\, dS \tag{2.40}$$

which for $U = T/\ell$ and $V = h$ yields:

$$\iint_S \bar{D}\left(\frac{T}{\ell}, h\right)\cos\beta\, dS = -\iint_S \frac{T}{\ell}\Delta_2 h \cos\beta\, dS \tag{2.41}$$

where Δ_2 is another operator defined as (Molodensky, et al., 1962, p.85):

$$\Delta_2 h = \frac{1}{h_1 h_2}\left[\frac{\partial_2}{\partial q_1}\left(\frac{h_0 h_2}{h_1}\frac{\partial_2 h}{\partial q_1}\right) + \frac{\partial_2}{\partial q_2}\left(\frac{h_0 h_1}{h_2}\frac{\partial_2 h}{\partial q_2}\right)\right] \tag{2.42}$$

Note that in the last equation h_1, h_2, and h_0 are functions of the coordinates q_1, q_2, and q_0 of an orthogonal curvilinear system. If q_1 and q_2 are identified as the geocentric latitude and longitude respectively, and q_0 as the elevation, then a line element in this system can be expressed as:

$$ds^2 = h_0^2\, dh^2 + h_1^2\, d\bar{\phi}^2 + h_2^2\, d\lambda^2$$

where (see in Molodensky, et al., ibid, p.86; Moritz, 1966, p.24):

$$\begin{aligned} h_0 &= 1 \\ h_1 &= r \\ h_2 &= r\cos\bar{\phi} \\ \text{and}\quad r &= R + h \end{aligned}$$

With this notation, (2.42) now becomes:

$$\Delta_2 h = \frac{1}{r\cos\bar{\phi}}\left[-\sin\bar{\phi}\,\frac{\partial_2 h}{\partial\bar{\phi}} + \cos\bar{\phi}\,\frac{\partial_2^2 h}{\partial\bar{\phi}^2} + \frac{1}{\cos\bar{\phi}}\,\frac{\partial_2^2 h}{\partial\lambda^2}\right] \tag{2.43}$$

If the first and second-order derivatives of the elevation at any surface point Q are known, it is possible to use (2.39) for the disturbing potential, or to differentiate it for the components of the gravity disturbance, as it will be done in the next section. As we will see, the expressions for these components, not only require knowledge of the elevations h over the whole surface, but they also require the slopes $\tan\tau_x$ and $\tan\tau_y$ to be known. In addition, the operator (2.43) requires the second-order derivatives of the elevation to be known over the whole surface S. At this point we will make the assumption that the earth's surface is a <u>smooth</u> surface,

whose second-order derivatives (of elevation) are equal to zero. This assumption of a smooth surface is also a condition which is required to fulfill Lyapunov's conditions (Molodensky et al., 1962, p.83). Under this assumption, (2.43) becomes:

$$\Delta_2 h = - \frac{1}{r^2} \tan\bar{\phi} \frac{\partial_2 h}{\partial \bar{\phi}} \qquad (2.44)$$

For any function F defined on the surface S, such as the elevation h, or the reciprocal of the distance $1/\ell$, we have (Molodensky et al., 1962, p.84; Moritz, 1966, p.22):

$$\frac{\partial_2 F}{\partial q_1} = \frac{\partial F}{\partial q_1}$$

$$\frac{\partial_2 F}{\partial q_2} = \frac{\partial F}{\partial q_2}$$

Therefore, (2.44) becomes:

$$\Delta_2 h = - \frac{1}{r^2} \tan\bar{\phi} \frac{\partial h}{\partial \bar{\phi}} \qquad (2.45)$$

In (2.43) there is no first-order derivative of the elevation with respect to longitude λ, and this is why this term is missing from (2.45) too. If we evaluate the partial derivative of h with respect to the latitude $\bar{\phi}$, we obtain:

$$\frac{\partial h}{\partial \bar{\phi}} = \frac{\partial h}{\partial x} \frac{\partial x}{\partial \bar{\phi}} + \frac{\partial h}{\partial y} \frac{\partial y}{\partial \bar{\phi}}$$

The transformation from one cartesian coordinate system to another, is usually done by applying a series of roatations and an origin shift to the coordinate system being transformed. In the present report we will use the following three matrices to denote a positive rotation θ around each one of the three axes:

$$R_1(\theta) = \begin{vmatrix} 1 & 0 & 0 \\ 0 & \cos\theta & \sin\theta \\ 0 & -\sin\theta & \cos\theta \end{vmatrix}$$

$$R_2(\theta) = \begin{vmatrix} \cos\theta & 0 & -\sin\theta \\ 0 & 1 & 0 \\ \sin\theta & 0 & \cos\theta \end{vmatrix}$$

$$R_3(\theta) = \begin{vmatrix} \cos\theta & \sin\theta & 0 \\ -\sin\theta & \sin\theta & 0 \\ 0 & 0 & 1 \end{vmatrix}$$

Starting from the transformation equation between the topocentric (x,y,z) and the geocentric (X,Y,Z) systems:

$$\begin{vmatrix} x \\ y \\ z + r_Q \end{vmatrix} = R_2[-(90^\circ - \bar{\phi}_Q)]\, R_3[-(180^\circ - \lambda_Q)] \begin{vmatrix} X \\ Y \\ Z \end{vmatrix}$$

it is very easy to show that:

$$\frac{\partial x}{\partial \bar{\phi}} = r_Q = R + h_Q$$

$$\frac{\partial y}{\partial \bar{\phi}} = 0$$

and hence

$$\frac{\partial h}{\partial \bar{\phi}} = \frac{\partial h}{\partial x}\,\frac{\partial x}{\partial \bar{\phi}} = r \tan \tau_x$$

Therefore, (2.45) can now be written as:

$$\Delta_2 h = -\frac{\tan\bar{\phi}}{r} \tan \tau_x \qquad (2.46)$$

After the above first-order approximation has been obtained for $\Delta_2 h$, it remains to derive the expression for the disturbing potential T_P, Substituting (2.41) into (2.39) we obtain:

$$T_P = \frac{1}{4\pi} \iint_S \left\{ T \frac{\partial}{\partial n}\left(\frac{1}{\ell}\right) + \frac{\delta g}{\cos\beta\, \ell} - \cos\beta\, T\left(\bar{D}\left(\frac{1}{\ell}, h\right) + \frac{\Delta_2 h}{\ell}\right) \right\} dS$$

Next, we apply equation (2.33) with $1/\ell$ instead of T (the proof is completely analogous) to obtain:

$$\frac{\partial(\frac{1}{\ell})}{\partial n} = \frac{1}{\cos\beta}\frac{\partial(\frac{1}{\ell})}{\partial n} - \cos\beta\ \bar{D}\ (\frac{1}{\ell},h) \qquad (2.48)$$

and then, (2.47) with (2.48) yield:

$$T_p = \frac{1}{4\pi}\iint_S \frac{\delta g}{\ell\cdot\cos\beta}\ dS + \frac{1}{4\pi}\iint_S T\ \{\frac{1}{\cos\beta}\frac{\partial}{\partial h}(\frac{1}{\ell}) - 2\cos\beta\ \bar{D}(\frac{1}{\ell},h) - \frac{\cos\beta}{\ell}\Delta_2 h\}\ dS \qquad (2.49)$$

As we have already mentioned, $1/\ell$ is a surface function and hence (2.35) yields:

$$\bar{D}\ (\frac{1}{\ell},h) = \frac{\partial(\frac{1}{\ell})}{\partial x}\tan\tau_x + \frac{\partial(\frac{1}{\ell})}{\partial y}\tan\tau_y \qquad (2.50)$$

As a final step, substitute (2.50) and (2.46) into (2.49) to obtain the expression for the disturbing potential T at a space point P from gravity and topography data on the earth's surface, without neglecting the topography of the earth or its inclinations. Only the second-order derivatives of the elevation are neglected under a "smooth-earth" approximation.

$$T_p = \frac{1}{4\pi}\iint_S \frac{\delta g}{\ell\cos\beta}\ dS + \frac{1}{4\pi}\iint_S T\{\frac{1}{\cos\beta}\frac{\partial}{\partial h}(\frac{1}{\ell}) - 2\cos\beta\ (\frac{\partial}{\partial x}(\frac{1}{\ell})\tan\tau_x + \frac{\partial}{\partial y}(\frac{1}{\ell})\tan\tau_y) + \cos\beta\ \frac{\tan\bar{\phi}\ \tan\tau_x}{\ell r}\}\ dS \qquad (2.51)$$

If we set the inclination components τ_x and τ_y in (2.51) equal to zero, and use (2.28-c), then (2.51) yields the following spherical formula (see Heiskanen and Moritz, 1967, p.12):

$$T_p = \frac{1}{4\pi}\iint_{S'} \{-\frac{\delta g}{\ell} + T\ \frac{\partial}{\partial n}\ (\frac{1}{\ell})\}\ dS \qquad (2.51')$$

where δg is now the gravity disturbance on the surface of the sphere (S') . In this case, (2.51') corresponds to the "classical" approach, where the topography is not considered.

It now remains to differentiate (2.51) with respect to $\bar{X}$, $\bar{Y}$, $\bar{Z}$, and then to rotate these components to the (X,Y,Z) system. This will be done in the next section.

2.5 Differentiation of the Disturbing Potential

In order to obtain the derivatives $\frac{\partial T}{\partial X}$, $\frac{\partial T}{\partial Y}$, $\frac{\partial T}{\partial Z}$, we first compute the partials $\frac{\partial T}{\partial \bar{X}}$, $\frac{\partial T}{\partial \bar{Y}}$, $\frac{\partial T}{\partial \bar{Z}}$ in the $(\bar{X}, \bar{Y}, \bar{Z})$ system (defined in section 2.2). From 2.51 we obtain:

$$\frac{\partial T}{\partial \bar{X}_p} = \frac{1}{4\pi} \iint_S \left\{ \frac{\delta g}{\cos\beta} + T \frac{\cos\beta \tan\bar{\phi}}{r} \tan\tau_x \right\} \frac{\partial}{\partial \bar{X}_p} \left(\frac{1}{\ell}\right) dS$$

$$+ \frac{1}{4\pi} \iint_S T \left\{ \frac{1}{\cos\beta} \frac{\partial}{\partial \bar{X}_p} \left(\frac{\partial}{\partial h} \left(\frac{1}{\ell}\right)\right) - 2\cos\beta \left[\frac{\partial}{\partial \bar{X}_p} \left(\frac{1}{\ell}\right)\right) \tan\tau_x \right.$$

$$\left. + \frac{\partial}{\partial \bar{X}_p} \left(\frac{\partial}{\partial y} \left(\frac{1}{\ell}\right)\right) \tan\tau_y \right] \right\} dS \qquad (2.52\text{-a})$$

$$\frac{\partial T}{\partial \bar{Y}_p} = \frac{1}{4\pi} \iint_S \left\{ \frac{\delta g}{\cos\beta} + T \frac{\cos\beta \tan\bar{\phi}}{r} \tan\tau_x \right\} \frac{\partial}{\partial \bar{Y}_p} \left(\frac{1}{\ell}\right) dS$$

$$+ \frac{1}{4\pi} \iint_S T \left\{ \frac{1}{\cos\beta} \frac{\partial}{\partial \bar{Y}_p} \left(\frac{\partial}{\partial h} \left(\frac{1}{\ell}\right)\right) - 2\cos\beta \left[\frac{\partial}{\partial \bar{Y}_p} \left(\frac{\partial}{\partial x} \left(\frac{1}{\ell}\right)\right) \tan\tau_x \right.\right.$$

$$\left.\left. + \frac{\partial}{\partial \bar{Y}_p} \left(\frac{\partial}{\partial y} \left(\frac{1}{\ell}\right)\right) \tan\tau_y \right] \right\} dS \qquad (2.52\text{-b})$$

$$\frac{\partial T}{\partial \bar{Z}_p} = \frac{1}{4\pi} \iint_S \left\{ \frac{\delta g}{\cos\beta} + T \frac{\cos\beta \tan\bar{\phi}}{r} \tan\tau_x \right\} \frac{\partial}{\partial \bar{Z}_p} \left(\frac{1}{\ell}\right) dS$$

$$+ \frac{1}{4\pi} \iint_S T \left\{ \frac{1}{\cos\beta} \frac{\partial}{\partial \bar{Z}_p} \left(\frac{\partial}{\partial h} \left(\frac{1}{\ell}\right)\right) - 2\cos\beta \left[\frac{\partial}{\partial \bar{Z}_p} \left(\frac{\partial}{\partial x} \left(\frac{1}{\ell}\right)\right) \tan\tau_x \right.\right.$$

$$\left.\left. + \frac{\partial}{\partial \bar{Z}_p} \left(\frac{\partial}{\partial y} \left(\frac{1}{\ell}\right)\right) \tan\tau_y \right] \right\} dS \qquad (2.52\text{-c})$$

We will now derive one-by-line all the partial derivatives which appear in the equations above. The spatial distance ℓ between the space point P and any surface point Q in the $(\bar{X}, \bar{Y}, \bar{Z})$ system is:

$$\ell = \left((\bar{X}_p - \bar{X}_Q)^2 + (\bar{Y}_p - \bar{Y}_Q)^2 + (\bar{Z}_p - \bar{Z}_Q)^2\right)^{\frac{1}{2}} \qquad (2.53)$$

From (2.53) we obtain:

$$\frac{\partial}{\partial \bar{X}_p}\left(\frac{1}{\ell}\right) = -\frac{\bar{X}_p - \bar{X}_Q}{\ell^3}$$

$$\frac{\partial}{\partial \bar{Y}_p}\left(\frac{1}{\ell}\right) = -\frac{\bar{Y}_p - \bar{Y}_Q}{\ell^3}$$

$$\frac{\partial}{\partial \bar{Z}_p}\left(\frac{1}{\ell}\right) = -\frac{\bar{Z}_p - \bar{Z}_Q}{\ell^3} \qquad (2.54)$$

We also have:

$$\frac{\partial}{\partial x}\left(\frac{1}{\ell}\right) = -\frac{1}{2\ell^3}\frac{\partial \ell^2}{\partial x}$$

$$\frac{\partial}{\partial y}\left(\frac{1}{\ell}\right) = -\frac{1}{2\ell^3}\frac{\partial \ell^2}{\partial y}$$

$$\frac{\partial}{\partial z}\left(\frac{1}{\ell}\right) = -\frac{1}{2\ell^3}\frac{\partial \ell^2}{\partial z} \qquad (2.55)$$

where

$$\frac{\partial \ell^2}{\partial x} = \frac{\partial \ell^2}{\partial \bar{X}_p}\frac{\partial \bar{X}_p}{\partial x} + \frac{\partial \ell^2}{\partial \bar{Y}_p}\frac{\partial \bar{Y}_p}{\partial x} + \frac{\partial \ell^2}{\partial \bar{Z}_p}\frac{\partial \bar{Z}_p}{\partial x}$$

$$\frac{\partial \ell^2}{\partial y} = \frac{\partial \ell^2}{\partial \bar{X}_p}\frac{\partial \bar{X}_p}{\partial y} + \frac{\partial \ell^2}{\partial \bar{Y}_p}\frac{\partial \bar{Y}_p}{\partial y} + \frac{\partial \ell^2}{\partial \bar{Z}_p}\frac{\partial \bar{Z}_p}{\partial y}$$

$$\frac{\partial \ell^2}{\partial z} = \frac{\partial \ell^2}{\partial \bar{X}_p}\frac{\partial \bar{X}_p}{\partial z} + \frac{\partial \ell^2}{\partial \bar{Y}_p}\frac{\partial \bar{Y}_p}{\partial z} + \frac{\partial \ell^2}{\partial \bar{Z}_p}\frac{\partial \bar{Z}_p}{\partial z} \qquad (2.56)$$

or in matrix form:

$$\begin{vmatrix} \frac{\partial \ell^2}{\partial x} \\ \frac{\partial \ell^2}{\partial y} \\ \frac{\partial \ell^2}{\partial z} \end{vmatrix} = \begin{vmatrix} \frac{\partial \bar{X}_p}{\partial x} & \frac{\partial \bar{Y}_p}{\partial x} & \frac{\partial \bar{Z}_p}{\partial x} \\ \frac{\partial \bar{X}_p}{\partial y} & \frac{\partial \bar{Y}_p}{\partial y} & \frac{\partial \bar{Z}_p}{\partial y} \\ \frac{\partial \bar{X}_p}{\partial z} & \frac{\partial \bar{Y}_p}{\partial z} & \frac{\partial \bar{Z}_p}{\partial z} \end{vmatrix} \begin{vmatrix} \frac{\partial \ell^2}{\partial \bar{X}_p} \\ \frac{\partial \ell^2}{\partial \bar{Y}_p} \\ \frac{\partial \ell^2}{\partial \bar{Z}_p} \end{vmatrix} \qquad (2.57)$$

Again, from (2.53) for a point Q fixed on S we obtain:

$$\frac{\partial \ell^2}{\partial \bar{X}_P} = 2\,(\bar{X}_P - \bar{X}_Q)$$

$$\frac{\partial \ell^2}{\partial \bar{Y}_P} = 2\,(\bar{Y}_P - \bar{Y}_Q)$$

$$\frac{\partial \ell^2}{\partial \bar{Z}_P} = 2\,(\bar{Z}_P - \bar{Z}_Q) \qquad (2.58)$$

The partial derivatives in (2.57) can be computed from the transformation equation between the (x,y,z), and the $(\bar{X},\bar{Y},\bar{Z})$ coordinate systems:

$$\begin{vmatrix} X - X_P \\ Y - Y_P \\ Z - Z_P + r_P \end{vmatrix} = R_2(-(90^\circ - \bar{\phi}_P))\; R_3(-\Delta\lambda)\; R_2(90^\circ - \bar{\phi}_Q) \begin{vmatrix} x \\ y \\ z + r_Q \end{vmatrix} \qquad (2.59)$$

where $\bar{\phi}_P$, $\bar{\phi}_Q$ are the geocentric latitudes of the points P and Q respectively, and r_P, r_Q are the geocentric radii to these points (see figure 2.1). The term $\Delta\lambda$ is the difference in longitude:

$$\Delta\lambda = \lambda_Q - \lambda_P \qquad (2.60)$$

The matrix:

$$R = R_2(-(90^\circ - \bar{\phi}_P))\; R_3(-\Delta\lambda)\; R_2(90^\circ - \bar{\phi}_Q)$$

in equation (2.59) can be easily shown to be equal to

$$R = \begin{vmatrix} \sin\bar{\phi}_P \cos\Delta\lambda \sin\bar{\phi}_P + \cos\bar{\phi}_P \cos\bar{\phi}_Q & -\sin\bar{\phi}_P \sin\Delta\lambda & -\sin\bar{\phi}_P \cos\Delta\lambda \cos\bar{\phi}_Q + \cos\bar{\phi}_P \sin\bar{\phi}_Q \\ \sin\Delta\lambda \sin\bar{\phi}_Q & \cos\Delta\lambda & -\sin\Delta\lambda \cos\bar{\phi}_Q \\ -\cos\bar{\phi}_P \cos\Delta\lambda \sin\bar{\phi}_Q + \sin\bar{\phi}_Q \cos\bar{\phi}_Q & \cos\bar{\phi}_P \sin\Delta\lambda & \cos\bar{\phi}_P \cos\Delta\lambda \cos\bar{\phi}_Q + \sin\bar{\phi}_P \sin\bar{\phi}_Q \end{vmatrix}$$

(2.61)

Therefore, equation (2.57) combined with (2.58) and (2.61) yields:

$$\begin{vmatrix} \frac{\partial \ell^2}{\partial x} \\ \frac{\partial \ell^2}{\partial y} \\ \frac{\partial \ell^2}{\partial z} \end{vmatrix} = -R^T \begin{vmatrix} \frac{\partial \ell^2}{\partial \bar{X}_p} \\ \frac{\partial \ell^2}{\partial \bar{Y}_p} \\ \frac{\partial \ell^2}{\partial \bar{Z}_p} \end{vmatrix} = -2R^T \begin{vmatrix} \bar{X}_p - \bar{X}_Q \\ \bar{Y}_p - \bar{Y}_Q \\ \bar{Z}_p - \bar{Z}_Q \end{vmatrix} \tag{2.62}$$

and therefore (2.55) becomes:

$$\begin{vmatrix} \frac{\partial}{\partial x}(\frac{1}{\ell}) \\ \frac{\partial}{\partial y}(\frac{1}{\ell}) \\ \frac{\partial}{\partial z}(\frac{1}{\ell}) \end{vmatrix} = \frac{1}{\ell^3} R^T \begin{vmatrix} \bar{X}_p - \bar{X}_Q \\ \bar{Y}_p - \bar{Y}_Q \\ \bar{Z}_p - \bar{Z}_Q \end{vmatrix} \tag{2.63}$$

Introducing the notation:

$$W = -R^T = \begin{vmatrix} w_{11} & w_{12} & w_{13} \\ w_{21} & w_{22} & w_{23} \\ w_{31} & w_{32} & w_{33} \end{vmatrix} \tag{2.64}$$

and differentiating (2.63) with respect to $\bar{X}_p$, $\bar{Y}_p$, $\bar{Z}_p$, we obtain:

$$\frac{\partial}{\partial \bar{X}_p}\left(\frac{\partial}{\partial x}\left(\frac{1}{\ell}\right)\right) = w_{11}\frac{\partial}{\partial \bar{X}_p}\left(\frac{\bar{X}_Q - \bar{X}_p}{\ell^3}\right) + w_{12}\frac{\partial}{\partial \bar{X}_p}\left(\frac{\bar{Y}_Q - \bar{Y}_p}{\ell^3}\right) + w_{13}\frac{\partial}{\partial \bar{X}_p}\left(\frac{\bar{Z}_Q - \bar{Z}_p}{\ell^3}\right)$$

$$\frac{\partial}{\partial \bar{Y}_p}\left(\frac{\partial}{\partial x}\left(\frac{1}{\ell}\right)\right) = w_{11}\frac{\partial}{\partial \bar{Y}_p}\left(\frac{\bar{X}_Q - \bar{X}_p}{\ell^3}\right) + w_{12}\frac{\partial}{\partial \bar{Y}_p}\left(\frac{\bar{Y}_Q - \bar{Y}_p}{\ell^3}\right) + w_{13}\frac{\partial}{\partial \bar{Z}_p}\left(\frac{\bar{Z}_Q - \bar{Z}_p}{\ell^3}\right)$$

$$\frac{\partial}{\partial \bar{Z}_p}\left(\frac{\partial}{\partial x}\left(\frac{1}{\ell}\right)\right) = w_{11}\frac{\partial}{\partial \bar{Z}_p}\left(\frac{\bar{X}_Q - \bar{X}_p}{\ell^3}\right) + w_{12}\frac{\partial}{\partial \bar{Z}_p}\left(\frac{\bar{Y}_Q - \bar{Y}_p}{\ell^3}\right) + w_{13}\frac{\partial}{\partial \bar{Z}_p}\left(\frac{\bar{Z}_Q - \bar{Z}_p}{\ell^3}\right)$$

$$\frac{\partial}{\partial \bar{X}_p}\left(\frac{\partial}{\partial y}\left(\frac{1}{\ell}\right)\right) = w_{21}\frac{\partial}{\partial \bar{X}_p}\left(\frac{\bar{X}_Q-\bar{X}_p}{\ell^3}\right)+w_{22}\frac{\partial}{\partial \bar{X}_p}\left(\frac{\bar{Y}_Q-\bar{Y}_p}{\ell^3}\right)+w_{23}\frac{\partial}{\partial \bar{X}_p}\left(\frac{\bar{Z}_Q-\bar{Z}_p}{\ell^3}\right)$$

$$\frac{\partial}{\partial \bar{Y}_p}\left(\frac{\partial}{\partial y}\left(\frac{1}{\ell}\right)\right) = w_{21}\frac{\partial}{\partial \bar{Y}_p}\left(\frac{\bar{X}_Q-\bar{X}_p}{\ell^3}\right)+w_{22}\frac{\partial}{\partial \bar{Y}_p}\left(\frac{\bar{Y}_Q-\bar{Y}_p}{\ell^3}\right)+w_{23}\frac{\partial}{\partial \bar{Y}_p}\left(\frac{\bar{Z}_Q-\bar{Z}_p}{\ell^3}\right)$$

$$\frac{\partial}{\partial \bar{Z}_p}\left(\frac{\partial}{\partial y}\left(\frac{1}{\ell}\right)\right) = w_{21}\frac{\partial}{\partial \bar{Z}_p}\left(\frac{\bar{X}_Q-\bar{X}_p}{\ell^3}\right)+w_{22}\frac{\partial}{\partial \bar{Z}_p}\left(\frac{\bar{Y}_Q-\bar{Y}_p}{\ell^3}\right)+w_{23}\frac{\partial}{\partial \bar{Z}_p}\left(\frac{\bar{Z}_Q-\bar{Z}_p}{\ell^3}\right)$$

$$\frac{\partial}{\partial \bar{X}_p}\left(\frac{\partial}{\partial z}\left(\frac{1}{\ell}\right)\right) = w_{21}\frac{\partial}{\partial \bar{X}_p}\left(\frac{\bar{X}_Q-\bar{X}_p}{\ell^3}\right)+w_{22}\frac{\partial}{\partial \bar{X}_p}\left(\frac{\bar{Y}_Q-\bar{Y}_p}{\ell^3}\right)+w_{23}\frac{\partial}{\partial \bar{X}_p}\left(\frac{\bar{Z}_Q-\bar{Z}_p}{\ell^3}\right)$$

$$\frac{\partial}{\partial \bar{Y}_p}\left(\frac{\partial}{\partial z}\left(\frac{1}{\ell}\right)\right) = w_{21}\frac{\partial}{\partial \bar{Y}_p}\left(\frac{\bar{X}_Q-\bar{X}_p}{\ell^3}\right)+w_{22}\frac{\partial}{\partial \bar{Y}_p}\left(\frac{\bar{Y}_Q-\bar{Y}_p}{\ell^3}\right)+w_{23}\frac{\partial}{\partial \bar{Y}_p}\left(\frac{\bar{Z}_Q-\bar{Z}_p}{\ell^3}\right)$$

$$\frac{\partial}{\partial \bar{Z}_p}\left(\frac{\partial}{\partial z}\left(\frac{1}{\ell}\right)\right) = w_{21}\frac{\partial}{\partial \bar{Z}_p}\left(\frac{\bar{X}_Q-\bar{X}_p}{\ell^3}\right)+w_{22}\frac{\partial}{\partial \bar{Z}_p}\left(\frac{\bar{Y}_Q-\bar{Y}_p}{\ell^3}\right)+w_{23}\frac{\partial}{\partial \bar{Z}_p}\left(\frac{\bar{Z}_Q-\bar{Z}_p}{\ell^3}\right)$$

(2.65)

It can be easily shown that the nine derivatives in the right-hand side of (2.65) are equal to:

$$\frac{\partial}{\partial \bar{X}_p}\left(\frac{\bar{X}_Q-\bar{X}_p}{\ell^3}\right) = \frac{3(\bar{X}_Q-\bar{X}_p)^2-\ell^2}{\ell^5}$$

$$\frac{\partial}{\partial \bar{X}_p}\left(\frac{\bar{Y}_Q-\bar{Y}_p}{\ell^3}\right) = \frac{3(\bar{X}_Q-\bar{X}_p)(\bar{Y}_Q-\bar{Y}_p)}{\ell^5}$$

$$\frac{\partial}{\partial \bar{X}_p}\left(\frac{\bar{Z}_Q-\bar{Z}_p}{\ell^3}\right) = \frac{3(\bar{X}_Q-\bar{X}_p)(\bar{Z}_Q-\bar{Z}_p)}{\ell^5}$$

$$\frac{\partial}{\partial \bar{Y}_p}\left(\frac{\bar{X}_Q-\bar{X}_p}{\ell^3}\right) = \frac{3(\bar{Y}_Q-\bar{Y}_p)(\bar{X}_Q-\bar{X}_p)}{\ell^5}$$

$$\frac{\partial}{\partial \bar{Y}_p}\left(\frac{\bar{Y}_Q-\bar{Y}_p}{\ell^3}\right) = \frac{3(\bar{Y}_Q-\bar{Y}_p)^2-\ell^2}{\ell^5}$$

$$\frac{\partial}{\partial \bar{Y}_p}\left(\frac{\bar{Z}_Q-\bar{Z}_p}{\ell^3}\right) = \frac{3(\bar{Y}_Q-\bar{Y}_p)(\bar{Z}_Q-\bar{Z}_p)}{\ell^5}$$

$$\frac{\partial}{\partial \bar{Z}_p}\left(\frac{\bar{X}_Q-\bar{X}_p}{\ell^3}\right) = \frac{3(\bar{Z}_Q-\bar{Z}_p)(\bar{X}_Q-\bar{X}_p)}{\ell^5}$$

$$\frac{\partial}{\partial \bar{Z}_p}\left(\frac{\bar{Y}_Q-\bar{Y}_p}{\ell^3}\right) = \frac{3(\bar{Z}_Q-\bar{Z}_p)(\bar{Y}_Q-\bar{Y}_p)}{\ell^5}$$

$$\frac{\partial}{\partial \bar{Z}_p}\left(\frac{\bar{Z}_Q-\bar{Z}_p}{\ell^3}\right) = \frac{3(\bar{Z}_Q-\bar{Z}_p)^2-\ell^2}{\ell^5}$$

(2.66)

Let us now substitute the partial derivatives (2.54), (2.65), and (2.66) into (2.52). Since we want to evaluate the components of $\vec{x}$ at the space point P, let us also set $X_p = X_P = Z_p = 0$. From (2.52) we obtain:

$$\frac{\partial T}{\partial \bar{X}_p} = \frac{1}{4\pi}\iint_S \left\{\frac{\delta g}{\cos\beta} + T\,\frac{\cos\beta\tan\bar{\phi}}{r}\tan\tau_x\right\}\frac{\bar{X}}{\ell^3}\,dS$$
$$+\frac{3}{4\pi}\iint_S \frac{T}{\ell^5}\left\{\frac{w_{31}(\bar{X}^2-\frac{\ell^2}{3})+w_{32}\bar{X}\bar{Y}+w_{33}\bar{X}\bar{Z}}{\cos\beta}\right.$$
$$-2\cos\beta\,[(w_{11}(\bar{X}^2-\tfrac{\ell^2}{3})+w_{12}\bar{X}\bar{Y}+w_{13}\bar{X}\bar{Z})\tan\tau_x$$
$$\left.+(w_{21}(\bar{X}^2-\tfrac{\ell^2}{3})+w_{22}\bar{X}\bar{Y}+w_{23}\bar{X}\bar{Z})\tan\tau_y]\right\}dS \qquad (2.67\text{-a})$$

$$\frac{\partial T}{\partial \bar{Y}_p} = \frac{1}{4\pi}\iint_S \left\{\frac{\delta g}{\cos\beta} + T\,\frac{\cos\beta\tan\bar{\phi}}{r}\tan\tau_x\right\}\frac{\bar{Y}}{\ell^3}\,dS$$
$$+\frac{3}{4\pi}\iint_S \frac{T}{\ell^5}\,\frac{w_{31}\bar{Y}\bar{X}+w_{32}(\bar{Y}^2-\frac{\ell^2}{3})+w_{33}\bar{Y}\bar{Z}}{\cos\beta}$$
$$-2\cos\beta[(w_{11}\bar{Y}\bar{X}+w_{12}(\bar{Y}^2-\tfrac{\ell^2}{3})+w_{13}\bar{Y}\bar{Z})\tan\tau_x$$
$$+(w_{21}\bar{Y}\bar{X}+w_{22}(\bar{Y}^2-\tfrac{\ell^2}{3})+w_{23}\bar{Y}\bar{Z})\tan\tau_y]\Big\}\,dS \qquad (2.67\text{-b})$$

$$\frac{\partial T}{\partial \bar{Z}_p} = \frac{1}{4\pi}\iint_S \left\{\frac{\delta g}{\cos\beta} + T\,\frac{\cos\beta\tan\bar{\phi}}{r}\tan\tau_x\right\}\frac{\bar{Z}}{\ell^3}\,dS$$
$$+\frac{3}{4\pi}\iint_S \frac{T}{\ell^5}\left\{\frac{w_{31}\bar{Z}\bar{X}+w_{32}\bar{Z}\bar{Y}+w_{33}(\bar{Z}^2-\frac{\ell^2}{3})}{\cos\beta}\right.$$
$$-2\cos\beta\,[(w_{11}\bar{Z}\bar{X}+w_{12}\bar{Z}\bar{Y}+w_{13}(\bar{Z}^2-\tfrac{\ell^2}{3}))\tan\tau_x$$
$$\left.+[w_{21}\bar{Z}\bar{X}+w_{22}\bar{Z}\bar{Y}+w_{23}(\bar{Z}^2-\tfrac{\ell^2}{3}))\tan\tau_y]\right\}dS \qquad (2.67\text{-c})$$

Finally, rearranging the terms in (2.67) we arrive at the following equations:

$$\frac{\partial T}{\partial \bar{X}_p} = \frac{1}{4\pi} \iint_S \left\{ \frac{\delta g}{\cos\beta} + T \frac{\cos\beta \tan\bar{\phi}}{r} \tan\tau_x \right\} \frac{\bar{X}}{\ell^3} dS$$

$$+ \frac{3}{4\pi} \iint_S \frac{T}{\ell^5} \left\{ (\bar{X}^2 - \frac{\ell^2}{3}) \left[\frac{w_{31}}{\cos\beta} - 2\cos\beta (w_{11}\tan\tau_x + w_{21}\tan\tau_y) \right] \right.$$

$$+ \bar{X}\bar{Y} \left[\frac{w_{32}}{\cos\beta} - 2\cos\beta (w_{12}\tan\tau_x + w_{22}\tan\tau_y) \right]$$

$$\left. + \bar{X}\bar{Z} \left[\frac{w_{33}}{\cos\beta} - 2\cos\beta (w_{13}\tan\tau_x + w_{23}\tan\tau_y) \right] \right\} dS \qquad (2.68\text{-a})$$

$$\frac{\partial T}{\partial \bar{Y}_p} = \frac{1}{4\pi} \iint_S \left\{ \frac{\delta g}{\cos\beta} + T \frac{\cos\beta \tan\bar{\phi}}{r} \tan\tau_x \right\} \frac{\bar{Y}}{\ell^3} dS$$

$$+ \frac{3}{4\pi} \iint_S \frac{T}{\ell^5} \left\{ \bar{Y}\bar{X} \left[\frac{w_{31}}{\cos\beta} - 2\cos\beta (w_{11}\tan\tau_x + w_{21}\tan\tau_y) \right] \right.$$

$$+ (\bar{Y}^2 - \frac{\ell^2}{3}) \left[\frac{w_{32}}{\cos\beta} - 2\cos\beta (w_{12}\tan\tau_x + w_{22}\tan\tau_y) \right]$$

$$\left. + \bar{Y}\bar{Z} \left[\frac{w_{33}}{\cos\beta} - 2\cos\beta (w_{13}\tan\tau_x + w_{23}\tan\tau_y) \right] \right\} dS \qquad (2.68\text{-b})$$

$$\frac{\partial T}{\partial \bar{Z}_p} = \frac{1}{4\pi} \iint_S \left\{ \frac{\delta g}{\cos\beta} + T \frac{\cos\beta \tan\bar{\phi}}{r} \tan\tau_x \right\} \frac{\bar{Z}}{\ell^3} dS$$

$$+ \frac{3}{4\pi} \iint_S \frac{T}{\ell^5} \left\{ \bar{Z}\bar{X} \left[\frac{w_{31}}{\cos\beta} - 2\cos\beta (w_{11}\tan\tau_x + w_{21}\tan\tau_y) \right] \right.$$

$$+ \bar{Z}\bar{Y} \left[\frac{w_{32}}{\cos\beta} - 2\cos\beta (w_{12}\tan\tau_x + w_{22}\tan\tau_y) \right]$$

$$\left. + (\bar{Z}^2 - \frac{\ell^2}{3}) \left[\frac{w_{33}}{\cos\beta} - 2\cos\beta (w_{13}\tan\tau_x + w_{23}\tan\tau_y) \right] \right\} dS \qquad (2.68\text{-c})$$

The differential surface element dS in all the equations above, is given (in general form for an ellipsoidal surface) in (Hotine, 1969, eq. 30.72) as:

$$dS = \frac{1}{\cos\beta} (N + h)(M + h) \cos\phi \; d\phi \; d\lambda \qquad (2.69\text{-a})$$

where N, M are the principal radii of curvature along the prime vertical and the meridian, and h is the height above the reference ellipsoid. Under the spherical approximation of our solution, this equation becomes:

$$dS = \frac{1}{\cos\beta} r^2 \cos\bar{\phi} \; d\bar{\phi} \; d\lambda \qquad (2.69\text{-b})$$

If the surface element is defined by the intersections of parallels and meridians on the reference sphere, (2.69-b) reduced to:

$$\Delta S = \frac{1}{\cos\beta} r^2 (\lambda_{EAST} - \lambda_{WEST}) (\sin\bar{\phi}_{NORTH} - \sin\bar{\phi}_{SOUTH}) \qquad (2.69\text{-c})$$

The data that is needed for the application of equations (2.68-a,b,c) is the following. (a) Gravity disturbances (δg) and disturbing potentials (T) on the surface of the earth, (b) the elevations of the surface points, and (c) the two components (τ_x , τ_y) of the surface inclinations. In the following chapters we will describe how this data is computed for our simulation studies.

2.6 Rotation to the Geocentric System

The derivatives (2.68) are referred to the cartesian coordinate system ($\bar{X}$, $\bar{Y}$, $\bar{Z}$) located at the space point P . They are related to the components of the deflection of the vertical and to the gravity disturbance δg at P through the equations (2.28-a,b,c):

$$\frac{\partial T}{\partial \bar{X}_p} = -\gamma\xi \qquad (2.70\text{-a})$$

$$\frac{\partial T}{\partial \bar{Y}_p} = +\gamma\eta \qquad (2.70\text{-b})$$

$$\frac{\partial T}{\partial \bar{Z}_p} = -\delta g \qquad (2.70\text{-c})$$

If we wish to transform these partial derivatives to a geocentric system (X, Y, Z), we start from the transformation between ($\bar{X}$, $\bar{Y}$, $\bar{Z}$,), and (X, Y, Z):

$$\begin{vmatrix} \bar{X} \\ \bar{Y} \\ \bar{Z} \end{vmatrix} = R_2 (-(90° - \bar{\phi}_p)) \; R_3 (-(180° - \lambda_p)) \begin{vmatrix} X \\ Y \\ Z \end{vmatrix}$$

or

$$\begin{vmatrix} \bar{X} \\ \bar{Y} \\ \bar{Z} + r_p \end{vmatrix} = \begin{vmatrix} -\sin\bar{\phi}_p \cos\lambda_p & -\sin\bar{\phi}_p \sin\lambda_p & \cos\bar{\phi}_p \\ \sin\lambda_p & -\cos\lambda_p & 0 \\ \cos\bar{\phi}_p \cos\lambda_p & \cos\bar{\phi}_p \sin\lambda_p & \sin\bar{\phi}_p \end{vmatrix} \begin{vmatrix} X \\ Y \\ Z \end{vmatrix}$$

where

$$r_p = (X_p^2 + Y_p^2 + Z_p^2)^{\frac{1}{2}} \tag{2.72}$$

The transformation of the partials in (2.68) to the geocentric system is based on the following set of equations:

$$\frac{\partial T}{\partial X} = \frac{\partial T}{\partial \bar{X}} \frac{\partial \bar{X}}{\partial X} + \frac{\partial T}{\partial \bar{Y}} \frac{\partial \bar{Y}}{\partial X} + \frac{\partial T}{\partial \bar{Z}} \frac{\partial \bar{Z}}{\partial X}$$

$$\frac{\partial T}{\partial Y} = \frac{\partial T}{\partial \bar{X}} \frac{\partial \bar{X}}{\partial Y} + \frac{\partial T}{\partial \bar{Y}} \frac{\partial \bar{Y}}{\partial Y} + \frac{\partial T}{\partial \bar{Z}} \frac{\partial \bar{Z}}{\partial Y}$$

$$\frac{\partial T}{\partial Z} = \frac{\partial T}{\partial \bar{X}} \frac{\partial \bar{X}}{\partial Z} + \frac{\partial T}{\partial \bar{Y}} \frac{\partial \bar{Y}}{\partial Z} + \frac{\partial T}{\partial \bar{Z}} \frac{\partial \bar{Z}}{\partial Z}$$

or in matrix form:

$$\begin{vmatrix} \frac{\partial T}{\partial X} \\ \frac{\partial T}{\partial Y} \\ \frac{\partial T}{\partial Z} \end{vmatrix} = J \left(\frac{(\bar{X},\bar{Y},\bar{Z})}{(X,Y,Z)}\right) \begin{vmatrix} \frac{\partial T}{\partial \bar{X}} \\ \frac{\partial T}{\partial \bar{Y}} \\ \frac{\partial T}{\partial \bar{Z}} \end{vmatrix} \tag{2.73}$$

where the Jacobian matrix J is computed from (2.71) as:

$$J \left(\frac{(\bar{X},\bar{Y},\bar{Z})}{(X,Y,Z)}\right) = \begin{vmatrix} -\sin\bar{\phi}_p \cos\lambda_p & \sin\lambda_p & \cos\bar{\phi}_p \cos\lambda_p \\ -\sin\bar{\phi}_p \sin\lambda_p & -\cos\lambda_p & \cos\bar{\phi}_p \sin\lambda_p \\ \cos\bar{\phi}_p & 0 & \sin\bar{\phi}_p \end{vmatrix} \tag{2.74}$$

In summary, equations (2.68) have been derived for the evaluation of the derivatives of T in the local $(\bar{X}, \bar{Y}, \bar{Z})$ system, while (2.73) with (2.74) can be used to compute the partials of T in the geocentric (X, Y, Z) system.

2.7 Computation of the Gravity Vector.

After the partial derivatives of T have been rotated to the geocentric (X,Y,Z) system, and the gravity disturbance vector has been determined:

$$\vec{\delta} = \text{grad } T = \left(\frac{\partial T}{\partial X}, \frac{\partial T}{\partial Y}, \frac{\partial T}{\partial Z}\right) \qquad (2.3)$$

the components of the gravity vector $\vec{g}$ are given from equation (2.5):

$$\vec{g} = \text{grad } W = \vec{\delta} + \vec{\gamma} = \left(\frac{\partial T}{\partial X}, \frac{\partial T}{\partial Y}, \frac{\partial T}{\partial Z}\right) + \left(\frac{\partial T}{\partial X}, \frac{\partial T}{\partial Y}, \frac{\partial T}{\partial Z}\right) \qquad (2.3)$$

U being the normal gravity potential of the equipotential of the equipotential ellipsoid. The expressions for the partial derivatives of U with respect to X,Y,Z are given in (Heiskanen and Moritz, 1967, chapter 6).

For some purposes we need the vector of gravitation $\vec{f}$, that is the vector of the pure attraction of the earth without the centrifugal force $\vec{f} = \text{grad}\Phi$ (Heiskanen and Moritz, 1967, p.228):

$$\vec{f} = \text{grad } V = \text{grad } (W - \Phi) = \vec{g} - \text{grad}\Phi = \vec{g} - (\omega^2 X, \omega^2 Y, 0) \qquad (2.75)$$

The vector $\vec{g}$ contains the effect of the rotation of the earth, while the vector $\vec{f}$ does not. The vector of gravitation is of considerable interest in Geodesy, because it is the effect of the gravitation potential $(V = W - \Phi)$ of the earth at a space point, which is not affected by its rotation (for example, an artificial satellite which is orbiting around the earth).

Chapter 3

THE TERRAIN MODEL

3.1 Introduction

In order to avoid the errors which exist in real data and for the purpose of testing equations (2.68-a,b,c) for the gravity disturbance components, we decided to use a simple terrain model, with synthetic data on its surface. As it will be described later in this chapter two disturbing masses are located below this model on its axis of symmetry, and from those, the exact gravity disturbance vector can be computed at any space point. The gravity disturbance δg , and the disturbing potential T can also be computed at any point on the surface of the model. This data, and the inclinations of the model at these points are then used in (2.68) to compute the three components of $\overset{+}{\delta}$ at any space point P , and to compare them with the exact components evaluated from the model's disturbing masses.

The idea of using this type of simulation tests is not new, and the details will follow along the lines of this chapter. For gravity anomaly and deflection of the vertical computations, a conical mountain was used by Molodensky et al., (1962, p.217), and by Reit, (1966). For a slightly more general case (the model is on a sphere rather than on a plane as above), see Sjöberg (1975, p.82). Bjerhammar (1963) has used another type of model which is a homogeneous spherical cap on a spherical earth. This model has also been discussed by (Sjöberg, ibid, p.79). In order to find estimates for the effect of the topographic elevations on the external gravity anomalies, Moritz (1965) has used two models (a conical mountain, and a two-dimensional model e.g. two planes intersecting each other). Other simulations were performed by Koch (1967-a, 1968-a) with a pyramid and a cone. These models are similar to those mentioned above, but they have the advantage of allowing the model's inclination to vary within certain limits.

Among the simulations above, those by Koch and by Moritz test the accuracy of the computed quantities following the Green's identity approach The rest are studies on the accuracy in the computation of surface or space quantities from one of the Bjerhammar's discrete methods. In this paper we are dealing with both approaches. The simulations for testing the Green's approach are reported in chapter 4, and those for the discrete (Dirac) approach are reported

in chapter 6. In the present chapter, the geometric and the dynamic characteristics of the model are described.

3.2 The Geometry of the Model

The terrain model which has been selected for this study, consists of a cone on a spherical earth, with its top replaced by a spherical cap of certain radius, such that the spherical and the conical surfaces are tangent to each other at their intersection (figure 3.1). In theory, this rounding of the model's top is a necessity to satisfy Lyapunov's conditions (Molodensky et al., 1962, p.217).

Assume that the axis of the cone intersects the surface of the mean earth sphere ($R = 6371$ km) at the point ($\bar{\phi}_0$, λ_0, $h=0$), and that it passes through the center of mass 0. Let ($\bar{\phi}_Q$, λ_Q, h_Q) be the coordinates of any point on the surface of the model. The height h_Q is the distance from Q to the sphere along the radius from 0 to Q. Let also ($\bar{\phi}_P$, λ_P, h_P) be the coordinates of the space point P where the gravity disturbance vector is to be computed. At the point M_1 and M_2 on the axis, there are two point masses m_1 and m_2 respectively, which generate the disturbing potential. Their distances from the surface of the sphere (point A_0) are a_1 and a_2. As inclination of the model (i), we define the angle between its surface and the plane tangent to the sphere R at A_0.

As we will show, there are only three parameters which are needed to completely describe the geometry of the model in terms of size and shape:

1. The height of the cone's vertex above the spherical earth (h_A)
2. The extent of the cone, in terms of the angle Ω, and
3. The radius of the spherical cap (ρ).

All the quantities involved with the model's geometry are computed below as functions of the three parameters above. Let $\bar{\omega}$ be the angle at the geocenter 0 between the axis and the radius to point D where the cone and the spherical cap meet each other. Let also ω be the angle at the geocenter 0 between the axis and the radius to an arbitrary point Q on the model. There are three possible cases for the location of Q on the model:

Q on the spherical cap: $0 \leq \omega \leq \bar{\omega}$

Q on the conical surface: $\bar{\omega} \leq \omega \leq \Omega$

Q on the mean sphere R: $\Omega \leq \omega \leq 180°$

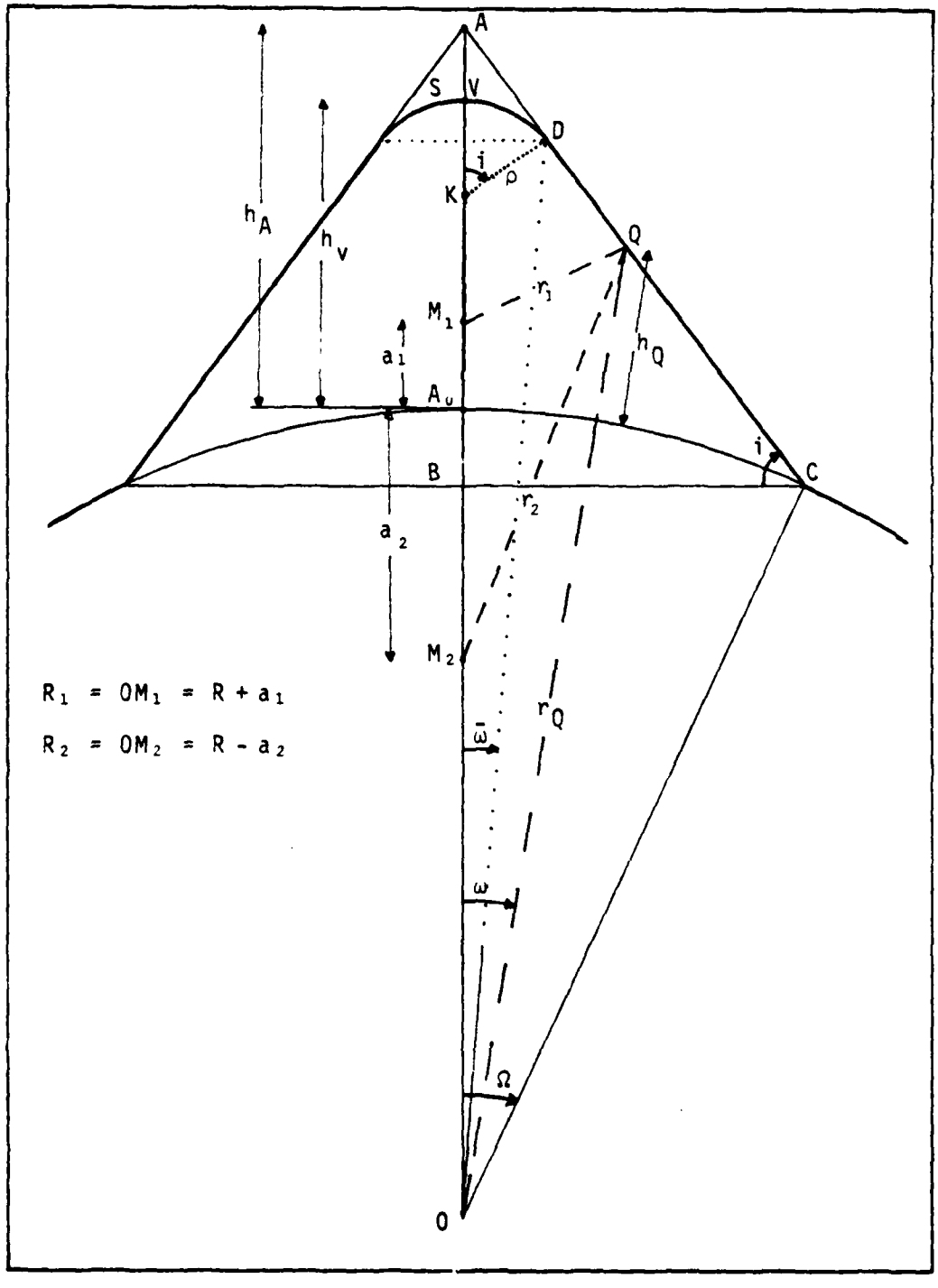

Figure 3.1: The Geometry of the Model.

ω can be computed from:

$$\cos\omega = \cos\theta_0 \cos\theta_Q \sin\theta_0 \sin\theta_Q \cos\Delta\lambda \tag{3.1}$$

where

$$\theta_0 = 90° - \bar{\Phi}_0$$
$$\theta_Q = 90° - \bar{\Phi}_Q$$
$$\Delta\lambda = \lambda_Q - \lambda_0$$

From figure 3.1 we easily obtain:

$$\overline{AB} = h_A + R\,(1 - \cos\Omega) \tag{3.2}$$

and the inclination i of the model is then computed as:

$$\tan i = \frac{\overline{AB}}{\overline{BC}} = \frac{h_A + R(1 - \cos\Omega)}{R \sin \Omega} \tag{3.3}$$

Then, the height h_V of the model's vertex V is given by:

$$h_V = h_A - \overline{AV} = h_A - (\overline{AK} - \rho) = h_A + \rho - \frac{\rho}{\cos i} \tag{3.4}$$

and since

$$\overline{AD} = \rho \tan i \tag{3.5}$$

we obtain:

$$\tan \bar{\omega} = \frac{\rho \sin i}{R + h_A - \overline{AD} \sin i} \tag{3.6}$$

The evaluation of the height of any surface point is done according to its location on the model (see the three conditions above).

Case-A Point Q on the surface of the cone ($\bar{\omega} \leq \omega \leq \Omega$, figure 3.1). Applying the law of consines to the triangle AOQ we obtain:

$$\frac{r_Q}{\cos i} = \frac{R + h_A}{\sin\,(180° - 90° + i - \omega)}$$

which gives:

$$r_Q = \frac{R + h_A}{\cos\omega + \tan i \sin\omega} \tag{3.7}$$

and hence:

$$h_Q = r_Q - R \tag{3.8}$$

The distances of the point Q from the two masses are:

$$r_1 = (R_1^2 + r_Q^2 - 2R_1 r_Q \cos\omega)^{\frac{1}{2}}$$

and

$$r_2 = (R_2^2 + r_Q^2 - 2R_2 r_Q \cos\omega)^{\frac{1}{2}} \tag{3.9}$$

where

$$R_1 = R + a_1$$

$$R_2 = R - a_2 \tag{3.10}$$

Case-B Point S on the spherical cap ($0° \leq \omega \leq \bar{\omega}$, figure 3.1). From the triangle OKS we obtain:

$$\rho^2 = r_S^2 + \overline{OK} - 2r_S \overline{OK} \cos\omega \tag{3.11}$$

which yields:

$$r_S = \overline{OK} \cos\omega + \sqrt{\rho^2 - \overline{OK}^2 \sin^2\omega} \tag{3.12}$$

where

$$\overline{OK} = R + h_V - \rho \tag{3.13}$$

and hence:

$$h_S = r_S - R \tag{3.14}$$

Case-C Point Q on the surface of the mean sphere ($\Omega \leq \omega \leq 180°$). In this case

$$h_Q = 0 \tag{3.15}$$

and hence:

$$r_Q = R \tag{3.15-a}$$

3.3 The Data on the Surface of the Model

After the geometry of the model has been established in terms of its size and shape, the disturbing field generated on its surface and in the exterior space is now determined.

Four more parameters are needed to describe the dynamic characteristics of the model. These parameters are:

1. The distances a_1 and a_2 of the two masses m_1 and m_2 from the surface of the sphere R, and
2. The gravity disturbances δg_1 and δg_2 produced by two masses at the vertex V of the model.

Therefore, for the simulation studies that we will conduct in this paper, we need to define the following set of seven parameters:

$$h_A \ , \ \Omega \ , \ \rho \ , \ a_1 \ , \ a_2 \ , \ \delta g_1 \ , \ \delta g_2$$

The disturbing potential at any point Q on the surface, or in the exterior space is computed from:

$$T_Q = \frac{km_1}{r_1} + \frac{km_2}{r_2} \tag{3.16}$$

where r_1 and r_2 are given by (3.9), and km_1, km_2 are determined from the given boundary conditions δg_1, and δg_2 as we will show below.

The normal component of the gravity disturbance at any surface point Q is computed from:

$$\delta g_Q = - \left(\frac{\partial T}{\partial r}\right)_Q \tag{3.17}$$

Using (3.9), (3.16), and (3.17) we obtain:

$$\delta g_Q = \frac{km_1(r_Q - R\cos\omega)}{r_1^3} + \frac{km_2(r_Q - R\cos\omega)}{r_2^3} \tag{3.18}$$

The geocentric distance r_Q in (3.18) is computed from:

1. equation (3.7), for Q on the conical surface, or
2. equation (3.12), for Q on the spherical cap, or
3. equation (3.15-a), for Q on the mean sphere R .

The terms km_1 and km_2 are determined from the solution of (3.18) using the boundary conditions δg_1 and δg_2 at V . In order to determine km_1 and km_2 , we have:

$$km_1 = \delta g_1 \, (R + h_V - R_1)^2 \qquad (3.19\text{-a})$$

and

$$km_2 = \delta g_2 \, (R + h_V - R_2)^2 \qquad (3.19\text{-b})$$

3.4 The Gravity Disturbance Vector in Space, Computed from the Model

It now remains to find the expressions for the components of the gravity disturbance vector as a space point, which is generated from the two disturbing masses:

$$\vec{\delta} = \text{grad } T = \left(\frac{\partial T}{\partial X} , \frac{\partial T}{\partial Y} , \frac{\partial T}{\partial Z}\right) \qquad (3.20)$$

The disturbing potential T is given by (3.16), where instead of (3.9) we now use:

$$r_1 = [(X - X_1)^2 + (Y - Y_1)^2 + (Z - Z_1)^2]^{\frac{1}{2}} \qquad (3.21\text{-a})$$

and

$$r_2 = [(X - X_2)^2 + (Y - Y_2)^2 + (Z - Z_2)^2]^{\frac{1}{2}} \qquad (3.21\text{-b})$$

where (X, Y, Z) are the geocentric cartesian coordinates of the space point P $(\bar{\phi}_P , \lambda_P , h_P)$, and (X_1 , Y_1 , Z_1), (X_2 , Y_2 , Z_2), are the cartesian geocentric coordinates of the two disturbing masses m_1 , and m_2 respectively:

$$X_1 = R_1 \cos\bar{\phi}_0 \cos\lambda_0$$

$$Y_1 = R_1 \cos\bar{\phi}_0 \sin\lambda_0$$

$$Z_1 = R_1 \sin\bar{\phi}_0 \qquad (3.22\text{-a})$$

and

$$X_2 = R_2 \cos\bar{\phi}_0 \cos\lambda_0$$

$$Y_2 = R_2 \cos\bar{\phi}_0 \sin\lambda_0$$

$$Z_2 = R_2 \sin\bar{\phi}_0 \qquad (3.22\text{-b})$$

Differentiating (3.16), and taking (3.21-a,b) into account we obtain the following expressions for the three components of the gravity disturbance vector P , as computed from the two masses:

$$\left(\frac{\partial T}{\partial X}\right)_P = -\frac{km_1(X-X_1)}{[(X-X_1)^2+(Y-Y_1)^2+(Z-Z_1)^2]^{3/2}} - \frac{km_2(X-X_2)}{[(X-X_2)^2+(Y-Y_2)^2+(Z-Z_2)]^{3/2}} \qquad (3.23\text{-a})$$

$$\left(\frac{\partial T}{\partial Y}\right)_P = -\frac{km_1(Y-Y_1)}{[(X-X_1)^2+(Y-Y_1)^2+(Z-Z_1)^2]^{3/2}} - \frac{km_2(Y-Y_2)}{[(X-X_2)^2+(Y-Y_2)^2+(Z-Z_2)^2]^{3/2}} \qquad (3.23\text{-b})$$

$$\left(\frac{\partial T}{\partial Z}\right)_P = -\frac{km_1(Z-Z_1)}{[(X-X_1)^2+(Y-Y_1)^2+(Z-Z_1)^2]^{3/2}} - \frac{km_2(Z-Z_2)}{[(X-X_2)^2+(Y-Y_2)^2+(Z-Z_2)^2]^{3/2}} \qquad (3.23\text{-c})$$

Equations (3.23) yield the three components directly from the model, and therefore these results are errorless. In the next chapter we will discuss the simulations tests we made in order to investigate how well equations (2.68-a, b,c) agree with the exact equations (3.23) in the case of the model, without integrating over the whole surface of the sphere.

3.5 The Effect of the Model's Symmetry and Center of Mass on the Simulations

The terrain model described above is rotationally symmetric, and the two point masses located on its axis obviously generate on its surface a disturbing field (δg and T), which is symmetric too. For the simulations which are described in the following chapters, four such models are used, and the seven parameters for each one of them are given in table 3.1 (these parameters were defined in sections 3.2 and 3.3).

Table 3.1

Parameters Defining the Models for the Simulations

	i=10°.543 inclination Model	i=20°.040 inclination Model	i=39°.976 inclination Model	Spherical Cap Model
h_A	4100 m	4100 m	4100 m	23682973.2 m
Ω	12'	6.08'	2.64'	45°
ρ	200 m	200 m	200 m	4975838.5 m
a_1	2000 m	2000 m	2000 m	2000 m
a_2	4000 m	4000 m	4000 m	4000 m
δg_1	50 mgal	50 mgal	50 mgal	50 mgal
δg_2	100 mgal	100 mgal	100 mgal	100 mgal

Note: The inclinations are computed from equation (3.3). The three conical models will be referred to as 10°-, 20°-, and 40°- inclination models.

Note that the large values for h_A and ρ in the list of parameters for the spherical cap model, were selected such that equation (3.4) will yield a height h_V of the model's vertes V above the mean sphere R (figure 2.1) equal to 4099.8 meters, i.e. of the same magnitude as the heights of the conical models. The last four parameters are the same for all models, and hence, there is a total gravity disturbance of 150 mgal at the vertices of the models. In figure 3.2 through 3.5 the gravity disturbances and the disturbing potentials are plotted against the spherical distance of the surface points from the model's axis. The elevation of the surface points above the mean-earth sphere R are also given at 2-km intervals.

In the derivation of equations (2.68) following the Green's approach (chapter 2), no assumption was made about the location of the earth's center of mass with respect to the origin of the (X,Y,Z) coordinate system. The origin O of this system was placed at the earth's geocenter (see figure 2.1), but there is no theoretical requirement for such a choice. The transformation equation (2.59) from the (x,y,z) system to the $(\bar{X},\bar{Y},\bar{Z})$ system has been derived by using a "geocentric" (X,Y,Z) system whose origin does not have to coincide with the true center of mass of the earth. In other words, there will be no effect of the model's center of mass on our simulation tests with the Green's approach. As long as we have the boundary values δg and T on the surface of the earth, and the elevations / inclinations with respect to a reference surface (the surface of the mean-earth sphere in our case), equation (2.68) can be used to evaluate the components $\partial T/\partial\bar{X}$, $\partial T/\partial\bar{Y}$, $\partial T/\partial\bar{Z}$ in the topocentric $(\bar{X},\bar{Y},\bar{Z})$ system centered at the space point P .

The rotation from this system to the "geocentric" (X,Y,Z) system may be done in order to express all vectors $\vec{\delta}$ in a unique system.

It must be pointed-out that due to the symmetric characteristics of the models, there are only two distinct components of the gravity disturbance vectors $\vec{\delta} = \text{grad}T$, namely $\partial T/\partial r$, and $(1/r)\ \partial T/\partial \psi$, where ψ is the angle between the model's axis and the radius to the space point P where $\vec{\delta}$ is computed. On the other hand, we decided to derive the equations for the computation of $\vec{\delta}$ in such a way that theycan be used without modification, or re-derivation for a future application with real-data (when this kind of information becomes available). This is why we have expressed the components of $\vec{\delta}$ (equation 2.68) not in a polar (r, ψ) system, but in a cartesian one. Nevertheless, the transformation of these components from the cartesian to the polar coordinate systems can be easily done, using (2.73), and then:

$$\begin{vmatrix} \frac{\partial T}{\partial r} \\ \frac{\partial T}{\partial \phi} \\ \frac{\partial T}{\partial \lambda} \end{vmatrix} = J\left(\frac{(X,Y,Z)}{(r,\bar{\phi},\lambda)}\right) \begin{vmatrix} \frac{\partial T}{\partial X} \\ \frac{\partial T}{\partial Y} \\ \frac{\partial T}{\partial Z} \end{vmatrix} \qquad (3.24)$$

Finally, the component $(1/r)\ \partial T/\partial \psi$ is computed from the components $\partial T/\partial \phi$, and $\partial T/\partial \lambda$ as:

$$\frac{1}{r}\ \frac{\partial T}{\partial \psi} = -\frac{1}{r}\left[\left(\frac{\partial T}{\partial \bar{\phi}}\right)^2 + \left(\frac{\partial T}{\partial \lambda}\right)^2\right]^{\frac{1}{2}} \qquad (3.25)$$

The direction of this component is defined from the space point P to the point on the model's axis where the plane perpendicular to the radius r at P interjects the axis.

The Jacobian of the transformation from (X,Y,Z) to $(r, \bar{\phi}, \lambda)$ can be computed from the transformation equations between these two systems:

$$\begin{aligned} X &= r \cos \bar{\phi} \cos \lambda \\ Y &= r \cos \bar{\phi} \sin \lambda \\ Z &= r \sin \bar{\phi} \end{aligned} \qquad (3.26)$$

and then:

$$J\left(\frac{(X,Y,Z)}{(r,\bar{\phi},\lambda)}\right) = \begin{vmatrix} \cos\bar{\phi}\cos\lambda & \cos\bar{\phi}\sin\lambda & \sin\bar{\phi} \\ -r\sin\bar{\phi}\cos\lambda & -r\sin\bar{\phi}\sin\lambda & r\cos\bar{\phi} \\ -r\cos\bar{\phi}\sin\lambda & r\cos\bar{\phi}\cos\lambda & 0 \end{vmatrix} \tag{3.27}$$

For the simulation tests which are described in the following chapters, the components of $\vec{\delta}$ will be compared to the exact components (from the model) in the polar (r, ψ) coordinate system, in order to have results independent of the location $(\bar{\phi}_0 , \lambda_0)$ of the model's center on the sphere R . In summary, these components will be transformed from the topocentric $(\bar{X},\bar{Y},\bar{Z})$ system to the polar system (r, ψ) using equations (2.73), (3.24), and (3.25).

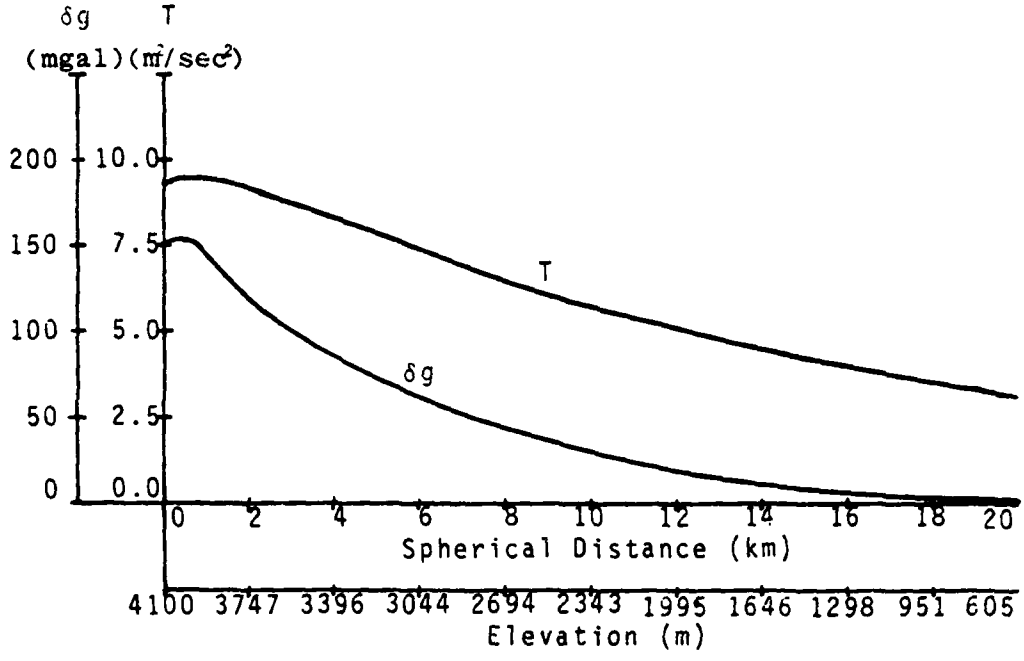

Figure 3.2: Simulation Data on the Surface of a 10°-Inclination Conical Model

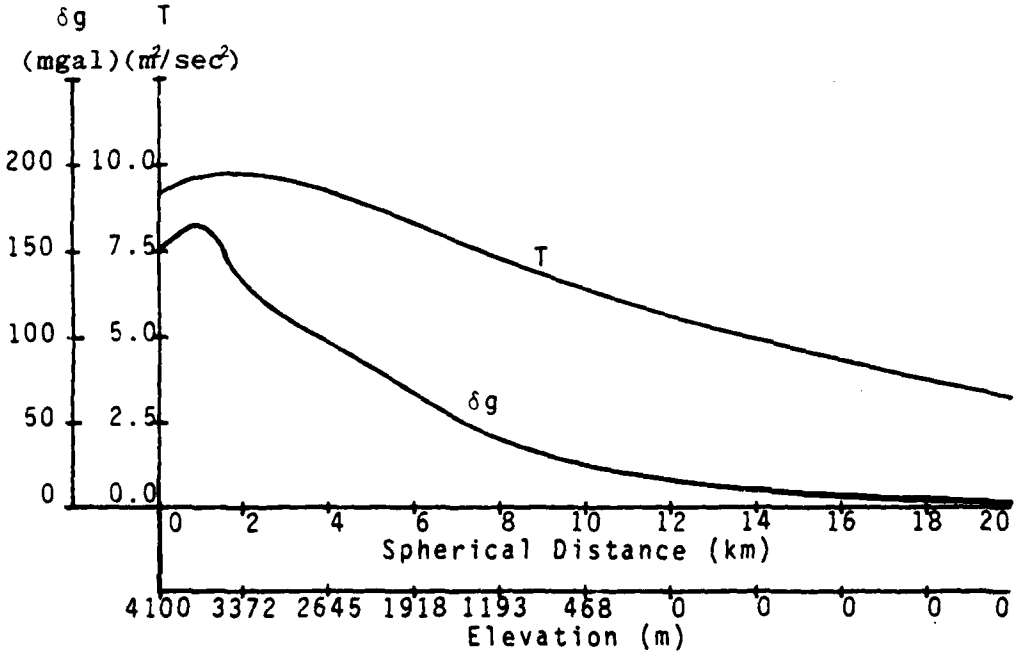

Figure 3.3: Simulation Data on the Surface of a 20°-Inclination Conical Model

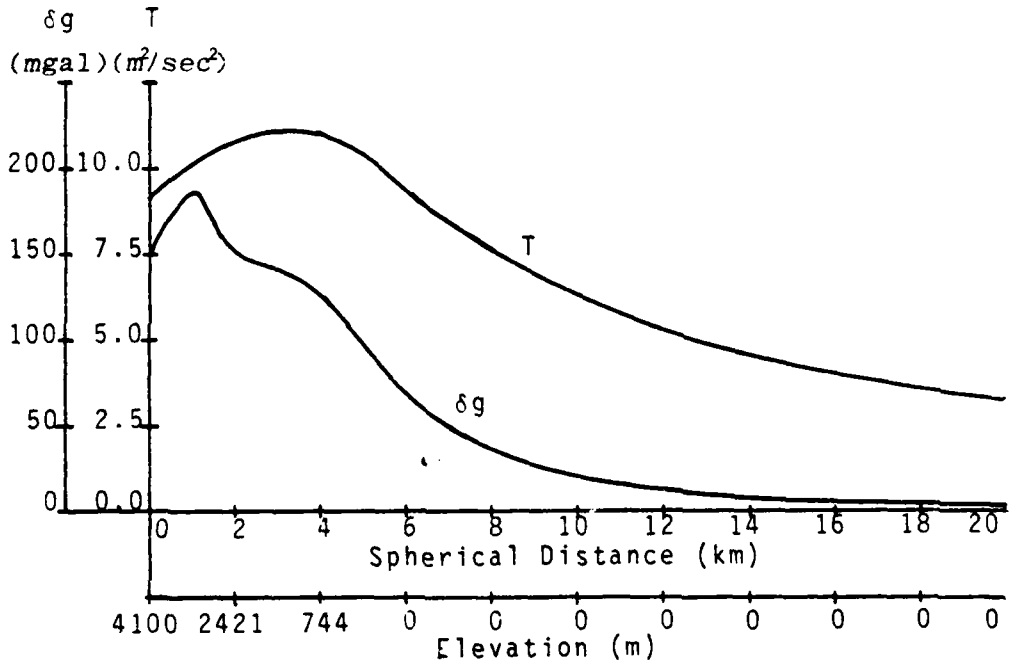

Figure 3.4: Simulation Data on the Surface of a 40°-Inclination Conical Model

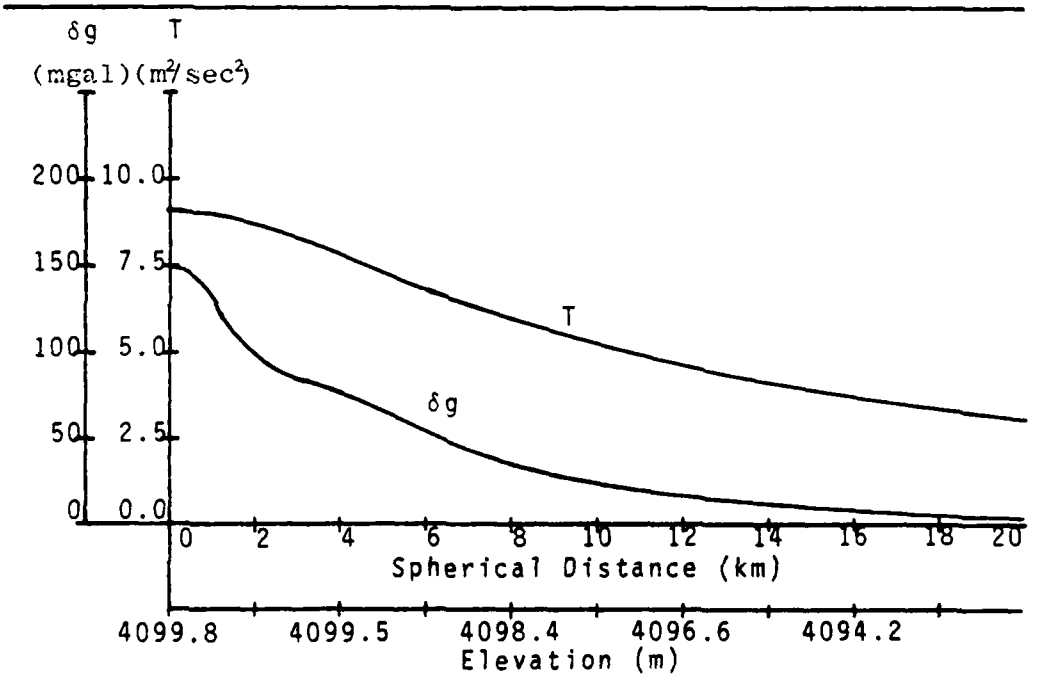

Figure 3.5: Simulation Data on the Surface of a Spherical Cap Model

Chapter 4

SIMULATION TESTS WITH THE GREEN'S APPROACH

4.1 Introduction

The idea of the simulation is to compare the exact gravity vectors as computed from the model, with those evaluated from Green's approach, using surface data also computed from the model.

There is a number of factors that will affect this agreement. The inclination of the model's surface, the altitude of the space point, the "density" of the observations, or in other words the grid interval, the extent of the area of integration, and the geometry of the model itself (size and shape), are among these factors. Throughout this chapter we will discuss the simulations that were done to investigate the effect of these factors on the agreement between the exact and the computed vectors. Each simulation is a four-step procedure, summarized as follows:

Step-1. Compute the exact components of the gravity disturbance vector, using equations (3.23), (3.24), and (3.25).

Step-2. Compute the normal gravity disturbance component δg and the disturbing potential T on the surface of the model and everywhere else within the specified area (at the center of the blocks which are formed from the specified grid). Equations (3.18) and (3.16) are used.

Step-3. Compute the components of the gravity disturbance vector at the space point P, in the $(\bar{X},\bar{Y},\bar{Z})$ coordinate system from (2.68-a,b,c), and the data generated from step 2. Then, rotate these three components to the geocentric (X,Y,Z) system using (2.73). Finally, compute the radial and the horizontal components of $\vec{\delta}$ in the polar (r, ψ) system using (3.24), and (3.25).

Step-4. Compare the gravity disturbance components from steps 1 and 3 in terms of their percentage relative difference:

$$\% \text{ rel. error in } \partial T/\partial r = \left| \frac{(\frac{\partial T}{\partial r})_{exact} - (\frac{\partial T}{\partial r})_{computed}}{(\frac{\partial T}{\partial r})_{exact}} \right| \times 100$$

$$\% \text{ rel. error in } \frac{1}{r}\frac{\partial T}{\partial \psi} = \left| \frac{\frac{1}{r}(\frac{\partial T}{\partial \psi})_{exact} - \frac{1}{r}(\frac{\partial T}{\partial \psi})_{computed}}{(\frac{\partial T}{\partial \psi})_{exact}} \right| \times 100 \qquad (4.1)$$

Assume that the cone-like terrain model is located on the surface of the earth (more specifically, on the surface of the mean sphere R), with its axis intersecting R at the point $(\bar{\phi}_0 , \lambda_0)$. The parameters which define the three conical models are listed in table 3.1.

In order to apply (2.68-a,b,c) in the case of the conical model, we divide the sphere below the model into blocks which are bounded by meridians and parallels. The grid spacing determines the density of the data. The radii passing through the intersections of the grid, form on the surface of the model another grid(see figure 4.1). If Q' is the center of the block on the sphere, the radius through Q' intersects the surface at the point Q . Equations (3.16) and (3.18) yield the disturbing potential T and the gravity disturbance δg at Q . Depending on the location of the block on the model (on the spherical cap, on the conical surface, or on the sphere), equations (3.8), (3.14), or (3.15) are used to compute the height of Q above the mean sphere. The inclinations τ_x and τ_y in the north-south, and west-east directions at Q , are computed using the height of Q and the heights of the neighboring blocks to the north, and to the west of Q , according to equations below:

$$\tan\tau_x = \frac{h_{north} - h}{s_x}$$

$$\tan\tau_y = \frac{h_{west} - h}{s_y} \qquad (4.2)$$

where h : the height at the center (Q) of the block, where the inclinations are to be determined.

h_{north}, h_{west} : the heights at the centers of the blocks to the north, and to the west of Q .

s_x , s_y : the distances from the centers of the blocks to the north and to the west of Q , from it.

The disturbing potential T , the gravity disturbance δg , and the two components of the inclination (τ_x , τ_y) are the data needed in equations (2.68), along with the coordinates

of the surface points Q . These equations yield the three components of the vector at the space point P in the $(\bar{X}, \bar{Y}, \bar{Z})$ system located at P , and (2.73) rotates them to the geocentric (X,Y,Z) system. Then, (3.24) and (3.25) yield the two distinct components of $\vec{\delta}$ in the polar (r, ψ) system. The exact and the computed vectors are finally compared in terms of their percentage differences from equations (4.1). For the investigation of the effect of the height (h_p) of the space point P , these vectors are computed at different altitudes, at equally-spaced points above the sphere, from the model's axis to the east of the model.

4.2 Simulation Tests

A number of tests were made to investigate the influence of the following parameters on the accuracy of the computed gravity vector components:

a. The inclination of the model.
b. The geometry of the model (cone vs. sphere).
c. The grid interval.
d. The size of the integration area, which, along with the grid interval determines the "density" of the data. Note that the center of the integration area coincides with the center of the model.
e. The altitude of the space point.

For all of these tests we assumed that the model's axis is located at

$$\bar{\phi}_0 = 45^\circ \ , \ \lambda_0 = 250^\circ$$

This choice is arbitrary, but since our software was designed for real as well as for simulated data, we had to select a "site" for the model in terms of latitude and longitude. In table 4.1 the specifications of 15 tests are summarized for easy comparison. The space points are 10' apart from each other, at the same altitude for each test, from 250° to 251° east longitude. Therefore, there are seven points where the components of $\vec{\delta}$ are computed and compared for each test.

The first five tests are referred to a conical model whose inclination is 10°. From tables 4.2 through 4.4 we see that by increasing the integration area from 2°x 2° to 3°x 3°, and then to 8°x 8°, the errors at the distant space points (away from the model) are reduced dramatically, but the errors above the model are almost the same. Larger integration areas do not improve the results above the model because of the local characteristic of the disturbing potential

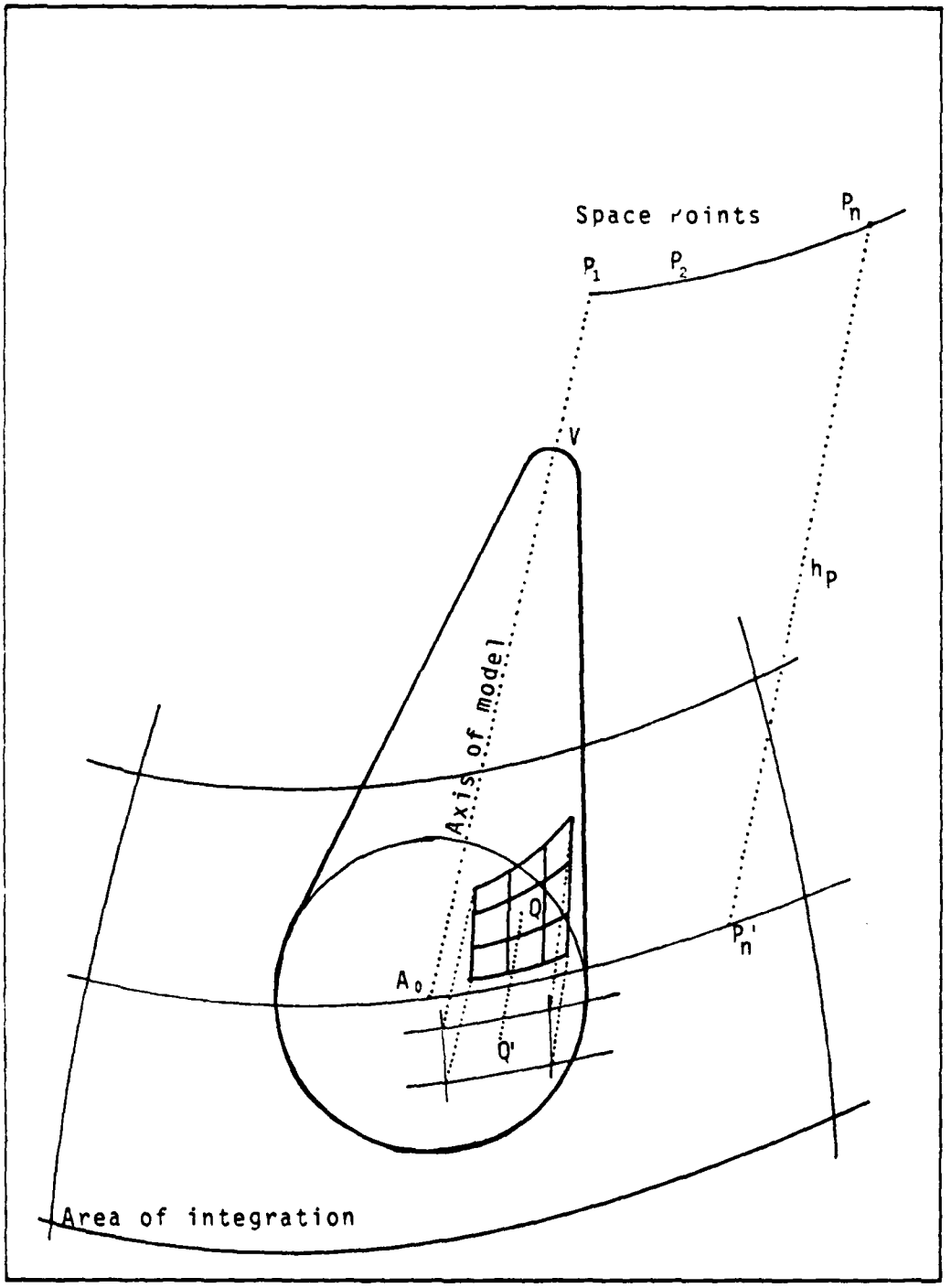

Figure 4.1: The Surface Grid on the Model

Table 4.1

Description of the Tests with the Model Topography (Green's Approach)

Test	Inclination	Elevation*	Area of Integration	Grid Interval	Number of blocks	Table
1	10°.543	10 km	2°x 2°	2'	3600	4.2
2	10°.543	10 km	3°x 3°	2'	8100	4.3
3	10°.543	10 km	8°x 8°	2'	57600	4.4
4	10°.543	20 km	2°x 2°	2'	3600	4.5
5	10°.543	10 km	4°x 4°	1'	57600	4.6
6	20°.040	10 km	4°x 4°	1'	57600	4.7
7	20°.040	10 km	inner:0°.3 x 0°.3 outer:4° x 4°	0'.5 1'	1296 57276	4.8
8	20°.040	10 km	inner:0°.3 x 0°.3 outer:4° x 4°	0'.1 1'	32400 57276	4.9
9	20°.040	100 km	4°x 4°	1'	57600	4.10
10	39°.976	10 km	4°x 4°	1'	57600	4.11
11	spherical cap	10 km	8°x 8°	2'	57600	4.12
12	10°.543	5 km	0°.4x 0°.4	1'	576	4.13
13	10°.543	10 km	0°.4x 0°.4	1'	576	4.14
14	10°.543	20 km	0°.4x 0°.4	1'	576	4.15
15	10°.543	100 km	0°.4x 0°.4	1'	576	4.16

*Note: Elevation of the space point above the mean-earth sphere (R =6371 km).

of the two masses at its center. However for the distant points, larger integration area is required such that there is enough gravity data below these points.

By increasing the altitude of the space points from 10 km to 20 km, the errors are reduced both over the model, and at the distant points (table 4.2 vs 4.5). From tables 4.6 and 4.7 we see that the errors for a 10°-inclination are slightly smaller over the cone than the errors for a 20°-inclination. Tests 6 through 9 are referred to a 20°-inclination model.

All the results indicate clearly that the errors above the model are larger than the errors at the distant points. Originally, we thought that the reason might be that we should have used a finer grid over the model, than over the neighboring area on the sphere, because of the fact that most of the disturbing field is close to the model's masses. However, by using 0.5' grid in the inner 0°.3x0°.3 area, rather than a 1'-grid (table 4.7, vs. 4.8) throughout the entire 4°x 4° area, we did not see any improvement in the results. The errors were not significantly reduced neither with more fine 0.1'-grid in the inner zone (table 4.7, vs. 4.9).

For an altitude of 100 km above the mean sphere (table 4.10), the errors in both components are smaller than 5%, that is much smaller than the corresponding errors at an altitude 10 km (table 4.7).

On table 4.11 we see the errors for a 40°-inclination model. If we compare these errors with those on table 4.7 (20°-inclination), we see that they are much smaller. This is probably due to the fact that a 40°-model has a more "local" effect on the gravity vector, than a 20°-model. The inclinations τ_x and τ_y for the 40°-model are larger as compared to those on a 20°-model, but for a smaller geographical extent.

In order to further investigate the errors from a very smooth-topography-model, we substituted the conical model by the spherical model, whose parameters are listed in table 3.1. These parameters imply a height of the model's vertex V above the mean-earth sphere R :

$$h_V = 4099.8 \text{ meters}$$

which is of the same magnitude as the height of the vertices of the conical models. In other words, the topography is now a sphere of radius ρ , at 4.1 km above R . From table

4.12 we can see that the errors are now very small. The components of the gravity disturbance vector are computed from the surface data on the sphere ρ, with an error which is smaller than 1%. These results clearly indicate that the Green's approach works very well for a smooth topography.

From the eleven tests just described, we can draw the following general conclusions:

1. The higher the space point, the smaller the relative errors of the components of $\vec{\delta}$ become.
2. The errors are larger over the model, then over the distant zones.
3. For a given grid spacing, and for a fixed altitude, the increase of the integration area does not improve the results over the model.
4. The use of a finer grid in the inner zone (0'.5, or 0'.1 vs. 1'-grid), does not improve the results over the model.
5. The errors are very small for a smooth topography (the case of a spherical cap), or for a very large but local topographic feature (the case of a 40°-inclination cone).

Because of the very local characteristics of the models, there are no truncation errors (i.e. errors caused by neglecting the information outside of the working area). In addition, there are no errors in the surface data, since both δg and T are rigorously computed from the model.

The only factors that affect the results, and cause the errors in the computed vectors, are the following:

1. The approximation of the integral equations by finite summations, and evaluations of the kernels at the center point of the elementary areas.
2. The neglect of the second-order variations of the topography (see equation (2.43)).

These factors are responsible for the larger errors right above the models, as compared to the errors far away from the model, or to the errors from the very smooth topography of the spherical cap model.. However, as we will see in chapter 8, the errors from the classical approach (the direct integration method), where the topography is neglected, are larger by a factor of 2 than the errors from the Green's approach, indicating the significant improvement of the later method in the computation of $\vec{\delta}$.

The last four tests in table 4.1 are applications of the Green's approach with a very limited amount of data on the surface of the model. These tests will be used for comparison purposes with the Dirac approach in chapter 6. Only 576

blocks have been formed on a 1'-grid within a 0°.4x0°.4 area on a 10°-inclination cone. The components of $\frac{T}{\delta}$ are computed at 5, 10, 20, and 100 km above the sphere R . Note how large the errors are at a 5-km altitude (table 4.13). Also, comparing table 4.6 with 4.14, we see that at 10 km the errors are of the same order of magnitude, indicating once more that the effect of truncation is not significant (for these two tests, only the size of area is different).

4.3 Related Work, and Comparison with Koch's Method

Among the papers which have been published on the computation of certain components of the gravity disturbance vector using the Green's third identity, the most elegant approach in our opinion is the one by Koch (1968-a). Therefore, it is essential to comment on the similarities and on the differences between his and our approaches, and to discuss his results under the light of ours.

Koch's approach is a simulation study with a cone-like model as in our case, but the solution for the disturbing potential and its partial derivatives is obtained through an iterative procedure. In addition, the computed quantities are surface quantities, and not at space points. Furthermore, his equations have been derived specifically for the simulation studies that he performed, and allow for the maximum inclination of the cone (β) only (not a two-component τ_x , τ_y description of the topography). Therefore, his equations cannot be used for a real-world application without additional work. Also, the whole approach is based on a planar approximation.

The large errors that were found by Koch in the case of inclinations larger than 20°, we believe that are due to the fact that the term $T(P_0)$ is included in his integral equation (21), while the integration is not carried out over the whole surface of the earth (according to the discussion below our equation (2.9')). In addition, the fact that Koch's equations were derived for computations of the derivatives of T on the surface of the earth only, does not permit comparison of our results with his.

Table 4.2: Comparison of Gravity Disturbance Vector Components in Space Computed Rigorously, and From Integration Procedures Using the Green's Identity (values in mgal; height in meters)

Region Size (Degrees): 2.00 x 2.00
Grid Interval (Minutes): 2.0

Inclination (Degrees): 10.543

LAT	LON	HEIGHT	EXACT: RADIAL	EXACT: HORIZ	COMPUTED: RADIAL	COMPUTED: HORIZ	DIFFERENCES: RADIAL	DIFFERENCES: HORIZ	PERCENTAGE DIF RADIAL	PERCENTAGE DIF HORIZ
45	250 0'	10000.	-36.89	0.0	-30.38	-2.54	-6.52	2.54	17.66	*******
45	250 10'	10000.	-13.52	-9.17	-11.11	-7.58	-2.40	-1.59	17.79	17.34
45	250 20'	10000.	-3.59	-4.83	-3.52	-4.12	-0.08	-0.71	2.10	14.74
45	250 30'	10000.	-1.30	-2.60	-1.45	-2.36	0.15	-0.24	11.52	9.12
45	250 40'	10000.	-0.60	-1.57	-0.87	-1.51	0.28	-0.06	46.40	3.97
45	250 50'	10000.	-0.32	-1.04	-0.76	-1.24	0.44	0.20	138.27	18.83
45	251 0'	10000.	-0.19	-0.74	0.06	-1.50	-0.25	0.76	134.03	102.87

Table 4.3: Comparison of Gravity Disturbance Vector Components in Space Computed Rigorously, and From Integration Procedures Using the Green's Identity (values in mgal; height in meters)

Region Size (Degrees): 3.00 x 3.00
Grid Interval (Minutes): 2.0

Inclination (Degrees): 10.543

LAT	LON	HEIGHT	EXACT: RADIAL	EXACT: HORIZ	COMPUTED: RADIAL	COMPUTED: HORIZ	DIFFERENCES: RADIAL	DIFFERENCES: HORIZ	PERCENTAGE DIF RADIAL	PERCENTAGE DIF HORIZ
45	250 0'	10000.	-36.89	0.0	-30.24	-2.54	-6.66	2.54	18.04	*******
45	250 10'	10000.	-13.52	-9.17	-10.99	-7.57	-2.53	-1.60	18.68	17.48
45	250 20'	10000.	-3.59	-4.83	-3.41	-4.10	-0.19	-0.72	5.22	15.00
45	250 30'	10000.	-1.30	-2.60	-1.30	-2.33	0.00	-0.27	0.34	10.37
45	250 40'	10000.	-0.60	-1.57	-0.65	-1.43	0.06	-0.14	9.93	9.19
45	250 50'	10000.	-0.32	-1.04	-0.42	-0.96	0.10	-0.09	30.93	8.30
45	251 0'	10000.	-0.19	-0.74	-0.33	-0.70	0.14	-0.04	75.37	5.31

Table 4.4: Comparison of Gravity Disturbance Vector Components in Space Computed Rigorously, and From Integration Procedures Using the Green's Identity (values in mgal; height in meters)

Region Size (Degrees: 8.00 x 8.00
Grid Interval (Minutes): 2.0

Inclination (Degrees): 10.543

LAT	LON	HEIGHT	EXACT: RADIAL	EXACT: HORIZ	COMPUTED: RADIAL	COMPUTED: HORIZ	DIFFERENCES: RADIAL	DIFFERENCES: HORIZ	PERCENTAGE DIF RADIAL	PERCENTAGE DIF HORIZ
45	250 0'	10000.	-36.89	0.0	-30.23	-2.54	-6.66	2.54	18.06	*******
45	250 10'	10000.	-13.52	-9.17	-10.95	-7.58	-2.56	-1.59	18.96	17.37
45	250 20'	10000.	-3.59	-4.83	-3.33	-4.10	-0.26	-0.73	7.20	15.10
45	250 30'	10000.	-1.30	-2.60	-1.22	-2.32	-0.08	-0.28	5.86	10.66
45	250 40'	10000.	-0.60	-1.57	-0.56	-1.42	-0.04	-0.15	5.91	9.81
45	250 50'	10000.	-0.32	-1.04	-0.31	-0.95	-0.01	-0.10	3.87	9.46
45	251 0'	10000.	-0.19	-0.74	-0.19	-0.67	-0.00	-0.07	1.11	9.40

Table 4.5: Comparison of Gravity Disturbance Vector Components in Space Computed Rigorously, and From Integration Procedures Using the Green's Identity (values in mgal; height in meters)

Region Size (Degrees): 2.00 x 2.00
Grid Interval (Minutes): 2.0

Inclination (Degrees): 10.543

LAT	LON	HEIGHT	EXACT: RADIAL	EXACT: HORIZ	COMPUTED: RADIAL	COMPUTED: HORIZ	DIFFERENCES: RADIAL	DIFFERENCES: HORIZ	PERCENTAGE DIF RADIAL	PERCENTAGE DIF HORIZ
45	250 0'	20000.	-12.07	0.0	-10.51	-0.31	-1.56	0.31	12.92	*******
45	250 10'	20000.	-8.06	-3.15	-7.02	-2.73	-1.04	-0.43	12.88	13.53
45	250 20'	20000.	-3.63	-2.63	-3.38	-2.47	-0.25	-0.35	6.79	12.52
45	250 30'	20000.	-1.66	-1.94	-1.70	-1.78	0.04	-0.16	2.49	8.25
45	250 40'	20000.	-0.85	-1.31	-0.99	-1.31	0.14	-0.01	16.02	0.43
45	250 50'	20000.	-0.48	-0.92	-0.61	-1.10	0.13	0.17	26.57	18.67
45	251 0'	20000.	-0.30	-0.68	-0.13	-0.97	-0.17	0.30	57.60	43.62

Table 4.6: Comparison of Gravity Disturbance Vector Components in Space Computed Rigorously, and From Integration Procedures Using the Green's Identity (values in mgal; height in meters)

Region Size (Degrees): 4.00 x 4.00
Grid Interval (Minutes): 1.0

Inclination (Degrees): 10.543

LAT	LON	HEIGHT	EXACT: RADIAL	EXACT: HORIZ	COMPUTED: RADIAL	COMPUTED: HORIZ	DIFFERENCES: RADIAL	DIFFERENCES: HORIZ	PERCENTAGE DIF RADIAL	PERCENTAGE DIF HORIZ
45	250 0'	10000.	-36.89	0.0	-29.98	-1.50	-6.91	1.50	18.73	*******
45	250 10'	10000.	-13.51	-9.17	-11.11	-7.61	-2.40	-1.56	17.75	16.99
45	250 20'	10000.	-3.60	-4.82	-3.33	-4.14	-0.26	-0.68	7.36	14.08
45	250 30'	10000.	-1.30	-2.60	-1.25	-2.33	-0.05	-0.27	3.84	10.35
45	250 40'	10000.	-0.59	-1.57	-0.60	-1.42	0.01	-0.15	1.65	9.79
45	250 50'	10000.	-0.32	-1.04	-0.35	-0.95	0.03	-0.10	10.48	9.41
45	251 0'	10000.	-0.19	-0.74	-0.24	-0.68	0.05	-0.06	25.73	8.56

Table 4.7: Comparison of Gravity Disturbance Vector Components in Space Computed Rigorously, and From Integration Procedures Using the Green's Identity (values in mgal; height in meters)

Region Size (Degrees): 4.00 x 4.00
Grid Interval (Minutes): 1.0

Inclination (Degrees): 20.040

LAT	LON	HEIGHT	EXACT: RADIAL	EXACT: HORIZ	COMPUTED: RADIAL	COMPUTED: HORIZ	DIFFERENCES: RADIAL	DIFFERENCES: HORIZ	PERCENTAGE DIF RADIAL	PERCENTAGE DIF HORIZ
45	250 0'	10000.	-36.75	0.0	-29.22	-2.64	-7.53	2.64	20.49	*******
45	250 10'	10000.	-13.51	-9.15	-11.91	-7.66	-1.60	-1.48	11.84	16.21
45	250 20'	10000.	-3.58	-4.81	-3.33	-4.34	-0.24	-0.47	6.81	9.75
45	250 30'	10000.	-1.29	-2.59	-1.24	-2.36	-0.05	-0.22	4.03	8.66
45	250 40'	10000.	-0.60	-1.57	-0.60	-1.43	0.00	-0.13	0.35	8.55
45	250 50'	10000.	-0.32	-1.04	-0.35	-0.95	0.03	-0.08	9.64	8.13
45	251 0'	10000.	-0.19	-0.74	-0.24	-0.68	0.05	-0.06	25.66	7.59

Table 4.8: Comparison of Gravity Disturbance Vector Components in Space Computed Rigorously, and From Integration Procedures Using the Green's Identity (values in mgal; height in meters)

Inner Region (Degrees): 0.30 x 0.30
Inner Grid (Minutes): 0.5
Outer Region (Degrees): 4.00 x 4.00
Outer Grid (Minutes): 1.0
Inclination (Degrees): 20.040

LAT	LON	HEIGHT	EXACT: RADIAL	EXACT: HORIZ	COMPUTED: RADIAL	COMPUTED: HORIZ	DIFFERENCES: RADIAL	DIFFERENCES: HORIZ	PERCENTAGE DIF RADIAL	PERCENTAGE DIF HORIZ
45	250 0'	10000.	-36.75	0.0	-28.90	-1.40	-7.85	1.40	21.37*******	
45	250 10'	10000.	-13.51	-9.15	-11.93	-7.75	-1.57	-1.40	11.66	15.29
45	250 20'	10000.	-3.58	-4.81	-3.32	-4.35	-0.25	-0.46	7.11	9.58
45	250 30'	10000.	-1.29	-2.59	-1.24	-2.37	-0.06	-0.22	4.56	8.49
45	250 40'	10000.	-0.60	-1.57	-0.60	-1.44	0.00	-0.13	0.06	8.13
45	250 50'	10000.	-0.32	-1.04	-0.35	-0.96	0.03	-0.08	8.71	7.51
45	251 0'	10000.	-0.19	-0.74	-0.24	-0.68	0.05	-0.06	24.82	7.53

Table 4.9: Comparison of Gravity Disturbance Vector Components in Space Computed Rigorously, and From Integration Procedures Using the Green's Identity (values in mgal; height in meters)

Inner Region (Degrees): 0.30 x 0.30
Inner Grid (Minutes): 0.1
Outer Region (Degrees): 4.00 x 4.00
Outer Grid (Minutes): 1.0
Inclination (Degrees): 20.040

LAT	LON	HEIGHT	EXACT: RADIAL	EXACT: HORIZ	COMPUTED: RADIAL	COMPUTED: HORIZ	DIFFERENCES: RADIAL	DIFFERENCES: HORIZ	PERCENTAGE DIF RADIAL	PERCENTAGE DIF HORIZ
45	250 0'	10000.	-36.75	0.0	-28.78	-0.23	-7.97	0.23	21.69*******	
45	250 10'	10000.	-13.51	-9.15	-12.01	-7.85	-1.50	-1.30	11.08	14.23
45	250 20'	10000.	-3.58	-4.81	-3.31	-4.36	-0.27	-0.45	7.42	9.41
45	250 30'	10000.	-1.29	-2.59	-1.24	-2.37	-0.06	-0.22	4.40	8.49
45	250 40'	10000.	-0.60	-1.57	-0.60	-1.44	0.00	-0.13	0.20	8.13
45	250 50'	10000.	-0.32	-1.04	-0.35	-0.96	0.03	-0.08	9.14	7.49
45	251 0'	10000.	-0.19	-0.74	-0.24	-0.68	0.05	-0.05	25.07	7.44

Table 4.10: Comparison of Gravity Disturbance Vector Components in Space Computed Rigorously, and From Integration Procedures Using the Green's Identity (values in mgal; height in meters)

Region Size (Degrees): 4.00 x 4.00
Grid Interval (Minutes): 1.0

Inclination (Degrees): 20.040

LAT	LON	HEIGHT	EXACT: RADIAL	EXACT: HORIZ	COMPUTED: RADIAL	COMPUTED: HORIZ	DIFFERENCES: RADIAL	DIFFERENCES: HORIZ	PERCENTAGE DIF RADIAL	PERCENTAGE DIF HORIZ
45	250 0'	100000.	-0.63	0.0	-0.60	-0.00	-0.03	0.00	4.68	*******
45	250 10'	100000.	-0.61	-0.05	-0.58	-0.05	-0.03	-0.00	4.62	4.52
45	250 20'	100000.	-0.57	-0.10	-0.55	-0.10	-0.02	-0.00	4.32	4.22
45	250 30'	100000.	-0.51	-0.14	-0.49	-0.13	-0.02	-0.01	4.05	3.83
45	250 40'	100000.	-0.45	-0.16	-0.43	-0.15	-0.02	-0.01	3.54	3.18
45	250 50'	100000.	-0.38	-0.17	-0.37	-0.17	-0.01	-0.00	2.60	1.90
45	251 0'	100000.	-0.32	-0.17	-0.31	-0.17	-0.01	0.00	2.32	0.11

Table 4.11: Comparison of Gravity Disturbance Vector Components in Space Computed Rigorously, and From Integration Procedures Using the Green's Identity (values in mgal; height in meters)

Region Size (Degrees): 4.00 x 4.00
Grid Interval (Minutes): 1.0

Inclination (Degrees): 39.976

LAT	LON	HEIGHT	EXACT: RADIAL	EXACT: HORIZ	COMPUTED: RADIAL	COMPUTED: HORIZ	DIFFERENCES: RADIAL	DIFFERENCES: HORIZ	PERCENTAGE DIF RADIAL	PERCENTAGE DIF HORIZ
45	250 0'	10000.	-36.23	0.0	-38.31	-2.84	2.08	2.84	5.74	*******
45	250 10'	10000.	-13.31	-9.02	-12.95	-9.10	-0.36	0.08	2.70	0.93
45	250 20'	10000.	-3.53	-4.74	-3.43	-4.68	-0.11	-0.06	3.08	1.34
45	250 30'	10000.	-1.28	-2.55	-1.26	-2.51	-0.02	-0.05	1.53	1.94
45	250 40'	10000.	-0.58	-1.55	-0.61	-1.52	0.02	-0.03	3.82	2.15
45	250 50'	10000.	-0.31	-1.03	-0.35	-1.01	0.04	-0.02	12.73	2.24
45	251 0'	10000.	-0.19	-0.73	-0.24	-0.71	0.05	-0.01	27.92	1.75

Table 4.12: Comparison of Gravity Disturbance Vector Components in Space Computed Rigorously, and From Integration Procedures Using the Green's Identity (values in mgal; height in meters)

Region Size (Degrees): 8.00 x 8.00
Grid Interval (Minutes): 2.0

Spherical Cap Model

LAT	LON	HEIGHT	EXACT: RADIAL	EXACT: HORIZ	COMPUTED: RADIAL	COMPUTED: HORIZ	DIFFERENCES: RADIAL	DIFFERENCES: HORIZ	PERCENTAGE DIF RADIAL	PERCENTAGE DIF HORIZ
45	250 0'	10000.	-36.89	0.0	-36.53	-0.04	-0.37	0.04	1.00*******	
45	250 10'	10000.	-13.52	-9.17	-13.49	-9.16	-0.02	-0.01	0.17	0.14
45	250 20'	10000.	-3.59	-4.83	-3.57	-4.82	-0.02	-0.01	0.50	0.24
45	250 30'	10000.	-1.30	-2.60	-1.29	-2.59	-0.01	-0.01	0.71	0.35
45	250 40'	10000.	-0.60	-1.57	-0.60	-1.57	0.00	-0.01	0.04	0.42
45	250 50'	10000.	-0.32	-1.04	-0.32	-1.04	0.00	-0.01	0.31	0.68
45	251 0'	10000.	-0.19	-0.74	-0.19	-0.74	0.00	-0.00	1.25	0.36

Table 4.13: Comparison of Gravity Disturbance Vector Components in Space Computed Rigorously, and From Integration Procedures Using the Green's Identity (values in mgal; height in meters)

Region Size (Degrees): 0.40 x 0.40
Grid Interval (Minutes): 1.0

Inclination (Degrees): 10.543

LAT	LON	HEIGHT	EXACT: RADIAL	EXACT: HORIZ	COMPUTED: RADIAL	COMPUTED: HORIZ	DIFFERENCES: RADIAL	DIFFERENCES: HORIZ	PERCENTAGE DIF RADIAL	PERCENTAGE DIF HORIZ
45	250 0'	5000.	-105.36	0.0	34.26	-10.55	-139.62	10.55	132.52*******	
45	250 2'	5000.	-82.06	-21.19	-22.78	-12.11	-59.28	-9.08	72.24	42.84
45	250 4'	5000.	-55.21	-25.21	-40.43	-19.17	-14.79	-6.04	26.78	23.96
45	250 6'	5000.	-35.67	-23.38	-31.81	-19.94	-3.86	-3.44	10.83	14.73
45	250 8'	5000.	-22.93	-19.64	-23.34	-18.82	0.41	-0.82	1.77	4.17
45	250 10'	5000.	-14.98	-15.93	-16.74	-19.11	1.76	3.18	11.75	19.95
45	250 12'	5000.	-10.10	-12.87	-5.21	-19.89	-4.90	7.02	48.48	54.55

Figure 4.14: Comparison of Gravity Disturbance Vector Components in Space Computed Rigorously, and From Integration Procedures Using the Green's Identity (values in mgal; height in meters)

Region Size (Degrees): 0.40 x 0.40
Grid Interval (Minutes): 1.0

Inclination (Degrees): 10.543

LAT	LON	HEIGHT	EXACT: RADIAL	EXACT: HORIZ	COMPUTED: RADIAL	COMPUTED: HORIZ	DIFFERENCES: RADIAL	DIFFERENCES: HORIZ	PERCENTAGE DIF RADIAL	PERCENTAGE DIF HORIZ
45	250 0'	10000.	-36.89	0.0	-32.52	-1.50	-4.37	1.50	11.84*******	
45	250 2'	10000.	-34.66	-4.88	-30.39	-4.87	-4.27	-0.01	12.33	0.22
45	250 4'	10000.	-29.48	-8.21	-26.13	-7.73	-3.36	-0.48	11.38	5.83
45	250 6'	10000.	-23.43	-9.66	-21.20	-9.47	-2.24	-0.19	9.54	1.93
45	250 8'	10000.	-17.93	-9.78	-16.24	-10.29	-1.69	0.52	9.43	5.31
45	250 10'	10000.	-13.51	-9.17	-11.43	-10.39	-2.09	1.22	15.44	13.36
45	250 12'	10000.	-10.15	-8.24	-6.91	-9.79	-3.24	1.55	31.89	18.81

Figure 4.15: Comparison of Gravity Disturbance Vector Components in Space Computed Rigorously, and From Integration Procedures Using the Green's Identity (values in mgal; height in meters)

Region Size (Degrees): 0.40 x 0.40
Grid Interval (Minutes): 1.0

Inclination (Degrees): 10.543

LAT	LON	HEIGHT	EXACT: RADIAL	EXACT: HORIZ	COMPUTED: RADIAL	COMPUTED: HORIZ	DIFFERENCES: RADIAL	DIFFERENCES: HORIZ	PERCENTAGE DIF: RADIAL	PERCENTAGE DIF: HORIZ
45	250 0'	20000.	-12.06	0.0	-10.79	-0.16	-1.27	0.16	10.57	*******
45	250 2'	20000.	-11.84	-0.93	-10.54	-1.03	-1.30	0.10	11.01	10.65
45	250 4'	20000.	-11.21	-1.76	-9.87	-1.90	-1.34	0.14	11.96	8.05
45	250 6'	20000.	-10.29	-2.42	-8.89	-2.60	-1.40	0.18	13.61	7.45
45	250 8'	20000.	-9.19	-2.88	-7.70	-3.10	-1.50	0.22	16.27	7.77
45	250 10'	20000.	-8.05	-3.15	-6.42	-3.39	-1.63	0.24	20.26	7.47
45	250 12'	20000.	-6.95	-3.26	-5.16	-3.46	-1.79	0.20	25.82	6.19

Table 4.16: Comparison of Gravity Disturbance Vector Components in Space Computed Rigorously, and From Integration Procedures Using the Green's Identity (values in mgal; height in meters)

Region Size (Degrees): 0.40 x 0.40
Grid Interval (Minutes): 1.0

Inclination (Degrees): 10.543

LAT	LON	HEIGHT	EXACT: RADIAL	EXACT: HORIZ	COMPUTED: RADIAL	COMPUTED: HORIZ	DIFFERENCES: RADIAL	DIFFERENCES: HORIZ	PERCENTAGE DIF: RADIAL	PERCENTAGE DIF: HORIZ
45	250 0'	100000.	-0.63	0.0	-0.33	-0.00	-0.30	0.00	48.20	*******
45	250 2'	100000.	-0.63	-0.01	-0.33	-0.01	-0.30	-0.00	48.17	35.67
45	250 4'	100000.	-0.63	-0.02	-0.32	-0.01	-0.30	-0.01	48.18	36.80
45	250 6'	100000.	-0.62	-0.03	-0.32	-0.02	-0.30	-0.01	48.37	36.65
45	250 8'	100000.	-0.62	-0.04	-0.32	-0.03	-0.30	-0.02	48.49	37.29
45	250 10'	100000.	-0.61	-0.05	-0.32	-0.03	-0.30	-0.02	48.66	37.44
45	250 12'	100000.	-0.61	-0.07	-0.31	-0.04	-0.30	-0.02	48.09	37.79

Chapter 5

DISCRETE APPROACHES FOR THE COMPUTATION OF THE GRAVITY DISTURBANCE VECTOR IN SPACE

5.1 Introduction

Throughout the three previous chapters, we developed and tested the equations for the computation of the components of the gravity disturbance vector at a space point. The described solution is based on the application of Green's third identity, the data being given on the physical surface of the earth. Hence, the method follows the modern approach for the solution of the boundary value problem for the determination of the external gravity field of the earth. Both, the coventional solution to the geodetic BVP (using the Stokes' integral), and the modern solution to the geodetic BVP (following Molodensky), require the data be given as mean values over small surface elements. Furthermore, the conventional approach requires gravity reduction to the geoid, a process which assumes knowledge of the earth's densities, while Molodensky's solution does not require any reductions.

In practice, gravity measurements are taken at a finite number of stations only. The need to solve the BVP in space from a finite number of gravity observations, let Bjerhammar to develop some methods (documented in a number of papers which are referenced below), in general called discrete approaches to the solution of the BVP of physical Geodesy.

The formal statement by Bjerhammar (1963) reads as follows:

> "A finite number of gravity data (Δg) is given for a non-spherical surface, and it is required to find such a solution that the boundary values for the gravity data are satisfied in all given points".

For a given finite set of gravity observations (or more specifically gravity anomalies which will be defined more precisely in the next section), there is always a fictitious field of gravity anomalies on an internal sphere that satisfies the given boundary values on the surface. This sphere is completely imbedded inside the earth, and appears in the literature under the names "Bjerhammar sphere", or "geosphere". Bjerhammar's methods are applications of the Poisson's integral equation and Stokes' formula (Bjerhammar, 1976, 1978; Sjöberg, 1978). Earlier solutions

considered the gravity anomalies on the geosphere as mean anomalies, but later solutions have been formulated on the basis that the reduced anomalies are point anomalies on the geosphere with no block size associated with them (Bjerhammar, 1978, p.220). The common characteristic of all methods is that a finite set of point gravity anomalies is given on the physical surface of the earth

A special case of Bjerhammar's reflexive prediction method (Bjerhammar, ibid), is the Dirac approach, which has been compared to collocation by Sjöberg (1978). This approach is based on the computation of the fictitious gravity anomalies at the so-called carrier points, located at the intersections of the radii to the observation points, with the geosphere. The radius (R_B) of the geosphere was found to be a critical parameter in this type of solutions. As (Sjöberg, 1978, p.64) reported, the optimum depth of the geosphere from the mean earth sphere R , is approximately half the mean distance between surface neighboring observations.

In the sections that follow, we will review the theory behind these discrete approaches, with emphasis on two methods, namely the mean-value approach, and the Dirac approach. Then, the Dirac approach will be applied to simulated data from the model described in chapter 3, and the results (the components of the disturbance vectors) will be compared to the exact vectors from the model, just as we did with Green's approach in chapter 4.

5.2 Theoretical Development

Let us start from the statement on the Dirichlet's problem or the first BVP of potential theory (Heiskanen and Moritz, 1967, p.34):

> "Given an arbitrary function on a surface S , determine a function V which is harmonic either inside or outside S , and which assumes on S the values of the prescribed function".

Dirichlet's problem can always be solved if S is the surface of a sphere, an explicit solution being given by the Poisson's integral equation (Heiskanen and Moritz, 1967, p.35), which for the exterior of S is written as:

$$V_e(r,\theta,\lambda) = \frac{R(r^2-R^2)}{4\pi}\int_0^{2\pi}\int_0^{\pi}\frac{V(R,\theta,\lambda)}{\ell^3}\sin\theta'\,d\theta'\,d\lambda' \qquad (5.1)$$

V is an arbitrary harmonic function on S and in the exterior space, (θ', λ') are the polar coordinates of the variable point on the sphere (R), (r, θ, λ) are the coordinates of the exterior point, and ℓ is the distance from (r, θ, λ) to (R, θ', λ'):

$$\ell = (r^2 + R^2 - 2R\, r \cos\psi)^{\frac{1}{2}} \tag{5.2}$$

$$\cos\psi = \cos\theta \cos\theta' + \sin\theta \sin\theta' \cos(\lambda' - \lambda) \tag{5.3}$$

The function $r\Delta g$ is a harmonic function (Heiskanen and Moritz, 1967, p.90), and hence, Poisson's Integral can be applied for any point in space as:

$$r_p \Delta g_p = \frac{R(r_p^2 - R^2)}{4\pi} \iint_\sigma \frac{R\, \Delta g}{\ell^3}\, d\sigma \tag{5.4}$$

where

$$d\sigma = \sin\theta'\, d\theta'\, d\lambda' \tag{5.5}$$

is the surface element on a unit sphere. For the geosphere (R_B), equation (5.4) becomes:

$$\Delta g_p = \frac{r_p^2 - R_B^2}{4\pi r_p} \iint_B \frac{\Delta g^*}{\ell^3}\, dS \tag{5.6}$$

where

$$dS = R_B^2\, d\sigma \tag{5.7}$$

S being the area of the geosphere B $(S = 4\pi R_B^2)$. The quantities which appear in (5.6) are defined as follows (see also in figure 5.1):

Δg_p : The gravity anomaly at the space point P

$$\Delta g_p = g_p - \gamma_p$$

where P' is that point along the vertical through P for which $U_{P'} = W_P$ (cf. Sjöberg, 1978);

Δg^* : The fictitious gravity anomalies on the geosphere, which generate the surface Δg, and which have to be determined;

r_p : The geocentric distance to P.

Obviously, equation (5.6) also holds for any point Q on the physical surface of the earth, because the geosphere has been defined to be completely imbedded inside the topographic masses, and therefore, the requirement of the Poisson's integral (5.1) is met (the solution is given for points outside of the surface S , the surface being the sphere R_B in our case). Equation (5.6), applied for a surface point Q , becomes:

$$\Delta g_Q = \frac{r_Q^2 - R_B^2}{4\pi r_Q} \iint_B \frac{\Delta g^*}{\ell^3} \, dS \tag{5.8}$$

By substituting:

$$t_Q = \frac{R_B}{r_Q} \tag{5.9}$$

and

$$D_Q = \frac{\ell}{r_Q} = \sqrt{1 - 2\, t_Q \cos\psi + t_Q^2} \tag{5.10}$$

in equation (5.8), we obtain:

$$\Delta g_Q = \frac{t_Q^2 (1 - t_Q^2)}{4\pi R_B} \iint_B \frac{\Delta g^*}{D_Q^3} \, dS \tag{5.11}$$

The precise definition of the surface gravity anomaly Δg_Q is similar to the definition of the space anomaly Δg_P (see below equation (5.6)). In other words, Δg_Q is the difference between the measured gravity g_Q at the surface point Q , and the normal gravity γ_Q computed at that point Q' along the ellipsoidal normal through Q , for which $U_{Q'} = W_Q$. All points Q' form the surface of the telluroid (Heiskanen and Moritz, 1967, p.292).

The central idea in the Bherhammer's methods is to apply an integral equation like (5.8) or (5.11) to the given surface data Δg_Q , and to compute the fictitious Δg^* on the geosphere, in such a way that all Δg_Q are satisfied by the analytically determined Δg^* . Furthermore, the gravity anomaly at a space point P , determined from the anomalies on the geosphere, must be identical to the gravity anomaly computed from the measured surface Δg_Q , provided that there are no errors in the data, and that the integrations are performed over the whole surface of the earth. This is a consequence from the uniqueness of Stokes' theorem (Heiskanen and Moritz, 1967, p.17).

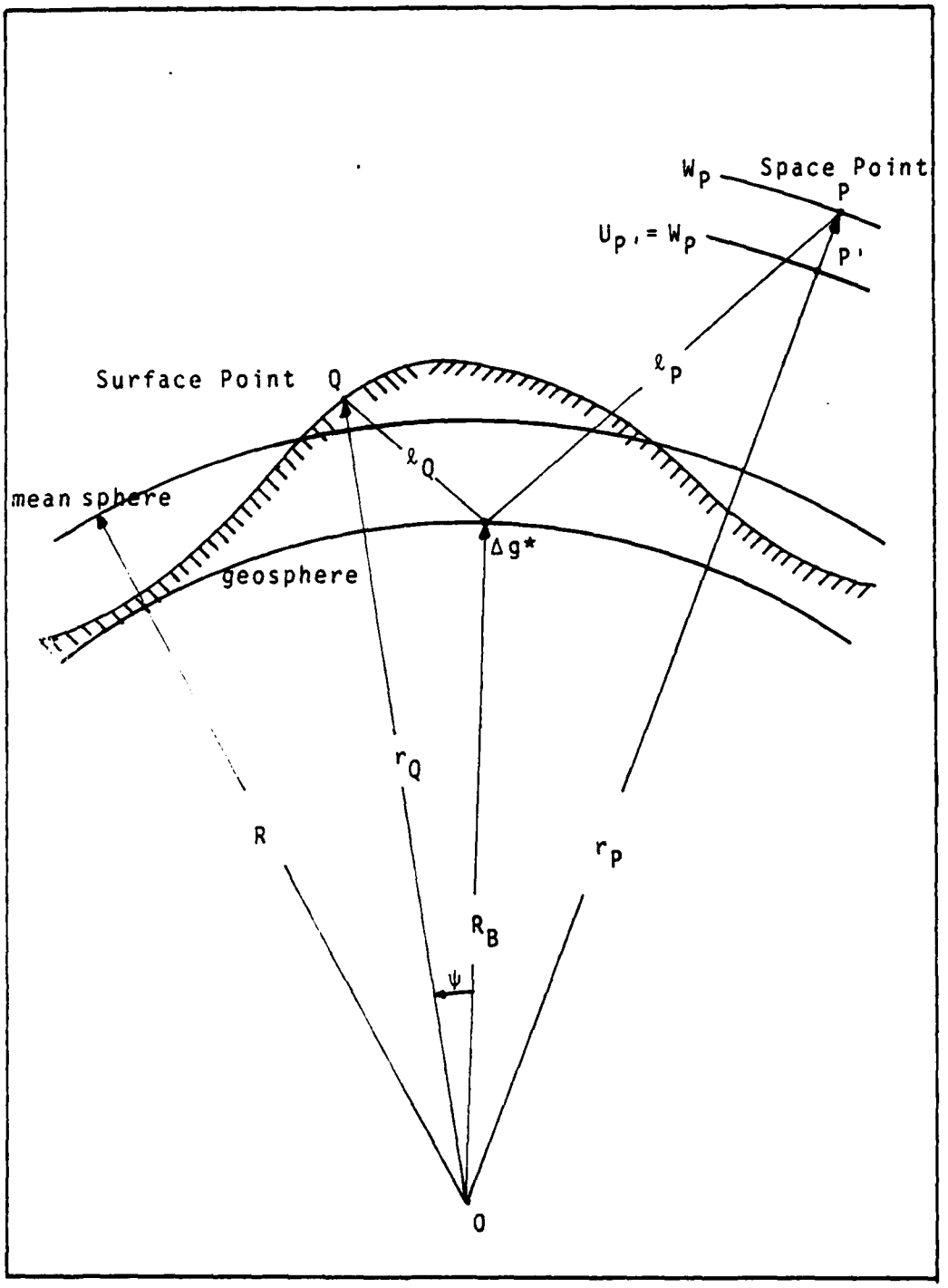

Figure 5.1: Geometrical Configuration for the Discrete Approaches.

Let us now show how an integral equation like (5.11) can be applied to a discrete approach.

5.2.1 The Mean-Value Approach

If the surface of the geosphere is divided into a finite number (N) of blocks (ΔS_i), equation (5.11) can be rigorously written as:

$$\Delta g_Q = \frac{t_Q^2 (1 - t_Q^2)}{4\pi R_B^2} \sum_{i=1}^{N} \iint_{\Delta S_i} \frac{\Delta g^*}{D_Q^3} \, dS \qquad (5.12)$$

or, approximately:

$$\Delta g_Q = \frac{t_Q^2 (1 - t_Q^2)}{4\pi R_B^2} \sum_{i=1}^{N} \frac{\Delta g_i^*}{D_{Qi}^3} \Delta S_i \qquad (5.13)$$

where Δg_i^* is evaluated at a certain (but unknown) point inside ΔS_i, usually assumed to be the center of the block, in which case (5.13) is an approximation. The conventional approach to convert a theoretical continuous integral transformation like (5.11), to a discrete summation transformation like (5.13), is called discretization (see for example in Robertson, 1978, p.4-1). *Discretizations are of great importance in geodesy, since we have to deal with finite sets of data, irregularly distributed on the surface of the earth.* The substitution of integral equations by finite summations is a common practice, especially for computer-oriented applications. Obviously, the best discretization process is the one which yields the minimum error of the computed quantity with respect to the true value. Robertson (ibid) discusses three discretization processes, and suggests a method for evaluating their accuracies by comparing their spectra.

The mean-value approach, requires the evaluation of the areas ΔS_i for each block, and from the theoretical point of view (5.13) holds as an approximation since the location of the point for evaluation Δg_i^* is unknown. The Dirac approach which will be discussed later avoids this problem because it determines Δg_i^* at the carrier points whose positions are pre-determined, and therefore are precisely known.

If the subdivision of the geospher in blocks is such that their number (N) is equal to the number of observations Δg_Q, then, a direct solution to (5.13) for the fictitious Δg_i^*, could be:

$$\underline{\Delta g^*} = \underline{A}^{-1}\underline{\Delta g} \tag{5.14}$$

where the underlines mean matrixes, or vectors, and the elements of $\underline{A}$ are:

$$\alpha_{ij} = \frac{t_i^2 (1 - t_j^2)}{4\pi R_B^2} \frac{\Delta S_j}{D_{ij}^3} \tag{5.15}$$

However, such an approach would be practically impossible if a large amount of surface data is available. Earlier solutions to the Bjerhammar's problem used an iterative approach to compute Δg^* from Δg (see for example Heiskanen and Moritz, (1967, p.318), or Emrick, (1973)). In the next section we describe the Gauss-Seidel iteration technique, and we investigate the possibility for employing an acceleration procedure.

5.2.2 Gauss-Seidel Iteration Method

For a linear system of n equations with n unknowns:

$$\underline{B}\,\underline{x} = \underline{u} \tag{5.16}$$

or

$$\begin{aligned} b_{11} x_1 + b_{12} x_2 + \ldots + b_{1n} x_n &= u_1 \\ b_{21} x_1 + b_{22} x_2 + \ldots + b_{2n} x_n &= u_2 \\ &\vdots \\ b_{n1} x + b_{n2} x_2 + \ldots + b_{nn} x_n &= u_n \end{aligned} \tag{5.17}$$

the Gauss-Seidel iteration method to solve x_i is (Carnahan, et al., 1969, p.299):

$$x_i^{(k+1)} = \frac{1}{b_{ii}}\left[u_i - \sum_{j=i+1}^{n} b_{ij} x_j^{(k)} - \sum_{j=1}^{i-1} b_{ij} x_j^{(k+1)}\right] \tag{5.18}$$

where (k) denotes the iteration step. In this iterative method, the newly-computed components of the solution vector $\underline{x}$ are always used in the right-hand side of (5.18) as soon as they are obtained. A sufficient condition to guarantee the convergence of the iteration is:

$$\sum_{\substack{j=1 \\ j\neq i}}^{n} \left| \frac{b_{ij}}{b_{ii}} \right| < 1 , \quad 1 \leq i \leq N \tag{5.19}$$

This condition will later be used to compute the optimum radius of the geosphere in order to guarantee the convergence of the solution for Δg^* .

As an example, let us apply (5.18) to the linear system (5.13). Assume that N surface gravity anomalies Δg are given, and that we want to determine the N unknowns Δg^* on the geosphere. The surface Δg are point anomalies, but the Δg^* on the geosphere are mean anomalies, associated with a certain block size which depends on the density of the surface data. Let Q be the points on the surface where the data is given, and Q' be the center of the block on the geosphere (see figure 5.2).

With this notation, the linear system (5.13) becomes:

$$\Delta g_{Qj} = \frac{t_j^2 (1 - t_j^2)}{4\pi R_B^2} \sum_{i=1}^{N} \frac{\Delta g^*_{Q'i}}{D^3_{ji}} \Delta S_i \tag{5.20}$$

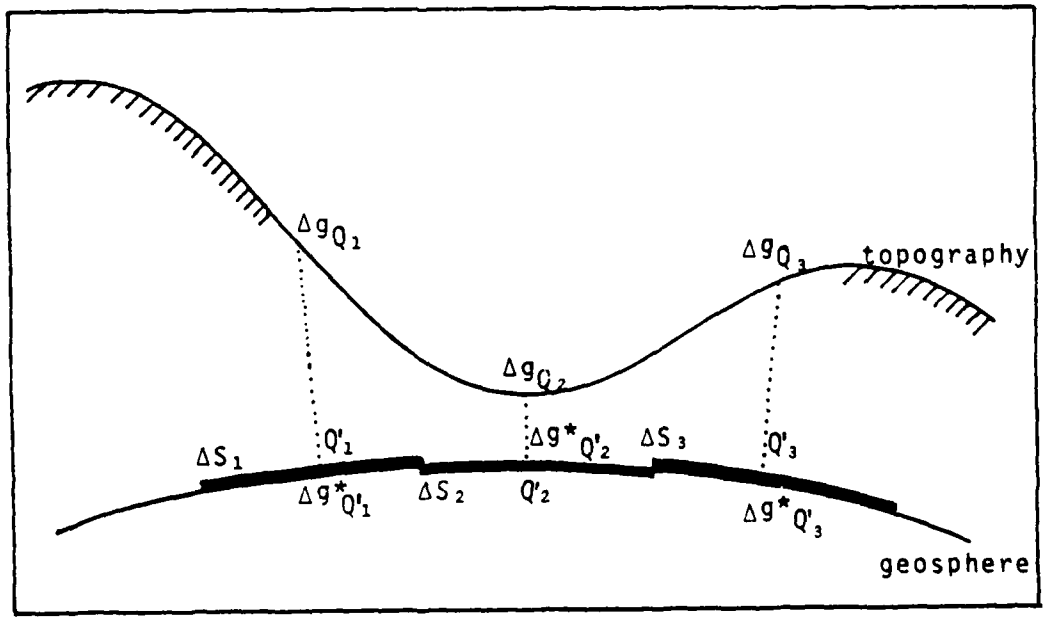

Figure 5.2: The Mean-Value Approach

with

$$t_j = t_{Qj} = \frac{R_B}{r_{Qj}}$$

The application of the Gauss-Seidel method (5.18) to the system (5.20) yields:

$$\Delta g^{*(k+1)}_{Q'i} = \frac{D^3_{ii}}{\Delta S_i}\left[\frac{4\pi R_B^2 \Delta g_{Qi}}{t_i^2 (1 - t_i^2)} - \sum_{\substack{j=1 \\ j\neq i}}^{N} \frac{\Delta g^{*(k)}_{Q'j}}{D^3_{ij}} \Delta S\right] \qquad (5.21)$$

where $i = 1, 2, \ldots, N$

$k = 1, 2, \ldots,$ maximum number of iterations allowed (k_{max})

and $\Delta g^{*(k=1)}_{Q'_J} = \Delta g_{Q_J}$ $j = 1, 2, \ldots, N$ as an initial approximation

An equation analogous to (5.21) but somewhat simpler will be derived later for the Dirac approach. The above iteration for the unknows Δg^* can be stoped either if we exceed the maximum number of iterations allowed, (say $k_{max} = 30$), or if two successive Δg^* at all points (iteration k and $k+1$) are different by no more than ε, a quantity which is as small as we desire.

Acceleration Techniques. Among the existing methods for the iterative solution of large systems of equations, the Gauss-Seidel ("successive iterations") method converges about two times faster than the Jacobi's ("simulation iterations") method (cf. Westlake, 1968, p.56). In addition, there ar certain acceration techniques, which yield a much larger rate of convergence than the two methods mentioned above. An acceleration technique requires the splitting of the matrix $\underline{B}$ according to (Isaacson and Keller, 1966, pp.73-80):

where $B = \underline{N}(\alpha) - \underline{P}(\alpha)$

$$\underline{N}(\alpha) = (1 + \alpha)\,\underline{N}_0$$

$$\underline{P}(\alpha) = (1 + \alpha)\,\underline{N}_0 - \underline{B} = \underline{P}_0 + \alpha \underline{N}_0$$

and

$$\underline{N}_0 = \begin{vmatrix} b_{11} & & & \\ b_{21} & b_{22} & & \\ \vdots & & & \\ b_{n1} & b_{n2} & \ldots & b_{nn} \end{vmatrix}$$

The estimation of the optimum parameter ($\alpha = \alpha_{opt}$) which yields the largest rate of convergence, requires the knowledge

of the minimum and of the maximum eigenvalues of the matrix $\underline{N}_0^{-1}\,\underline{P}_0$, according to the formula:

$$\alpha_{opt} = -\frac{\lambda_{min} + \lambda_{max}}{2}$$

After the parameter α_{opt} has been determined, the iterative solution to the system $\underline{B}\underline{x} = \underline{U}$ can be obtained as (Westlake, 1968, p.62, where $\omega = 1 + \alpha$):

$$x_i^{(k+1)} = \frac{1+\alpha}{b_{ii}} \left[u_i - \sum_{j=i+1}^{n} b_{ij}\, x_j^{(k)} - \sum_{j=1}^{i-1} b_{ij}\, x_i^{(k+1)} \right] - \alpha x_i^{(k)} \qquad (5.18\text{-b})$$

which for $\alpha = 0$ reduces to the Gauss-Seidel technique (5.18).

Clearly, from an application point of view, the employment of an acceleration technique requires that the user will follow one of the following two procedures.

(a). Form the matrix $\underline{N}_0^{-1}\underline{P}_0$, find its eigenvalues λ_{min} and λ_{max} , and then determine α_{opt} which yields fastest rate of convergence in (5.18-b).

(b). Empirically estimate a parameter α which yields a rate of convergence faster than that of the Gauss-Seidel technique. Such an empirical determination (used for the downward continuation of gravity anomalies), has been used by Koch (1968-b). Westlake (1968, pp.62-63) describes a procedures for the estimation of α but in the special case that $\underline{B}$ is a symmetric matrix. Finally, another empirical procedure for the estimation of α is described in (Isaacson and Keller, 1966, pp.78-80), but the method is graphical, and hence not suitable for computer-oriented applications.

For large matrices, the analytical procedure (a) above requires considerably additional work, before the actual iteration (5.18-b) starts. Furthermore, the empirical techniques (b) mentioned above are either not fully automatted, or not applicable for a general (not symmetric) matrix. Therefore, and for reasons of simplicity, we decided to use the Gauss-Seidel iterative method.

5.2.3 The Computation of the Gravity Disturbance Vectors in Space (Mean-Value Approach)

Once Δg^* have been determined, the evaluation of the three components of the gravity disturbance vector in space can be done following standard procedures. The three components of $\vec{\delta}$, are defined as (Heiskanen and Moritz, 1967, equ.6-29):

$$(\delta g_r)_P = (\frac{\partial T}{\partial r})_P$$

$$(\delta g_{\bar{\phi}})_P = \frac{1}{r_P}(\frac{\partial T}{\partial \bar{\phi}})_P$$

$$(\delta g_\lambda)_P = \frac{1}{r_P \cos\bar{\phi}_P}(\frac{\partial T}{\partial \lambda})_P \qquad (5.22)$$

where $(r_P, \bar{\phi}_P, \lambda_P)$ are the coordinates of the space point P where these components are to be computed. The disturbing potential at P is given by Pizzetti's generalization of Stokes' formula (*Heiskanen and Moritz, 1967, equ.8-88*):

$$T_P = T(r_P, \bar{\phi}_P, \lambda) = \frac{R_B}{4\pi} \iint_B \Delta g^* \, S(r,\psi) \, d\sigma \qquad (5.23)$$

From (5.22) and (5.23) follows that:

$$(\delta g_r)_P = \frac{R_B}{4\pi} \iint_B \Delta g^* \frac{\partial S(r,\psi)}{\partial r} d\sigma$$

$$(\delta g_{\bar{\phi}})_P = -\frac{R_B}{4\pi r_P} \iint_B \Delta g^* \frac{\partial S(r,\psi)}{\partial \psi} \cos\alpha \, d\sigma$$

$$(\delta g_\lambda)_P = -\frac{R_B}{4\pi r_P} \iint_B \Delta g^* \frac{\partial S(r,\psi)}{\partial \psi} \sin\alpha \, d\sigma \qquad (5.24)$$

Since Δg^* represents the value of the fictitious anomaly over a block on the geosphere, we apply the same approximation as we did in section 5.2.1, to obtain (Note: $dS = R_B^2 d\sigma$):

$$(\delta g_r)_P = \frac{1}{4\pi R_B} \sum_{i=1}^{N} \Delta g^*_{Q'_i} (\frac{\partial S(r,\psi)}{\partial r})_i \, \Delta S_i$$

$$(\delta g_{\bar{\phi}})_P = \frac{1}{4\pi r_P R_B} \sum_{i=1}^{N} \Delta g^*_{Q'_i} (\frac{\partial S(r,\psi)}{\partial \psi})_i \cos\alpha_i \, \Delta S_i$$

$$(\delta g_\lambda)_P = \frac{1}{4\pi r_P R_B} \sum_{i=1}^{N} \Delta g^*_{Q'_i} (\frac{\partial S(r,\psi)}{\partial \psi})_i \sin\alpha_i \, \Delta S_i \qquad (5.25)$$

The index i refers to the center of the block ΔS_i - this is in approximation, since the point to evaluate the kernels in (5.24) is unknown - , and α_i is the aximuth from the projection of P on the geospher to the point Q'_i :

$$\tan\alpha_i = \frac{\cos\bar{\phi}_i \sin(\lambda_i - \lambda_P)}{\cos\bar{\phi}_P \sin\bar{\phi}_i - \sin\bar{\phi}_P \cos\bar{\phi}_i \cos(\lambda_i - \lambda_P)} \qquad (5.26)$$

The partial derivatives of the Stokes' function with respect to r and ψ are computed as:

$$\cos\psi = \cos\psi_{Pi} = \sin\bar{\phi}_P \sin\bar{\phi}_i + \cos\bar{\phi}_P \cos\bar{\phi}_i \cos(\lambda_i - \lambda_P) \tag{5.27}$$

$$t = t_P = \frac{R_B}{r_P} \tag{5.28}$$

$$D = D_{Pi} = \frac{\ell}{r_P} = (1 - 2t\cos\psi + t^2)^{\frac{1}{2}} \tag{5.29}$$

and then, with the notation above we have:

$$\frac{\partial S(r,\psi)}{\partial r} = -\frac{t^2}{R_B}\left[\frac{1-t^2}{D^3} + \frac{4}{D} + 1 - 6D - t\cos\psi\left(13 + 6\ell n\,\frac{1 - t\cos\psi + D}{2}\right)\right] \tag{5.30}$$

$$\frac{\partial S(r,\psi)}{\partial \psi} = -t^2\sin\psi\left[\frac{2}{D^3} + \frac{6}{D} - 8 - 3\,\frac{1 - t\cos\psi - D}{D\sin^2\psi} - 3\ell n\left(\frac{1 - t\cos\psi + D}{2}\right)\right]$$

Finally, the components of the gravity disturbance vector in a geocentric coordinate system are (Heiskanen and Moritz, 1967, equ.6-18):

$$\begin{vmatrix} \frac{\partial T}{\partial X} \\ \frac{\partial T}{\partial Y} \\ \frac{\partial T}{\partial Z} \end{vmatrix}_P = \begin{vmatrix} \delta g_X \\ \delta g_Y \\ \delta g_Z \end{vmatrix}_P = \begin{vmatrix} \cos\bar{\phi}_P \cos\lambda_P & -\sin\bar{\phi}_P \cos\lambda_P & -\sin\lambda_P \\ \cos\bar{\phi}_P \sin\lambda_P & -\sin\bar{\phi}_P \sin\lambda_P & \cos\lambda_P \\ \sin\bar{\phi}_P & \cos\bar{\phi}_P & 0 \end{vmatrix} \begin{vmatrix} \delta g_r \\ \delta g_{\bar{\phi}} \\ \delta g_\lambda \end{vmatrix}_P \tag{5.32}$$

5.3 The Dirac Approach

The Dirac approach avoids the continuation of the surface anomalies to mean (fictitious) anomalies on the geosphere. Instead, the gravity information of the N surface point gravity anomalies Δg, is downward-continued to gravity anomaly impulses (spikes) Δg^S at a finite number of carrier points (defined in section 5.1). This downward continuation is an analytic continuation, by which is meant that the N spikes satisfy the surface data, without having any physical meaning (i.e. this is not a gravity reduction that yields the true anomaly on the geosphere).

If the number of the gravity impulses Δg^S on the geosphere is equal to the number of the given surface gravity

anomalies Δg , the case is called "non-singular" (Bjerhammar, 1977), and the carrier points can be selected at the projections of the surface points, on the geosphere, along the geocentric radii (see figure 5.3). Q_i are the surface points where the data is given, and Q'_i are their projections on the geosphere, where the spikes Δg^S are to be computed.

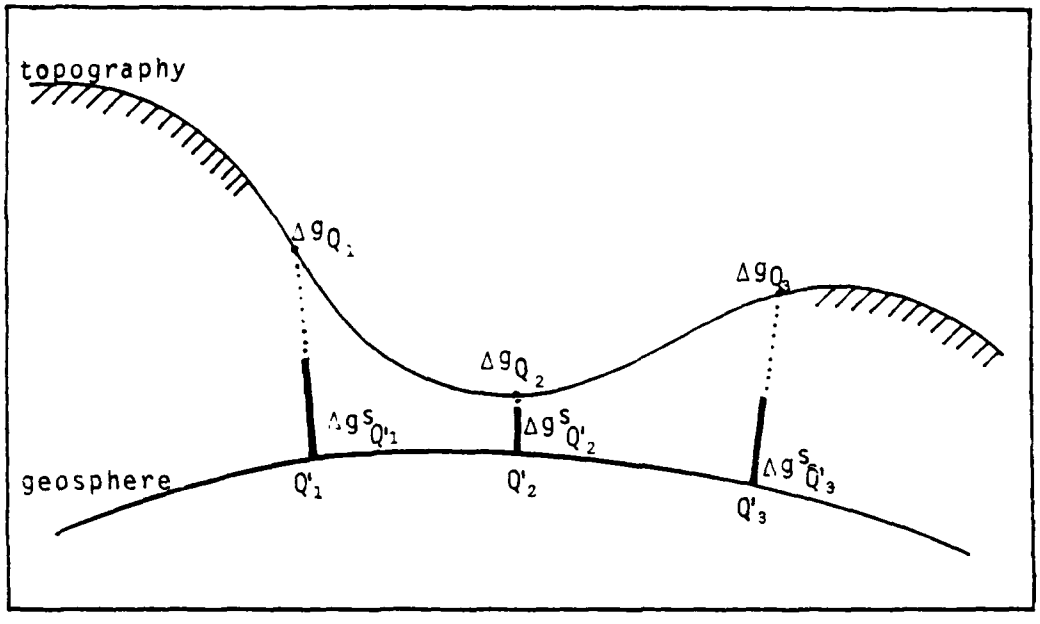

Figure 5.3: The Dirac Approach: The Spikes Δg^S at the Carrier Points

Let us now define the anomaly Δg^* which appears in (5.11) as:

$$\Delta g^* = \sum_{k=1}^{N} \Delta g_k^S \, \delta(r - r_k) \qquad (5.33)$$

where r : the radius to the current point on the geosphere.
r_k: the radius to the k^{th} spike Δg_k^S on the geosphere.
and $\delta(r - r_k)$: the Dirac "delta" function defined through the following integral equation for an arbitrary function $f(r)$ on the geosphere.

$$\frac{1}{4\pi R_B} \iint_B f(r) \, \delta(r - r_k) \, dS = f(r_k) \qquad (5.34)$$

Substituting (5.33) into (5.11) we obtain:

$$\Delta g_Q = \frac{t_Q^2 (1 - t_Q^2)}{4\pi R_B^2} \iint_B \frac{\sum_{k=1}^{N} \Delta g_k^s \, \delta(r - r_k)}{D_Q^3}$$

or

$$\Delta g_Q = \frac{t_Q^2 (1 - t_Q^2)}{4\pi R_B^2} \sum_{k=1}^{N} \Delta g_k^s \iint_B \frac{1}{D_Q^3} \, \delta(r - r_k) \, dS$$

and using (5.34) with $f(r) = 1/D_Q^3$, we obtain:

$$\Delta g_Q = t_Q^2 (1 - t_Q^2) \sum_{k=1}^{N} \frac{\Delta g_k}{D_{Qk}^3} \tag{5.35}$$

The reader can see that equation (5.35) of the Dirac approach, corresponds to equation (5.13) of the mean-value approach, the difference being that the former does not involve any areas ΔS_i associated with the spikes. Furthermore, the positions of the carrier points are precisely known, and hence the Dirac approach avoids the approximation of the mean-value approach, where the kernels are evaluated at the centers of the blocks.

5.3.1 Iterative solution for the Spikes Δg^s

The computation of the N spikes Δg^s from the given finite set of observations Δg, is done using the Gauss-Seidel iterative method described in section 5.2.2. More specifically, from (5.18) and (5.35) we obtain:

$$\Delta g_{Q'_i}^{s(k+1)} = D_{ii}^3 \left[\frac{\Delta g_{Q_i}}{t_{Q_i}^2 (1 - t_{Q_i}^2)} - \sum_{\substack{j=1 \\ j \neq i}}^{N} \frac{\Delta g_{Q'_j}^{s(k)}}{D_{Q_i j}^3} \right] \tag{5.36}$$

where $i = 1, 2, \ldots, N$
$k = 1, 2, \ldots,$ maximum number of iterations allowed

and since

$$D_{ii}^3 = (1 - 2t_i \cos\psi_{ii} + t_i^2)^{3/2} = (1 - t_i)^3$$

equation (5.36) yields:

$$\Delta g_{Q'_i}^{s(k)} = (1 - t_{Q_i})^3 \left[\frac{\Delta g_{Q_i}}{t_{Q_i}^2 (1 - t_{Q_i}^2)} - \sum_{\substack{j=1 \\ j \neq i}}^{N} \frac{\Delta g_{Q'_j}^{s(k)}}{D_{Q_i j}^3} \right] \tag{5.37}$$

As initial values we used $\Delta g_{Q_j}^{s(1)} = 0$, $j = 1, 2, \ldots N$, and not $\Delta g_{Q_j}^{s(1)} = \Delta g_{Q_j}$, because from our preliminary tests we found that the magnitude of the spikes is much smaller (or the order of 10^{-10} m.sec^{-2}) than the magnitude of the surface anomalies (from 10^{-2} to 10^{-6} m.sec^{-2}).

The iteration scheme (5.37) can be terminated either if it exceeds a specified maximum (k_{max}), or if two successive iterations for a spike yield values

$$\Delta g_j^{s(k)} \qquad \text{and} \qquad \Delta g_j^{s(k+1)}$$

which are different by less than a specified limit. For example, if we want to have a 12-digit agreement between these two values, we stop the iteration whenever the following condition is satisfied for every spike:

$$\left| \Delta g_j^{s(k+1)} - \Delta g_j^{s(k)} \right| < \left| \frac{\Delta g_j^{s(k+1)}}{10^{12}} \right| \qquad (5.38)$$

5.3.2 The Convergence of the Iterative Solution, and the Radius of the Geosphere

Let us now examine the conditions for the convergence of the Gauss-Seidel iterative method for the spikes. A sufficient condition for the convergence of this method was given in section 5.2.2 as inequality (5.19). By applying this condition in the case of the Dirac spikes (5.35) we obtain:

$$j = 1, 2, \ldots, N: \quad \sum_{\substack{i=1 \\ i \neq j}}^{N} \left| \frac{\frac{t_j^2 (1 - t_j^2)}{D^3_{ij}}}{\frac{t_j^2 (1 - t_j^2)}{(1 - t_j)^3}} \right| < 1$$

which becomes:

$$j = 1, 2, \ldots, N: \quad \sum_{\substack{i=1 \\ i \neq j}}^{N} \frac{(1 - t_j)^3}{(1 - 2t_j \cos\psi_{ji} + t_j^2)^{3/2}} < 1 \qquad (5.39)$$

because all the terms are positive ($t \leq 1$). Our goal is to use (5.39), to determine a radius R_B of the geosphere which will guarantee the convergence of the solution. It would be very difficult to use all the terms of the above inequality to determine R_B, for large N values. Below, we present a much simpler

method to estimate this R_B radius, without having to solve a large inequality (such as (5.39)) each time that we seek a solution. At first, note that each term in the sum above is a function of the distance ψ_{ji}, and of the height of the point h_j k and that:

$$t_j = \frac{R_B}{R + h_j} \qquad (5.9)$$

which yields:

$$t_{min} = \frac{R_B}{R + h_{max}} \qquad (5.40)$$

The smaller the distance ψ_{Ji}, and the smaller the parameter t, the larger the term in the sum becomes. In other words, the maximum term in (5.39) corresponds to ψ_{min} and h_{max}. Some typical values for these terms are given in table 5.1, assuming $R - R_B = 100$ meters. From these results we can see that for very dense data (1' grid, or smaller), and for high elevations (above 4 km), each term in (5.39) becomes almost equal to 1.0, and therefore, the condition (5.39) might not be satisfied. However, (5.39), as well as its original condition (5.19), are both sufficient conditions. This means that the iteration might converge, even if this condition is not satisfied. We will see an example in our tests in the next chapter.

The Inequality (5.39) determines the minimum radius of the geosphere ($\bar{R}_B$) which guarantees the convergence of the iteration. For any radius R_B larger than this minimum value $\bar{R}_B$, and such that the geosphere is completely imbedded inside the earth, the convergence is certain:

$$\bar{R}_B < R_B \quad : \quad \text{guarantees convergence} \qquad (5.41)$$

If all the terms in (5.39) had the same magnitude, we could solve for $\bar{R}_B$ from an inequality of the form:

$$\frac{(1 - t_j)^3}{(1 - 2t_j \cos\psi_{ji} + t_j^2)^{\frac{1}{2}}} < \frac{1}{N} < \frac{1}{N - 1} \qquad (5.42)$$

but the magnitude of these terms varies very rapidly, especially with the value of the distance ψ (see in table 5.1). As we have already mentioned above, the largest value for these terms corresponds to the minimum distance, and to the maximum height.

Consequently, if the data is distributed on a regular grid - as in the simulations described in the next chapter, -

Table 5.1

Typical Values (dimensionless) of the Terms in Condition (5.39)

ψ \ h	0	100	500	1000	2000	3000	4000	5000
0'.1	0.12228	0.59055	0.93111	0.98026	0.98878	0.99770	0.99864	0.99766
0'.5	0.00127	0.00923	0.15833	0.44406	0.76864	0.87836	0.92721	0.95271
1'.0	0.00016	0.00124	0.02930	0.13331	0.42067	0.63284	0.75695	0.82935
2'.0	0.00002	0.00016	0.00408	0.02303	0.11996	0.26391	0.40793	0.52929
5'.0	1.10^{-6}	0.0001	0.00027	0.00164	0.01079	0.031915	0.06618	0.11199
10'.0	1×10^{-7}	1×10^{-6}	0.00003	0.00021	0.00143	0.00449	0.01007	0.01866
20'.0	2×10^{-8}	1×10^{-7}	4×10^{-6}	0.00003	0.00018	0.00058	0.00133	0.00253
30'.0	6×10^{-9}	5×10^{-8}	1×10^{-6}	7×10^{-6}	0.00005	0.00017	0.00040	0.00076

there will be four terms in (5.39) whose magnitudes are the largest: these terms correspond to the point Q_j with the maximum elevation, and to the four closests points in the vicinity (figure 5.4).

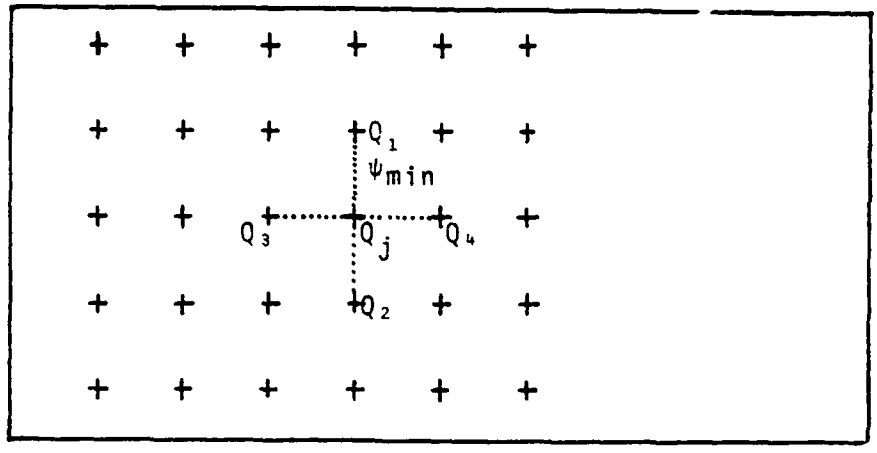

Figure 5.4: The Point Q_j with Maximum Elevation h_{max}, to which the Maximum Terms in (5.39) Correspond.

From the tests reported in the following chapter, we found that it would be sufficient to determine $\bar{R}_B$ by solving the equation below (the term 1/10 was determined empirically):

$$\frac{(1 - t_{min})^3}{(1 - 2t_{min}\cos\psi_{min} + t_{min}^2)^{3/2}} = \frac{1}{10} \qquad (5.43)$$

where

$$t_{min} = \frac{\bar{R}_B}{R + h_{max}} \qquad (5.44)$$

from which it can be easily found that:

$$t_{min} = p - \sqrt{p^2 - 1} \qquad (5.45)$$

in which

$$p = \frac{1 - \cos\psi_{min}\,(1/10)^{2/3}}{1 - (1/10)^{2/3}} \geq 1 \qquad (5.46)$$

and finally:

$$\bar{R}_B = (R + h_{max}) [P - \sqrt{P^2 - 1}] \qquad (5.47)$$

This equation has been used to determine nominal values for the depth $(R - \bar{R}_B)$ of the geosphere, for various values of the minimum distance ψ_{min} and the maximum height h_{max}. R is again the radius of the mean-earth sphere, and since the geosphere must be completely imbedded inside the earth, the iterative solution for the spikes will converge, if we select a radius R_B such that: $\bar{R}_B \leq R_B < R = 6371$ km (see condition (5.41)). These nominal values for the depth of the minimum geosphere are given in table 5.2. For those blocks in this table where no depth is given, the data is so dense, and at such a high elevation, that the iterative solution might not converge (as a matter of fact, we found that in these cases $\bar{R}_B$ is larger than R).

In the last column of table 5.2, we list the corresponding depth from the Sjöberg's (1978, p.64) "rule", that the optimum depth of the geosphere should be half the distance between neighboring surface points. We can see that Sjöberg's depths agree very well with ours (for the $h = 0$ case). This agreement will be demonstrated again in chapter 9, where some tests with real data and the Dirac approach are discussed. The advantage of equation (5.47) in computing the depth of the geosphere, is due to the fact that $\bar{R}_B$ is now a function of both the distance between the observations, and of the maximum elevation of the data points.

5.3.3 The Computation of the Gravity Disturbance Vectors in Space (Dirac Approach)

It remains to use the spikes Δg^S on the geosphere, to compute the components of $\vec{\delta}$ at a space point. This is done by substituting (5.33) into (5.24), and using the definition of the Delta Function (5.34). Thus we obtain (note $dS = R_B^2 \, d\sigma$):

$$\begin{aligned}
(\delta g_r)_P &= R_B \sum_{i=1}^{N} \Delta g_i^S \left(\frac{\partial S(r,\psi)}{\partial r}\right)_i \\
(\delta g_{\bar{\phi}})_P &= -\frac{R_B}{r_P} \sum_{i=1}^{N} \Delta g_i^S \left(\frac{\partial S(r,\psi)}{\partial \psi}\right)_i \cos\alpha_i \\
(\delta g_{\lambda})_P &= -\frac{R_B}{r_P} \sum_{i=1}^{N} \Delta g_i^S \left(\frac{\partial S(r,\psi)}{\partial \psi}\right)_i \sin\alpha_i
\end{aligned} \qquad (5.48)$$

Table 5.2

Maximum Sufficient Depths ($R - R_B$) of the Geosphere for a Convergent Solution

ψ_{min} \ h_{max}	0	100	500	1000	2000	3000	4000	5000	10000	Sjöberg's (1978) Rule $R-R_B=\frac{\psi_{mean}}{2}$
0'.1	0.									92
0'.5	493	393								462
1'.0	987	887	487							925
2'.0	1953	1853	1453	953						1850
5'.0	4850	4750	4350	3851	2852	1852	853			4625
10'.0	9705	9605	9206	8706	7708	6709	5711	4712		9250
20'.0	19395	19293	18895	18396	17399	16402	15405	14408	9423	18500
30.0	29068	28968	28570	28072	27707	26081	25086	24091	19113	27750

where the terms α_i , $\frac{\partial S}{\partial r}$, $\frac{\partial S}{\partial \psi}$, are given by (5.26), (5.30), and (5.31) respectively. The three components of the vector $\vec{\delta}$ at P are then computed from (5.32). Finally, equations (3.24) and (3.25) can be used to compute the two distinct components $\partial T/\partial r$, and $(1/r)\ \partial T/\partial \psi$ in the polar (r, ψ) coordinate system.

5.4 The Initial - Value Method

The mean value approach, and the Dirac approach which have been discussed in this chapter are the two most representative discretization techniques that can be found in the literature. Recently, a new method has been proposed, called the initial-value method (Nakiboglu and Lim, 1979). From the theoretical standpoint, this method is similar to the mean-value approach, because the given data and the reduced quantities on the geosphere are assumed to be given as mean values over a finite number of blocks. The number (m) of the fictitious gravity anomalies Δg^* on the geosphere, is not necessarily equal to the number (n) of the surface gravity anomalies Δg . The solution for Δg^* is obtained from the numerical solution of a set of ordinary first-order differential equations using the iterative Runge-Kutta's method. However, there is anumber of points we would like to emphasize concerning this approach, as compared to the methods described in this chapter.

a. For a real-world application, the Dirac-approach method with point anomalies on the surface of the earth, is more advantageous because it avoids the assumptions on the regular distribution of the data, on the location of the points where the kernels are evaluated, and the computation of the areas.

b. Nakiboglu and Lim (ibid), have restricted themselves in computations of geop-spherop separations (ζ), and deflections of the vertical (ξ , η) at the surface of their model only, and not in space. Furthermore, they do say that the Dirac approach would yield better results than their method.

c. In their numerical example, only a small number of subdivisions (40 or 80 blocks) has been used for the computation of ζ, ξ, and η .

d. As we have already shown in section 5.3.2, the Dirac approach permits a relatively easy way for determining the radius of the geosphere that will guarantee the convergence of the iterative solution, Nakiboglu and Lim (ibid), kept the radius of the geosphere fixed at 1 km below the mean earth sphere R .

Chapter 6

SIMULATION TESTS WITH THE DIRAC APPROACH

6.1 Introduction

In this chapter we describe the simulation tests which we performed in applying the Dirac approach to the terrain model, just as we did in chapter 4 with the Green's approach. Similar simulation studies are reported in (Reit, 1966), but they follow a flat-earth approximation for the ξ component of the deflection of the vertical only. It should be clear by now that the data needed for the Green's approach is gravity disturbances, and not gravity anomalies as in the discrete Dirac approach. Therefore, the gravity disturbances that are computed from the model (equation 3.18), have to be transformed to anomalies. This can be achieved by using the fundamental equation of physical geodesy (see in Heiskanen and Moritz, 1967, p.88):

$$\Delta g_Q = \delta g_Q - \frac{2}{r_Q} T_Q \qquad (6.1)$$

the gravity disturbance being computed from (3.18), and the disturbing potential from (3.16). This particular step has been ignored in similar simulation studies in the past (Molodensky, et al., 1962, p.217 ; Bjerhammar, 1976, p.43; Sjöberg, 1978, p.37), all of which use the conical Molodensky's model. However, the magnitude of the disturbing potential T on the model is not larger than 1 . kgal.m (see figures 3.2 through 3.5), and therefore, the magnitude of the second term in the right-hand side of (6.1) is no greater than 0.3 mgal. Out simulation studies for the Dirac approach consist of a six-step procedure, which can be described as follows:

Step-1. The exact values of the components of $\vec{\delta}$ are computed from equations (3.23), (3.24), and (3.25) at selected points, over and in the vicinity of the model.

Step-2. The gravity anomalies are computed on the surface of the model from equations (6.1) and (3.18). The extent of the area around the model, and the grid spacing are specified, and the data is generated on a regular grid.

Step-3. The radius of the (smallest) geosphere that will guarantee the convergence of the iterative solution is computed from (5.47).

Step-4. The Gauss-Seidel iterative method is applied for the computation of the gravity spikes Δg^S at the carrier points.

Step-5. The components (δg_r , δg_φ , δg_λ) are obtained from (5.48), and them, (5.52) yields the three components $\partial T/\partial X$, $\partial T/\partial Y$, $\partial T/\partial Z$ at the selected space points. Then, (3.24) and (3.25) can be used to compute the two distinct components $\partial T/\partial r$, $(1/r)\ \partial T/\partial \psi$ in the polar (r, ψ) system.

Step-5* (optional). The N spikes on the geosphere must satisfy all the surface gravity anomalies. Equation (5.35) can be used to compute the surface anomalies from the spikes, which can be compared ot the original data. Any difference between the given data and the computed anomalies are due to the fact that the iteration has been forced to stop before a 16-digit agreement was reached between successive approximations.

Step-6. The components from steps 1 and 5 are compared in terms of their relative percentage difference (from equations 4.1)).

6.2 Simulation Tests

The difficulty in applying the Dirac approach arises from the fact that an iterative procedure is used to solve for the gravity spikes on the geosphere (section 5.3.1). In terms of computer time (on an Amdahl 470 machine), it takes about 16 seconds to complete just one iteration for 576 spikes. Therefore, it would be practically impossible to handle a large amount of surface data (say more than 2000 data points), because of the large CPU time that is required to solve such a large system of equations. This is why we decided to make the simulation tests for the Dirac approach, using a relatively small amount of data points (up to 576 surface gravity anomalies). The characteristics of the models are defined from the parameters listed in table 3.1. A description of the tests is given in table 6.1 for easy comparison. It must be kept in mind that the iterative solution for the gravity spikes can be carried-out to any desirable level of accuracy, which is controlled by the convergence criterion (5.38), and by the maximum number of iterations allowed (k_{max}).

The question is now how many iterations are actually needed to compute the gravity spikes. In other words, a 12-digit agreement between successive iterations at all spikes according to conditon (5.38) might be too much, and that the iteration should rather be terminated whenever the RMS difference between the surface anomalies, and the anomalies computed from the spikes at the same points, is below a certain level (say 1. mgal).

Table 6.1

Description of the Tests with the Model Topography (Dirac Approach)

Model	Area Extent	Grid	Number of Points	$R - R_B$	$k_{max}^{(*)}$	Altitude of space point	RMS diff.(+)	Table
Sph. cap	2° x 2°	5'	576	753m	12	5 km	3×10^{-7} mgal	6.3
Sph. cap	0.4° x 0.4°	1'	576	50m	12	5 km	0.5 mgal	6.4
10° cone	0.4° x 0.4°	1'	576	50m	12	5 km	1.0 mgal	6.5
10° cone	0.4° x 0.4°	1'	576	50m	12	10 km	1.0 mgal	6.6
10° cone	0.4° x 0.4°	1'	576	50m	12	20 km	1.0 mgal	6.7
10° cone	0.4° x 0.4°	1'	576	50m	12	100 km	1.0 mga	6.8
40° cone	0.4° x 0.4°	1'	576	50m	12	10 km	0.4 mgal	6.9

(*) k_{max} : maximum number of iterations

(+) RMS diff : The Root Mean Squared difference between the surface anomalies, and the anomalies computed from the spikes at the same points.

Table 6.2

Gravity Disturbance Vector Components from the Dirac Approach, at Various Iteration Steps. Values in mgal. Spherical cap model, 1' grid, 576 anomalies.

space point coordinates	max.# iterations (k_{max})	∂T/∂X Diff.	∂T/∂Y Diff.	∂T/∂Z Diff.	RMS Diff. exact-comp.vect.	RMS Diff. orig.-comp. Δg
$\bar{\phi}$ = 45°, λ = 250°00'		25.51	70.09	-74.59		
02'	E	- 8.36	64.84	-58.08		
04'	X	-20.19	48.91	-39.07		
h = 5 km 06'	A	-22.53	35.03	-25.24		
08'	C	-20.67	24.71	-16.19		
10'	T	-17.63	17.64	-10.58		
12'		-14.67	12.90	- 7.13		
$\bar{\phi}$ = 45°, λ = 250°00'		24.56(0.95)	69.44(0.65)	-73.23(-1.36)		
02'		- 8.54(0.16)	64.80(0.04)	-58.05(-0.03)		
04'	k_{max}	-20.23(0.04)	48.92(-0.01)	-38.98(-0.09)		
h = 5 km 06'		-22.72(0.19)	35.13(-0.10)	-25.24(-0.00)	0.76	0.99
08'	= 8	-21.00(0.33)	24.82(-0.11)	-16.13(-0.06)		
10'		-18.02(0.39)	17.73(-0.09)	-10.51(-0.07)		
12'		-15.38(0.71)	13.00(-0.10)	- 6.97(-0.16)		
$\bar{\phi}$ = 45°, λ = 250°00'		24.79(0.72)	69.40(0.69)	-73.40(-1.19)		
02'		- 8.54(0.18)	64.86(-0.02)	-58.12(0.04)		
04'	k_{max}	-20.31(0.12)	48.94(-0.03)	-39.00(-0.07)		
h = 5 km 06'		-22.71(0.18)	35.09(-0.06)	-25.23(-0.01)	0.69	0.75
08'	= 10	-20.99(0.32)	24.83(-0.12)	-16.17(-0.02)		
10'		-18.04(0.41)	17.74(-0.10)	-10.52(-0.06)		
12'		-15.38(0.71)	13.00(-0.10)	- 6.97(-0.16)		
$\bar{\phi}$ = 45°, λ = 250°00'		24.98(0.53)	69.36(0.83)	-73.44(-1.15)		
02'		- 8.42(0.06)	64.80(0.04)	-58.15(0.07)		
04'	k_{max}	-20.27(0.06)	48.93(-0.02)	-39.05(-0.02)		
h = 5 km 06'		-22.66(0.13)	35.03(0.00)	-25.22(-0.02)	0.65	0.52
08'	= 12	-20.92(0.25)	24.79(-0.08)	-16.18(-0.01)		
10'		-17.99(0.36)	17.72(-0.08)	-10.53(-0.05)		
12'		-15.34(0.67)	12.97(-0.07)	- 6.98(-0.15)		

In order to investigate the effect of the number of iterations, on the accuracy of the components of $\vec{\delta}$, three tests were made using the spherical cap model (576 anomalies in a 0.4°x 0.4° area), and terminating the iteration process after 8, 10, and 12 iterations respectively. The exact components from the model, and the components computed from the spikes at 7 space points (at 5 km altitude above the mean sphere R), are listed in table 6.2. The differences between the exact and the computed components are also listed in parenthesis. The last two columns of table 6.2 contain:

(a). The RMS difference between the exact components, and the computed ones, and
(b). The RMS difference between the original surface anomalies and those computed at the same points from the spikes, after the iteration is terminated.

The fact that these RMS differences become smaller as the number of iterations increases, indicates that the numerical solution for the gravity spikes probably converges (the relative percentage errors from the $k_{max}= 12$, are given in table 6.4, and as we can see are quite small). Therefore, we decided to terminate the iteration for all tests at $k_{max}= 12$, for which the RMS differences between the original and the computed anomalies are smaller than 1. mgal (see also table 6.1).

The radius of the geosphere is computed from equation (5.47), but for most of our tests with very dense data (1' grid, see table 6.1), R_B was forced to be 50 meters smaller than R . This had to be done, because for very dense data at high elevations (as on our 4.1-km models), the radius R_B from (5.47) is larger than R . (note: the 50-meters depth for the geosphere was selected on a rather arbitrary basis, since the geosphere must be completely imbedded inside the earth, and therefore inside the mean-earth sphere R). This paradoxial result, i.e. R_B larger than R , actually means that this kind of data does not satisfy the sufficient condition (5.39), and hence, the iterative solution for the spikes might not converge. However, the tests that follow, indicate that even in this case the iteration converges, which is explained by the fact that (5.39) is only a <u>sufficient</u> condition for convergence.

Let us first start the discussion on the simulations with the errors from the spherical cap model, already used above for the determination of the maximum number of iterations. A total number of 576 anomalies were generated on its surface, within a 2° x 2° area on a 5' grid. This data implies a radius R_B 753 meters smaller than R . The errors in the components of $\vec{\delta}$ at 5 km altitude are large (table 6.3), but the reason is obvious: most of the gravity

information generated by the model is missing, since the data points are too far away from it. As we can see in table 6.4, by using data on a 1' grid within a 0.4° x 0.4° area - 576 points again-, the errors are two orders of magnitude smaller than with data on a 5' grid in a much larger area. The errors from these two tables indicate that for the very smooth topography of the spherical cap model, the results from the Dirac approach are very sensitive to the density of the surface data, but the method works very well with dense data (say on a 1' grid), provided that this data is not too dense if we want to avoid divergence of the iteration.

For a 10°-inclination conical model, with 576 anomalies ona 1' grid as above, the errors at 5, 10, 20, and 100 km altitude are given in tables 6.5, 6.6, 6.7, and 6.8 respectively. At altitude 5 km, the errors from the spherical cap model are slightly smaller than the errors from the 10°-inclination conical model (table 6.4 vs. 6.5). It is quite remarkable that even over the edge of the area at 5 km altitude, the errors are no more than 9%. Not only that, but comparing with the results from the Green's approach at 10 km are almost three times smaller, despite the fact that the amount of data is now two orders of magnitude smaller. More remarkable is the fact that directly above the model, at 5 km, 10 km, and 20 km altitude, the errors are less than 3%, as opposed to almost 25% errors from the Green's approach. However, as the altitude increases, the errors from the Dirac approach become slightly larger, in contrast to the results from the Green's approach. Nevertheless, at 100 km the errors from the Dirac approach are almost four times smaller than the errors from the Green's approach (table 6.8 vs. 4.16).

An overall examination of the two techniques, using identical data and models (10°-cone, 0.4° x 0.4° area, 1' grid, 576 anomalies), shows that the Dirac approach in general is superior to the Green's approach in terms of the magnitude of the errors. The problem with the Dirac approach is that it will fail with very dense data at high elevations, and it requires considerably more computer time because of the iterative solution for the gravity spikes.

For a 40°-inclination conical model (table 6.9), the errors are quite large, reaching almost 90% over the whole area. However, we have to realize that the extent of a 40° cone with 4.1 km height is $\Omega = 2.64'$, and thus, there are only 16 data points on the conical surface with a 1' grid. Apparently, this amoung of data is not enough to represent the model's gravity field (figure 3.4) for the Dirac approach. On the other hand, the Green's approach with the same model and data, and at the same altitude, has yielded considerably smaller errors (table 4.11). Attempts to use smaller grid

AD-A109 856 OHIO STATE UNIV COLUMBUS DEPT OF GEODETIC SCIENCE A--ETC F/G 8/5
SIMULATION STUDIES ON THE COMPUTATION OF THE GRAVITY VECTOR IN --ETC(U)
JUN 81 K E KATSAMBALOS F19628-79-C-0027
UNCLASSIFIED 314 AFGL-TR-81-0187 NL

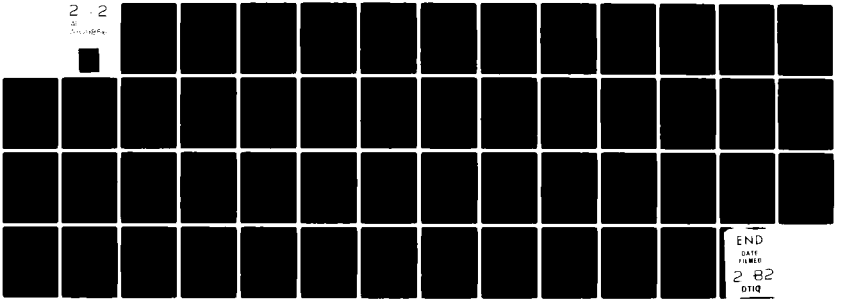

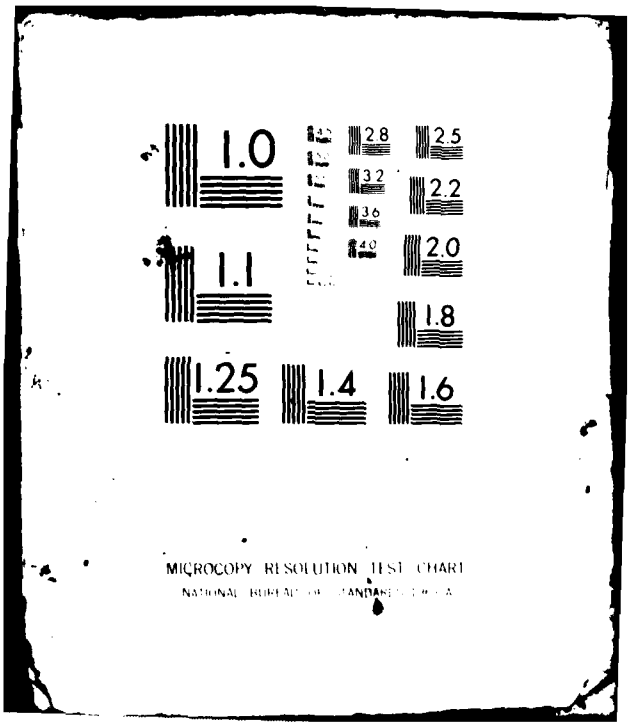
1.0
1.1
1.25
1.4
1.6
2.8
3.2
3.6
4.0
2.5
2.2
2.0
1.8
MICROCOPY RESOLUTION TEST CHART

spacing with the Dirac approach failed, because of the divergence of the iterative solution for the spikes.

All the tests in the present study use synthetic data on the surface of the models, and therefore, there are no data errors (the gravity anomalies are rigorously computed from the two point masses). In addition, and similarily to the simulations with the Green's approach, due to the very local characteristics of the models(figure 3.2 through 3.5), there are no significant truncation errors (i.e. errors caused by neglecting the information outside of the working area). The resulting errors which are given in tables 6.3 through 6.9 are due only to the following factors:

(a). Errors in the numerical solution for the gravity spikes, and
(b). Errors caused by using a small number of data points on the surface of the model.

From our experience with the simulations above, we can draw the following conclusions:

1. As the altitude of the space point increases, the errors increase too. This effect is opposite to that from the Green's approach. Possibly, the small amount of data points on the surface of the models (determined by the grid spacing), is responsible for this discrepancy.

2. In general, the errors over the model seem to be smaller than at the distant points, again in contrast to the Green's approach.

3. The finer the grid spacing, the smaller the errors become, but the disadvantage of the Dirac approach is that it will not converge with very dense data at high elevations.

4. The larger the inclination of the model, the larger the errors become, again in contrast to the results from the Green's approach. It seems that the Dirac approach is more sensitive to high inclinations than the Green's approach. For a smooth topography (the case of the spherical cap model, and of the 10°-inclination cone), the Dirac approach is superior to the Green's approach.

Table 6.3: Comparison of Gravity Disturbance Vector Components in Space Computed Rigorously, and From the Dirac Discrete Approach
(values in mgal; height in meters)

Region Size (Degrees): 2.00 x 2.00
Grid Interval (Minutes): 5.0

Spherical Cap Model

LAT	LON	HEIGHT	EXACT: RADIAL	EXACT: HORIZ	COMPUTED: RADIAL	COMPUTED: HORIZ	DIFFERENCES: RADIAL	DIFFERENCES: HORIZ	PERCENTAGE DIF: RADIAL	PERCENTAGE DIF: HORIZ
45	250 0'	5000.	-105.50	0.0	-36.24	-0.04	-69.26	0.04	65.65	*******
45	250 10'	5000.	-14.98	-15.93	-11.25	-10.90	-3.73	-5.03	24.93	31.60
45	250 20'	5000.	-2.83	-5.93	-2.42	-4.65	-0.41	-1.28	14.64	21.65
45	250 30'	5000.	-0.92	-2.88	-0.82	-2.32	-0.10	-0.56	10.55	19.60
45	250 40'	5000.	-0.41	-1.67	-0.38	-1.36	-0.03	-0.31	7.51	18.30
45	250 50'	5000.	-0.21	-1.09	-0.21	-0.90	-0.01	-0.19	3.86	17.37
45	251 0'	5000.	-0.13	-0.76	-0.11	-0.65	-0.01	-0.12	10.32	15.18

Table 6.4: Comparison of Gravity Disturbance Vector Components in Space Computed Rigorously, and From the Dirac Discrete Approach
(values in mgal; height in meters)

Region Size (Degrees): 0.40 x 0.40
Grid Interval (Minutes): 1.0

Spherical Cap Model

LAT	LON	HEIGHT	EXACT: RADIAL	EXACT: HORIZ	COMPUTED: RADIAL	COMPUTED: HORIZ	DIFFERENCES: RADIAL	DIFFERENCES: HORIZ	PERCENTAGE DIF: RADIAL	PERCENTAGE DIF: HORIZ
45	250 0'	5000.	-105.50	0.0	-103.82	-0.53	-1.67	0.53	1.59	*******
45	250 2'	5000.	-82.13	-21.20	-82.09	-21.32	-0.04	0.11	0.05	0.53
45	250 4'	5000.	-55.29	-25.21	-55.21	-25.21	-0.07	0.00	0.13	0.00
45	250 6'	5000.	-35.67	-23.38	-35.69	-23.54	0.02	0.16	0.05	0.67
45	250 8'	5000.	-22.91	-19.70	-22.83	-19.93	-0.08	0.22	0.33	1.14
45	250 10'	5000.	-14.98	-15.93	-14.88	-16.22	-0.10	0.29	0.67	1.82
45	250 12'	5000.	-10.10	-12.87	-9.89	-13.36	-0.21	0.49	2.12	3.80

Table 6.5: Comparison of Gravity Disturbance Vector Components in Space Computed Rigorously, and From the Dirac Discrete Approach
(values in mgal; height in meters)

Region Size (Degrees): 0.40 x 0.40
Grid Interval (Minutes): 1.0

Inclination (Degrees): 10.543

LAT	LON	HEIGHT	EXACT: RADIAL	EXACT: HORIZ	COMPUTED: RADIAL	COMPUTED: HORIZ	DIFFERENCES: RADIAL	DIFFERENCES: HORIZ	PERCENTAGE DIF: RADIAL	PERCENTAGE DIF: HORIZ
45	250 0'	5000.	-105.36	0.0	-103.90	-0.22	-1.45	0.22	1.38	*******
45	250 2'	5000.	-82.06	-21.19	-82.13	-21.20	0.07	0.01	0.08	0.06
45	250 4'	5000.	-55.21	-25.21	-55.30	-25.37	0.09	0.16	0.16	0.62
45	250 6'	5000.	-35.67	-23.38	-35.64	-23.67	-0.03	0.29	0.08	1.24
45	250 8'	5000.	-22.93	-19.64	-22.78	-20.06	-0.15	0.42	0.65	2.15
45	250 10'	5000.	-14.98	-15.93	-14.58	-16.46	-0.40	0.53	2.70	3.34
45	250 12'	5000.	-10.10	-12.87	-9.21	-13.31	-0.90	0.44	8.87	3.39

Table 6.6: Comparison of Gravity Disturbance Vector Components in Space Computed Rigorously, and From the Dirac Discrete Approach
(values in mgal; height in meters)

Region Size (Degrees): 0.40 x 0.40
Grid Interval (Minutes): 1.0

Inclination (Degrees): 10.543

LAT	LON	HEIGHT	EXACT: RADIAL	EXACT: HORIZ	COMPUTED: RADIAL	COMPUTED: HORIZ	DIFFERENCES: RADIAL	DIFFERENCES: HORIZ	PERCENTAGE DIF: RADIAL	PERCENTAGE DIF: HORIZ
45	250 0'	10000.	-36.89	0.0	-36.74	-0.03	-0.15	0.03	0.40	*******
45	250 2'	10000.	-34.66	-4.88	-34.49	-4.93	-0.17	0.06	0.48	1.14
45	250 4'	10000.	-29.48	-8.21	-29.30	-8.32	-0.19	0.11	0.63	1.32
45	250 6'	10000.	-23.43	-9.66	-23.16	-9.81	-0.27	0.16	1.16	1.61
45	250 8'	10000.	-17.93	-9.78	-17.57	-9.98	-0.36	0.20	2.01	2.07
45	250 10'	10000.	-13.51	-9.17	-12.97	-9.34	-0.54	0.17	4.02	1.90
45	250 12'	10000.	-10.15	-8.24	-9.54	-8.41	-0.60	0.17	5.95	2.04

Table 6.7: Comparison of Gravity Disturbance Vector Components in Space Computed Rigorously, and From the Dirac Discrete Approach
(values in mgal; height in meters)

Region Size (Degrees): 0.40 x 0.40
Grid Interval (Minutes): 1.0

Inclination (Degrees): 10.543

			EXACT:		COMPUTED:		DIFFERENCES:		PERCENTAGE DIF	
LAT	LON	HEIGHT	RADIAL	HORIZ	RADIAL	HORIZ	RADIAL	HORIZ	RADIAL	HORIZ
45	250	0' 20000.	-12.06	0.0	-11.72	-0.00	-0.34	0.00	2.80	*******
45	250	2' 20000.	-11.84	-0.93	-11.49	-0.94	-0.35	0.01	2.93	1.17
45	250	4' 20000.	-11.21	-1.76	-10.86	-1.78	-0.35	0.02	3.12	1.22
45	250	6' 20000.	-10.29	-2.42	-9.92	-2.44	-0.37	0.02	3.62	0.91
45	250	8' 20000.	-9.19	-2.88	-8.80	-2.91	-0.40	0.03	4.36	0.92
45	250	10' 20000.	-8.05	-3.15	-7.64	-3.17	-0.41	0.02	5.14	0.48
45	250	12' 20000.	-6.95	-3.26	-6.51	-3.26	-0.44	-0.00	6.27	0.09

Table 6.8: Comparison of Gravity Disturbance Vector Components in Space Computed Rigorously, and From the Dirac Discrete Approach
(values in mgal; height in meters)

Region Size (Degrees): 0.40 x 0.40
Grid Interval (Minutes): 1.0

Inclination (Degrees): 10.543

			EXACT:		COMPUTED:		DIFFERENCES:		PERCENTAGE DIF	
LAT	LON	HEIGHT	RADIAL	HORIZ	RADIAL	HORIZ	RADIAL	HORIZ	RADIAL	HORIZ
45	250	0' 100000.	-0.63	0.0	-0.55	-0.00	-0.08	0.00	12.15	*******
45	250	2' 100000.	-0.63	-0.01	-0.55	-0.01	-0.08	-0.00	12.17	3.19
45	250	4' 100000.	-0.63	-0.02	-0.55	-0.02	-0.08	-0.00	12.13	7.37
45	250	6' 100000.	-0.62	-0.03	-0.55	-0.03	-0.08	-0.00	12.24	7.44
45	250	8' 100000.	-0.62	-0.04	-0.54	-0.04	-0.08	-0.00	12.27	7.96
45	250	10' 100000.	-0.61	-0.05	-0.54	-0.05	-0.07	-0.00	12.21	7.95
45	250	12' 100000.	-0.61	-0.07	-0.53	-0.06	-0.08	-0.01	12.39	8.35

Table 6.9: Comparison of Gravity Disturbance Vector Components in Space Computed Rigorously, and From the Dirac Discrete Approach
(values in mgal; height in meters)

Region Size (Degrees): 0.40 x 0.40
Grid Interval (Minutes): 1.0

Inclination (Degrees): 39.976

				EXACT:		COMPUTED:		DIFFERENCES:		PERCENTAGE DIF	
LAT	LON		HEIGHT	RADIAL	HORIZ	RADIAL	HORIZ	RADIAL	HORIZ	RADIAL	HORIZ
45	250	0'	10000.	-36.23	0.0	-25.66	-0.06	-10.58	0.06	29.19	*******
45	250	2'	10000.	-34.11	-4.79	-23.49	-4.10	-10.62	-0.69	31.14	14.40
45	250	4'	10000.	-28.96	-8.03	-18.57	-6.49	-10.39	-1.54	35.88	19.16
45	250	6'	10000.	-23.06	-9.49	-13.36	-7.04	-9.69	-2.45	42.05	25.79
45	250	8'	10000.	-17.69	-9.63	-9.20	-6.51	-8.49	-3.11	48.01	32.36
45	250	10'	10000.	-13.31	-9.02	-6.30	-5.62	-7.01	-3.40	52.66	37.72
45	250	12'	10000.	-9.97	-8.10	-4.39	-4.71	-5.58	-3.39	55.96	41.87

6.3 Comparison of the Green's with the Dirac Approach

In section 4.2 and 6.2 we prsented the simulation studies with the two approaches. Let us now review the results, and compared the two methods.

The Green's approach requires as data gravity disturbances δg on the surface of the earth, the disturbing potential T, the elevation h, and the two components of the inclination at these points. Actually, δg, T, and h are referred to the center of the blocks, after a subdivision of the surface has been made using a certain grid spacing, and the whole approach is thus an approximation. The fact that the errors of δ are not reduced by using a finer grid, is an indication that this kind of approximation (combined with the neglect of 2nd order variations of the topography) is not sufficient. The method does not work on the surface, and close to it gives very large errors. As the altitude of the space point increases, the errors descrease. Because of the very local characteristic of the model used in the simulations, the increase of the integration area does not reduce the errors, and hence, there are no significant truncation errors. Also, as the inclination of the model increases, (beyond 20°), the errors become smaller. The method is much faster than the Dirac approach, but it requires the data be given on a regular grid.

The Dirac approach requires as data only surface gravity anomalies and elevations at points, not necessarily on a regular grid. The method requires an iterative solution for the anomalies on the geosphere, which might diverge for dense data at high elevations. As the inclination of the model increases, the errors increase. The same happens when the altitude of the space point increases, but the errors are stil smaller than those from the Green's approach. In general, this method works well, both close to the surface of the earth, and at high altitudes. Its basic disadvantage is the fact that it cannot be used for large amounts of data, since it involves an analytical solution for the anomalies on the geosphere, which is a very time-consuming process. Also, it might diverge for very dense data at high elevations.

If it is a matter of choice between the two methods, from our experience with these simulation studies, we would recommend the Green's approach for high altitudes, with a large number of data on the surface of the earth, and the Dirac approach close to the surface, if a small number of point data is available.

6.4 Related Work

A number of authors have applied Bjerhammar's methods for the computation of the external gravity field of the earth. Some of them followed the original method (based on the mean-value approach), and some other have developed methods based on the fitting of the surface data to an m-degree polynomial. To the best of my knowledge, the Dirac approach has never been applied to real or simulated data for the computaion of the complete gravity vector in space, without neglecting the topography.

The earliest work on this subject was published by Reit (1966). It is a flat-earth (planar approximation) simulation study, using two models, one of which is almost identical to the conical model described in chapter 3. The gravity anomalies on the geosphere (Δg^*), are computed iteratively, and the ξ -component of the deflection of the vertical is computed and compared to its exact value on the model's surface, and in space. The errors are almost two times larger than those found from our analysis. For example, from Reit's tables 5 and 6, the errors at 5 km above the cone are almost 10%, while at the same altitude the errors from the Dirac approach are less than 2% (tables 6.4 and 6.5). For reasons that will be explained in the chapter 9 we have to point out that Reit computed the ξ -component on the surface of the model at the same points where the "synthetic" data is given.

Forstner (1966) used 125 gravity anomalies in Cyprus, and performed four polynomial fittings to this data. However, these methods were applied in computing surface components of the gravity vector only. In addition, the RMS difference between the original data, and the anomalies computed from the reduced (Δg^*) data, was found to be between 7 and 22 mgal (Forstner, ibid, p.55). This difference is much larger than that found from our tests (see table 6.1), despite of the fact that the maximum elevation on our model is 4.1 km, as opposed to 1.8 km over Cyprus.

Barlik (1971) describes other methods which are proposed for areas with high elevations in order to avoid the divergence problems which are encountered by Forstner (ibid). An auxiliary sphere is used, not imbedded inside the earth as the geosphere, that the terms $t_j = R_B/r_j$ are not very small for the points at high elevations. However, the proposed method is not fully automatted, and the evaluation of terrain corrections is required.

The original work by Bjerhammar (1963, 1975, 1976, 1978), and that by Sjöberg (1975, 1978), have already been mentioned in section 5.1. Bjerhammar (1976) has presented some results from the application of the Dirac approach for the computation

of deflections of the vertical on the surface of the earth. Finally, Sjöberg (1975, 1978) has worked with a limited amount of real data for the computation of gravity anomalies on the surface of the earth. Because we feel that these results need some additional elaboration, we will repeat his tests in chapter 9 with some comments.

Chapter 7

COMPUTATION OF THE GRAVITY DISTURBANCE VECTOR IN SPACE USING THE METHOD OF LEAST SQAUARES COLLOCATION

7.1 Introduction

Let us now apply the method of least-Squares Collocation to the estimation of the components of $\vec{\delta}$, from the simulated data on the surface of the model. As with the other two methods in this report, it is easy to evaluate the applicability of collocation to our problem, because the exact components of $\vec{\delta}$ can be computed directly from the model.

A great number of papers have been published on applications of collocation to the determination of the gravity field of the earth, on its surface as well as in the exterior space. For the estimation of gravity anomalies, geoidal undulations, and deflections of the vertical see for example in (Lachapelle, 1977; Sjöberg, 1978; Tscherning and Forsberg, 1978; Forsberg and Tscherning, 1981). For computation of gravity anomalies in space see Rapp and Hajela (1975). For the computation of the covariance functions - the most essential quantities in any estimation through collocation, see Tscherning and Rapp (1974), Tscherning (1976), and Sünkel (1979). Advanced aspects on collocation are discussed in Moritz (1980), and Moritz and Sünkel (1978).

The collocation estimation of a quantity s from gravity anomalies Δg , can be done using the equation below (Moritz, 1972):

$$s = \underline{C}_{s,\Delta g} \, (\underline{C}_{\Delta g,\Delta g} + \underline{D})^{-1} \, \underline{\Delta g} \qquad (7.1)$$

where:

- $\underline{\Delta g}$: the vector of the m observations of gravity anomalies
- $\underline{C}_{\Delta g,\Delta g}$: the covariance matrix (m x m) of the observed anomalies.
- $\underline{D}$: the covariance matrix (m x m) of the measuring errors in the anomalies. This is taken to be a null matrix, since we assume errorless observations for our simulation study.
- $\underline{C}_{s,\Delta g}$: the cross-covariance vector (m), between the quantity s to be predicted, and the gravity observations.

The predicted s might be any quantity as long as the corresponding covariance function between s and the data (Δg) exists. For example, s may be geoidal undulation, gravity anomaly, first or higher order derivative of the disturbing potential, etc. The two problems that we encounter in any collocation prediction are (a) the inversion of a large matrix $(\underline{C}+\underline{D})$ in case of a large number of data, and (b) the computation of the auto - and cross-covariances between the various quantities in (7.1).

For the computation of the various covariances we decided to use the covariance approximation procedure which is documented in Sünkel (1979). In fact, we have used a new version of his computer program, documented in Sünkel (1980), the difference between the old and the new version being minor. The whole procedure is based on the generation of a sufficiently dense network of covariances, and then, on the computation of any other covariance at a point inside this network by a differentiation - interpolation procedure with spline functions. The accuracy of this procedure can be as high as we wish, depending on the density or the covariance network. Interpolating at any other point from the grid values, rather than computing the covariance directly, reduces the CPU time significantly (Sünkel, 1979, p.22).

7.2 Collocation Prediction of the Gravity Disturbance Vector

The computer program mentioned above, computes the auto- and cross-covariances between fourteen quantities, among which we find the radial component of the disturbing potential, and the components of the deflection of the vertical:

$$-\frac{\frac{\partial T}{\partial r}}{r} \qquad \text{in Eötvös} \quad (1\ E = 10^{-9}\,\text{sec}^{-2})$$

ξ in arcsec

η in arcsec

Δg in mgal

For simplicity, let us denote by $\underline{Q}$ the product $\underline{C}^{-1}\ \underline{\Delta g}$ in (7.1):

$$\underline{Q}_{,1} = \underline{C}^{-1}_{\Delta\rho\ \Delta g}\ \underline{\Delta g} = \begin{vmatrix} \text{cov}(\Delta g_1,\Delta g_1) & \cdots & \text{cov}(\Delta g_1,\Delta g_m) \\ \vdots & & \\ \text{cov}(\Delta g_m,\Delta g_1) & \cdots & \text{cov}(\Delta g_m,\Delta g_m) \end{vmatrix}^{-1} \begin{vmatrix} \Delta g \\ \vdots \\ \Delta g_m \end{vmatrix} \tag{7.2}$$

Then, the application of (7.1) to the determination of the quantities: $-(\partial T/\partial r)/r$, ξ , and η yields:

$$-(1/r)\partial T/\partial r = [\mathrm{cov}(-1/r)\partial T/\partial r,\ \Delta g_1],\ldots]\ \underline{Q}\ ,\ \text{in Eötvös}$$

$$\xi = [\mathrm{cov}(\xi,\Delta g_1),\ .\ .\ .]\ \underline{Q}\ ,\ \text{in arcsec}$$

$$\eta = [\mathrm{cov}(\eta,\Delta g_1),\ .\ .\ .]\ \underline{Q}\ ,\ \text{in arcsec}$$

The partial derivatives of the disturbing potential with respect to r , $\bar{\phi}$, and λ, are then given from the well-known equations (Sünkel, ibid, p.21):

$$\frac{\partial T}{\partial r} = -r\left(-\frac{\partial T/\partial r}{r}\right)\ ,\ \text{in } 10^{-9}\,\mathrm{m.sec^{-2}}$$

$$\frac{\partial T}{\partial \phi} = -r\,\gamma\,\xi\ ,\ \text{in m .sec}^{-2}\text{. arsec}$$

$$\frac{\partial T}{\partial \lambda} = -r\gamma\cos\bar{\phi}\,\eta\ ,\ \text{in m .sec}^{-2}\text{. arsec} \qquad (7.4)$$

The components of T can now be transformed to components of the gravity disturbance vector $\vec{\delta}$, using (5.22):

$$\delta g_r = \frac{\partial T}{\partial r} = -r\left(-\frac{\partial T/\partial r}{r}\right)10^{-9}\ ,\ \text{in m.sec}^{-2}$$

$$\delta g_{\bar{\phi}} = \frac{1}{r}\frac{\partial T}{\partial \bar{\phi}} = -\gamma\xi\,\frac{1}{206264.806}\ ,\ \text{in m.sec}^{-2}$$

$$\delta g_\lambda = \frac{1}{r\cos\bar{\phi}}\,\frac{\partial T}{\partial \lambda} = -\gamma\eta\,\frac{1}{206264.806}\ ,\ \text{in m.sec}^{-2} \qquad (7.5)$$

Then, equation (5.32) is used to rotate the components of $\vec{\delta}$ to a geocentric (X , Y , Z) system:

$$\begin{vmatrix} \frac{\partial T}{\partial X} \\ \frac{\partial T}{\partial Y} \\ \frac{\partial T}{\partial Z} \end{vmatrix} = \begin{vmatrix} \delta g_X \\ \delta g_Y \\ \delta g_Z \end{vmatrix} = \begin{vmatrix} \cos\bar{\phi}_p\cos\lambda_p & -\sin\bar{\phi}_p\cos\lambda_p & -\sin\lambda_p \\ \cos\bar{\phi}_p\sin\lambda_p & -\sin\bar{\phi}_p\sin\lambda_p & \cos\lambda_p \\ \sin\bar{\phi}_p & \cos\bar{\phi}_p & 0 \end{vmatrix} \begin{vmatrix} \delta g_r \\ \delta g_{\bar{\phi}} \\ \delta g_\lambda \end{vmatrix} \qquad (7.6)$$

where the index P means that the computations are made at the space point P (r_P , $\bar{\phi}_P$, λ_P).

Finally, equations (3.24) and (3.25) can be used to rotate these components to the polar (r , ψ) coordinate system in order to obtain the two distinct components $\partial T/\partial r$, and $(1/r)\ \partial T/\partial \psi$ for the simulation tests.

7.3 Simulation Tests with the Collocation Approach

As we described in sections 4.2 and 6.2 for the Green's and for the Dirac approaches respectively, the terrain model of chapter 3 is used again, and the gravity anomalies are generated on its surface from the two point masses to be used in the collocation prediction.

The covariance network which is the most time-consuming part in the covariance approximation procedure just mentioned, is also generated in space, from the surface of the sphere up to an altitude of 111 km in radial direction, and from the center of the model up to 125' in spherical distance. The grid has to be denser for smaller altitudes than for higher altitudes, and denser for smaller spherical distances than for larger ones (Sünkel, 1979, p.5). From our preliminary tests with the collocation approach, we found that a non-uniform grid as it is shown in figure 7.1 would be sufficient for the prediction of the components of the gravity disturbance vector up to an altitude of 100 km. The grid that we constructed has a spacing of 1 km up to the 11 km altitude, and then the spacing becomes 10 km up to the maximum 111 km radial distance. In the spherical direction, the grid spacing is 0'.5 for the first 5', then it is 1' for the next 20', and finally it becomes 10' up to the maximum spherical distance of 125'. It takes approximately 18 CPU-seconds in an Amdahl 470/6-II maching for the construcion of such a grid.

The Tscherning and Rapp (1974 , 4th model) anomaly degree variance model was used for the computation of the covariance network. This model corresponds to the 2nd model in Sünkel's program (see also equation (9.7), section 9.3). Preliminary tests indicated that the use of a "global" versus a "local" n^{th}-degree covariance function (the first n anomaly degree variances are set equal to zero), is not a critical factor for the computation of $\vec{\delta}$. The use of a global, of a 20th-degree, and of a 40th-degree covariance functions, resulted to components of $\vec{\delta}$, which are different by no more than 0.5 mgal. The fact that the collocation prediction is not sensitive to the covariance function being used, has been verified in numerous applications of collocation (see for example in: Rapp and Agajelu, 1975, p.9; Lachapelle, 1977; Rapp, 1979-a; Katsambalos, 1980).

One might argue that the covariance function being used should be consistent with the synthetic data on the models. Theoretically, this is necessary due to the fact that the center of mass of the models does not coincide with the center of the mass of the earth (the center of the sphere R in our case). The construction of a covariance function is a very laborious procedure, especially for our simulation tests where a great number of different models are used. In addition, as we mentioned above, from our preliminary tests it was found that the predicted quantities are not sensitive to the covariance function being used. Therefore, for simplicity we decided to use the global Tscherning-Rapp covariance function.

After the covariance network is set-up, the equations of the previous section can be used for the collocation prediction of the components of $\vec{\delta}$. The radii r_P, r_Q are computed as $r_P = R + h_P$, $r_Q = R + h_Q$, where h_P, h_Q are the heights of the space point P of the surface point Q above the mean-earth sphere R.

In table 7.1 the relative percentage errors of the vector $\vec{\delta}$ at 5 km altitude are shown in the usual form. 256 anomalies are generated on the surface of a 10° conical model, on a 3' grid within a 0.8°x 0.8° area. These errors are about 20% above the cone, they reach a maximum of 70%, and then they fall below the 10% level. By decreasing the grid spacing to 2' within the same area (576 anomalies on the surface of the model now), the errors at 5 km are now 10% (table 7.2), but they grow larger as we go away from the model's axis towards the boundary of the area.

Table 7.3 shows the errors at 10 km altitude using the 10° conical model again. Comparing these errors with those at 5 km (table 7.1), we see that they are almost an order of magnitude smaller right above the model's center, but they are larger away from it. At higher altitudes (100 km and above) the errors from the collocation approach were found to be very large (more than 100%). Any attempt to increase the size of the area with 2' or 3' grid spacing, would require the inversion of large matrix $\underline{C}$. Not that it takes about 4 minutes CPU time to form and invert a 576 X 576 symmetric matrix of the covariances (the IMSL subroutine LINV3P was used).

For a direct comparison between the Dirac and the collocation approaches, the components of $\vec{\delta}$ at 5 km altitude are tabulated in table 7.7 using the same model (10° cone), and the same data (576 anomalies on a 2' grid, within a 0.8°x 0.8° area). The results from the collocation approach are in a better agreement with the exact components of $\vec{\delta}$ right above the model's center, but the Dirac approach is obviously superior at the other points.

The errors from a 40°-inclination model (table 7.4 , compared to those from a 10°-model, (table 7.2), are larger over the cone, but smaller away from it. In order to decrease the errors at the points away from the model's axis, we should increase the working area beyond 1°x 1°, but that would require the inversion of a very large matrix. Therefore, the application of collocation to our problem seems to be a very time consuming approach.

For the very smooth topography of the spherical cap model which was described in section 3.5, the errors are smaller when compared to those from the conical model, and they become almost zero at point away from the model (tables 7.5 and 7.6). This is true not only at 5 km altitude, but also at 10 km altitude.

In order to investigate the effect of the topography on the collocation approach, we made an additional test for which the elevations of the surface points were forced to be equal to zero(the remaining specifications for this test are identical to those in table 7.2). The results from this test are given in table 7.8. Comparing the errors given in tables 7.2 and 7.8, we see that the effect of the topography is very significant, since the errors from the new test are much larger above the model's center, than those in table 7.2.

From our experience from the simulation tests with the collocation prediction of $\vec{\delta}$, we can make the following conclusions.

(a). Collocation is a very time consuming approach, especially in handling a large amount of surface data.
(b). The errors in $\vec{\delta}$ are very large for altitudes larger than 10 km (relative percentage errors at the 100% level and above)
(c). For data given on a very smooth topography, the errors at 5 km, and 10 km altitude are relatively small (compared to the errors from the conical models), but not as small as those from the Dirac approach.
(d). On an overall basis, the Dirac approach seems to be superior as compared to the collocation approach.

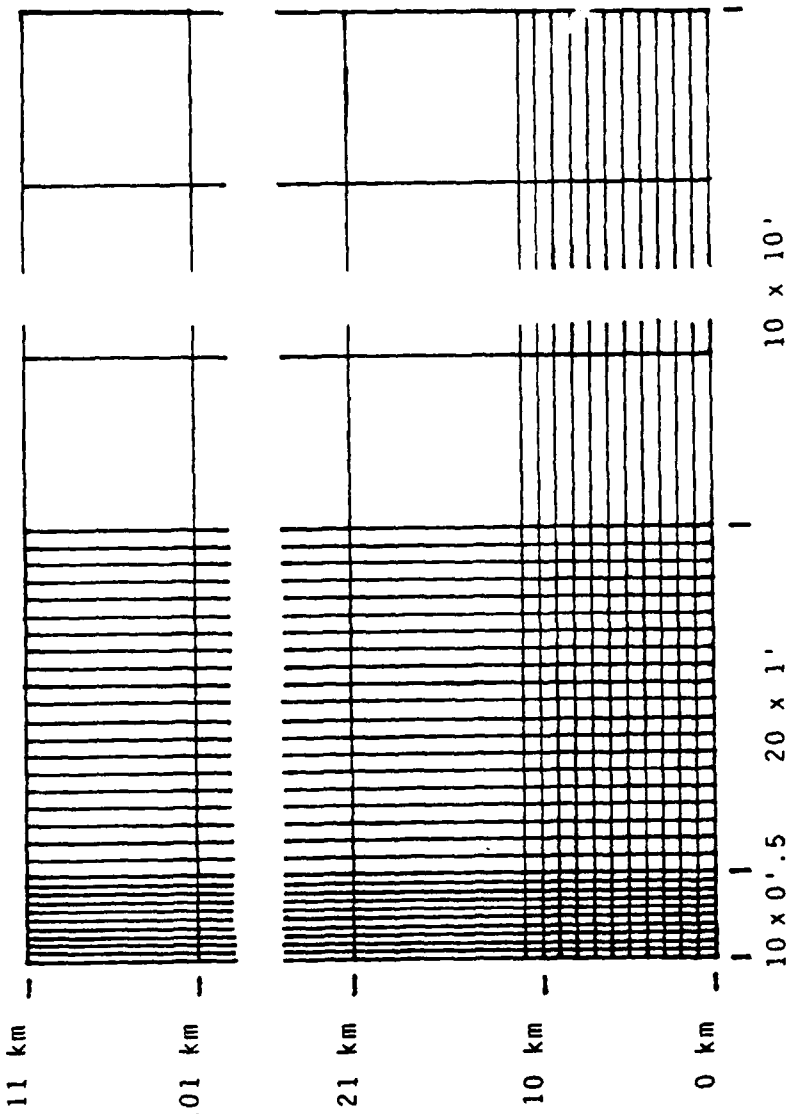

Figure 7.1

The Network for the Covariance Approximation Procedure

Table 7.1: Comparison of Gravity Disturbance Vector Components in Space Computed Rigorously, and From the Collocation Approach
(values in mgal; height in meters)

Region Size (Degrees): 0.80 x 0.80
Grid Interval (Minutes): 3.0

Inclination (Degrees): 10.543

LAT	LON	HEIGHT	EXACT: RADIAL	EXACT: HORIZ	COMPUTED: RADIAL	COMPUTED: HORIZ	DIFFERENCES: RADIAL	DIFFERENCES: HORIZ	PERCENTAGE DIF RADIAL	PERCENTAGE DIF HORIZ
45	250 0'	5000.	-105.36	0.0	-83.69	-0.04	-21.67	0.04	20.57	*******
45	250 2'	5000.	-82.06	-21.19	-74.39	-15.44	-7.67	-5.76	9.35	27.16
45	250 4'	5000.	-55.21	-25.21	-54.04	-22.74	-1.17	-2.48	2.12	9.82
45	250 6'	5000.	-35.67	-23.38	-35.37	-21.97	-0.31	-1.41	0.86	6.04
45	250 8'	5000.	-22.93	-19.64	-23.38	-18.37	0.45	-1.27	1.94	6.46
45	250 10'	5000.	-14.98	-15.93	-15.72	-14.86	0.74	-1.06	4.92	6.68
45	250 12'	5000.	-10.10	-12.87	-10.83	-11.65	0.73	-1.22	7.18	9.49

Table 7.2: Comparison of Gravity Disturbance Vector Components in Space Computed Rigorously, and From the Collocation Approach
(values in mgal; height in meters)

Region Size (Degrees): 0.80 x 0.80
Grid Interval (Minutes): 2.0

Inclination (Degrees): 10.543

LAT	LON	HEIGHT	EXACT: RADIAL	EXACT: HORIZ	COMPUTED: RADIAL	COMPUTED: HORIZ	DIFFERENCES: RADIAL	DIFFERENCES: HORIZ	PERCENTAGE DIF RADIAL	PERCENTAGE DIF HORIZ
45	250 0'	5000.	-105.36	0.0	-95.51	-0.05	-9.85	0.05	9.35	*******
45	250 2'	5000.	-82.06	-21.19	-85.18	-16.07	3.12	-5.12	3.80	24.16
45	250 4'	5000.	-55.21	-25.21	-62.99	-23.01	7.77	-2.20	14.08	8.74
45	250 6'	5000.	-35.67	-23.38	-43.20	-21.67	7.53	-1.72	21.10	7.33
45	250 8'	5000.	-22.93	-19.64	-30.40	-17.45	7.47	-2.19	32.58	11.14
45	250 10'	5000.	-14.98	-15.93	-22.81	-13.14	7.83	-2.79	52.24	17.51
45	250 12'	5000.	-10.10	-12.87	-18.14	-9.61	8.04	-3.26	79.57	25.34

Table 7.3: Comparison of Gravity Disturbance Vector Components in Space Computed Rigorously, and From the Collocation Approach
(values in mgal; height in meters)

Region Size (Degrees): 0.80 x 0.80
Grid Interval (Minutes): 3.0

Inclination (Degrees): 10.543

LAT	LON	HEIGHT	EXACT: RADIAL	EXACT: HORIZ	COMPUTED: RADIAL	COMPUTED: HORIZ	DIFFERENCES: RADIAL	DIFFERENCES: HORIZ	PERCENTAGE DIF RADIAL	PERCENTAGE DIF HORIZ
45	250 0'	10000.	-36.89	0.0	-36.09	-0.03	-0.80	0.03	2.18	*******
45	250 2'	10000.	-34.66	-4.88	-34.29	-4.29	-0.38	-0.59	1.08	12.00
45	250 4'	10000.	-29.48	-8.21	-29.72	-7.33	0.23	-0.88	0.79	10.68
45	250 6'	10000.	-23.43	-9.66	-24.06	-8.70	0.63	-0.95	2.68	9.85
45	250 8'	10000.	-17.93	-9.78	-18.93	-8.78	1.01	-1.00	5.61	10.19
45	250 10'	10000.	-13.51	-9.17	-14.73	-8.12	1.21	-1.05	8.98	11.48
45	250 12'	10000.	-10.15	-8.24	-11.52	-7.11	1.38	-1.13	13.59	13.70

Table 7.4: Comparison of Gravity Disturbance Vector Components in Space Computed Rigorously, and From the Collocation Approach
(values in mgal; height in meters)

Region Size (Degrees): 0.80 x 0.80
Grid Interval (Minutes): 2.0

Inclination (Degrees): 39.976

LAT	LON	HEIGHT	EXACT: RADIAL	EXACT: HORIZ	COMPUTED: RADIAL	COMPUTED: HORIZ	DIFFERENCES: RADIAL	DIFFERENCES: HORIZ	PERCENTAGE DIF RADIAL	PERCENTAGE DIF HORIZ
45	250 0'	5000.	-102.66	0.0	-81.07	-0.04	-21.61	0.04	21.20	*******
45	250 2'	5000.	-80.44	-20.61	-71.88	-14.29	-8.56	-6.33	10.64	30.70
45	250 4'	5000.	-54.31	-24.67	-52.68	-20.62	-1.64	-4.05	3.02	16.41
45	250 6'	5000.	-35.09	-22.97	-35.40	-20.03	0.31	-2.95	0.87	12.83
45	250 8'	5000.	-22.52	-19.34	-23.51	-16.74	0.99	-2.60	4.37	13.47
45	250 10'	5000.	-14.78	-15.68	-16.02	-12.97	1.24	-2.71	8.39	17.31
45	250 12'	5000.	-9.96	-12.62	-11.54	-9.76	1.58	-2.87	15.83	22.71

Table 7.5: Comparison of Gravity Disturbance Vector Components in Space Computed Rigorously, and From the Collocation Approach
(values in mgal; height in meters)

Region Size (Degrees): 0.80 x 0.80
Grid Interval (Minutes): 2.0

Spherical Cap Model

LAT	LON	HEIGHT	EXACT: RADIAL	EXACT: HORIZ	COMPUTED: RADIAL	COMPUTED: HORIZ	DIFFERENCES: RADIAL	DIFFERENCES: HORIZ	PERCENTAGE DIF RADIAL	PERCENTAGE DIF HORIZ
45	250 0'	5000.	-105.50	0.0	-88.95	-0.01	-16.55	0.01	15.69*******	
45	250 2'	5000.	-82.13	-21.20	-79.07	-16.24	-3.06	-4.96	3.73	23.41
45	250 4'	5000.	-55.29	-25.21	-56.76	-24.14	1.47	-1.08	2.66	4.27
45	250 6'	5000.	-35.67	-23.38	-35.94	-23.66	0.27	0.27	0.75	1.16
45	250 8'	5000.	-22.91	-19.70	-22.58	-19.79	-0.32	0.08	1.41	0.43
45	250 10'	5000.	-14.98	-15.93	-15.00	-15.86	0.02	-0.07	0.16	0.42
45	250 12'	5000.	-10.10	-12.87	-10.25	-12.83	0.15	-0.04	1.46	0.33

Table 7.6: Comparison of Gravity Disturbance Vector Components in Space Computed Rigorously, and From the Collocation Approach
(values in mgal; height in meters)

Region Size (Degrees): 0.80 x 0.80
Grid Interval (Minutes): 2.0

Spherical Cap Model

LAT	LON	HEIGHT	EXACT: RADIAL	EXACT: HORIZ	COMPUTED: RADIAL	COMPUTED: HORIZ	DIFFERENCES: RADIAL	DIFFERENCES: HORIZ	PERCENTAGE DIF RADIAL	PERCENTAGE DIF HORIZ
45	250 0'	10000.	-36.89	0.0	-36.09	-0.03	-0.80	0.03	2.18*******	
45	250 2'	10000.	-34.80	-4.90	-34.24	-4.42	-0.56	-0.48	1.61	9.73
45	250 4'	10000.	-29.55	-8.21	-29.44	-7.71	-0.11	-0.50	0.38	6.14
45	250 6'	10000.	-23.43	-9.66	-23.50	-9.46	0.07	-0.20	0.31	2.07
45	250 8'	10000.	-17.93	-9.78	-17.99	-9.82	0.06	0.04	0.34	0.38
45	250 10'	10000.	-13.52	-9.17	-13.53	-9.19	0.01	0.02	0.10	0.22
45	250 12'	10000.	-10.15	-8.24	-10.24	-8.27	0.09	0.02	0.86	0.29

Table 7.7

Comparison of Gravity Disturbance Vector Components in Space, from the Dirac Approach, and From Collocation.
(values in mgal; height in meters)

Region Size (Degrees): 0.80 x 0.80
Grid Interval (Minutes): 2.0

Inclination (Degrees): 10.543

Dirac Approach:

LAT	LON	HEIGHT	EXACT: RADIAL	EXACT: HORIZ	COMPUTED: RADIAL	COMPUTED: HORIZ	DIFFERENCES: RADIAL	DIFFERENCES: HORIZ	PERCENTAGE DIF: RADIAL	PERCENTAGE DIF: HORIZ
45	250 0'	5000.	-105.36	0.0	-90.92	-0.02	-14.44	0.02	13.70	*******
45	250 2'	5000.	-82.06	-21.19	-77.67	-18.36	-4.40	-2.83	5.36	13.37
45	250 4'	5000.	-55.21	-25.21	-53.31	-24.41	-1.90	-0.81	3.45	3.21
45	250 6'	5000.	-35.67	-23.38	-34.35	-22.99	-1.32	-0.40	3.70	1.70
45	250 8'	5000.	-22.93	-19.64	-21.65	-19.55	-1.28	-0.08	5.60	0.42
45	250 10'	5000.	-14.98	-15.93	-13.54	-15.82	-1.44	-0.11	9.62	0.67
45	250 12'	5000.	-10.10	-12.87	-8.57	-12.67	-1.53	-0.20	15.18	1.53

Collocation Approach:

LAT	LON	HEIGHT	EXACT: RADIAL	EXACT: HORIZ	COMPUTED: RADIAL	COMPUTED: HORIZ	DIFFERENCES: RADIAL	DIFFERENCES: HORIZ	PERCENTAGE DIF: RADIAL	PERCENTAGE DIF: HORIZ
45	250 0'	5000.	-105.36	0.0	-95.51	-0.05	-9.85	0.05	9.35	*******
45	250 2'	5000.	-82.06	-21.19	-85.18	-16.07	3.12	-5.12	3.80	24.16
45	250 4'	5000.	-55.21	-25.21	-62.99	-23.01	7.77	-2.20	14.08	8.74
45	250 6'	5000.	-35.67	-23.38	-43.20	-21.67	7.53	-1.72	21.10	7.33
45	250 8'	5000.	-22.93	-19.64	-30.40	-17.45	7.47	-2.19	32.58	11.14
45	250 10'	5000.	-14.98	-15.93	-22.81	-13.14	7.83	-2.79	52.24	17.51
45	250 12'	5000.	-10.10	-12.87	-18.14	-9.61	8.04	-3.26	79.57	25.34

Table 7.8: Comparison of Gravity Disturbance Vector Components in Space Computed Rigorously, and From the Collocation Approach (values in mgal) (Elevations set equal to zero)

Region Size (Degrees): 0.80 x 0.80
Grid Interval (Minutes): 2.0

Inclination (Degrees): 10.543

LAT	LON	HEIGHT	EXACT: RADIAL	EXACT: HORIZ	COMPUTED: RADIAL	COMPUTED: HORIZ	DIFFERENCES: RADIAL	DIFFERENCES: HORIZ	PERCENTAGE DIF RADIAL	PERCENTAGE DIF HORIZ
45	250 0'	5000.	-105.36	0.0	-44.99	-0.02	-60.37	0.02	57.30	*******
45	250 2'	5000.	-82.06	-21.19	-42.02	-6.54	-40.04	-14.65	48.79	69.14
45	250 4'	5000.	-55.21	-25.21	-34.68	-10.84	-20.54	-14.37	37.19	57.00
45	250 6'	5000.	-35.67	-23.38	-26.32	-12.44	-9.35	-10.95	26.22	46.81
45	250 8'	5000.	-22.93	-19.64	-18.85	-12.14	-4.08	-7.50	17.78	38.19
45	250 10'	5000.	-14.98	-15.93	-13.29	-10.90	-1.69	-5.03	11.31	31.58
45	250 12'	5000.	-10.10	-12.87	-9.28	-9.42	-0.83	-3.45	8.19	26.84

Chapter 8

COMPARISON OF THE IMPROVED TECHNIQUES WITH THE CLASSICAL APPROACH

As we have already mentioned in chapter 1 , there exist three methods for the computation of δ (using gravity data reduced to the geoid), which were called the "classical" approaches:

1. the Direct Integration Method,
2. the Coating Method, and
3. the Upward Continuation Method.

The theory behind these methods can be found in Hirvonen and Moritz (1963); Heiskanen and Moritz (1967); Mueller (1966). The Direct Integration method is computationally the most difficult to use, but it requires the least amount of data, since the other two methods require - in addition to the gravity anomalies which are needed by all three - , geoidal undulations, and deflections of the vertical on the physical surface of the earth. A computer program which is based on the Direct Integration Method is documented in (Rapp, 1966).

We decided to use the Direct Integration Method as our "classical" approach, because of its simplicity in terms of data required. The corresponding equations for the three components of δ , at a point P (ϕ_P λ_P , r_P) in space are (Heiskanen and Moritz, 1967, p.234):

$$(\delta g_r)_P = \frac{1}{4\pi R} \iint_S \Delta g \frac{\partial S(r,\psi)}{\partial r} dS$$

$$(\delta g_{\bar{\phi}})_P = -\frac{1}{4\pi R} \iint_S \Delta g \frac{\partial S(r,\psi)}{\partial \psi} \cos\alpha \, dS$$

$$(\delta g_\lambda)_P = -\frac{1}{4\pi R} \iint_S \Delta g \frac{\partial S(r,\psi)}{\partial \psi} \sin\alpha \, dS \qquad (8.1)$$

Strictly speaking, the gravity anomalies $\Delta g = g_G - \gamma_E$ in the equations above refer to the geoid; g_G is the gravity reduced in free-air from the surface of the earth to the geoid, and γ_E is the normal gravity on the ellipsoid. It must be pointed-out that in applications with real data, the normal gradient $\partial\gamma/\partial r = -0.3086$ mgal/meter is used for this type of reduction, instead of the gradient $\partial g/\partial r$ Therefore, the resulting anomalies are approximately surface

free-air gravity anomalies. However, the difference between the surface anomaly, and the anomaly at the geoid is small (ibid, p.241). Consequently, for our simulation tests with the classical approach we will be using gravity anomalies generated by the model on its surface (see equation (6.1)), similarily to the computations performed by Molodensky et al. (1962, pp.196-210).

Applying the same kind of approximation as in section 5.2.3, equations (8.1) yield:

$$(\delta g_r)_P = \frac{1}{4\pi R} \sum_{i=1}^{N} \Delta g_i \left(\frac{\partial S(r,\psi)}{\partial r}\right)_i \Delta S_i$$

$$(\delta g_{\bar{\phi}})_P = -\frac{1}{4\pi r_P R} \sum_{i=1}^{N} \Delta g_i \left(\frac{\partial S(r,\psi)}{\partial \psi}\right)_i \Delta S_i \cos\alpha_i$$

$$(\delta g_{\lambda})_P = -\frac{1}{4\pi r_P R} \sum_{i=1}^{N} \Delta g_i \left(\frac{\partial S(r,\psi)}{\partial \psi}\right)_i \Delta S_i \sin\alpha_i \qquad (8.2)$$

where N is the total number of elementary areas in which the sphere R is subdivided. The index i refers to the center of the block ΔS_i (this is an approximation too, since the point to evaluate the kernels in (8.1) is unknown). The aximuth α_i, the spherical distance ψ_i, and the derivatives of the Stokes' function with respect to r, and ψ, are given by equations (5.26) through (5.31). The differences between equations (8.2) of the classical approach, and equations (5.25) of the mean-value approach (following Bjerhammar), are:

(a). The geosphere R_B in (5.25), now becomes the mean-earth sphere R, and

(b). The gravity anomalies Δg^* in (5.25) do <u>not</u> have any physical meaning (they just satisfy the surface data), while the anomalies in (8.2) are the given free-air anomalies.

Let us now apply equations (8.2) using the data (surface gravity anomalies) generated by the terrain models, similarily to the simulations for the improved techniques. Using a 10°-inclination conical model, and gravity anomalies on a 2' grid within an area 8°x 8°, the errors in the components of $\vec{\delta}$ at 10 km altitude, are by a factor of 2 larger than those from the Green's approach (table 8.1 vs. table 4.4). The same difference was found using data on a 1' grid within a 0.4°x 0.4° area (table 8.3 vs. 4.14).

Comparing the errors from the Dirac approach at 5 km, 10 km, 20 km, and 100 km altitudes, to those from the classical approach, using identical model and data, we found them to be 2 to 10 times smaller (tables 6.5, 6.6, 6.7, and 6.8, versus tables 8.2, 8.3, 8.4, and 8.5 respectively).

For an easier comparison among the results from the various techniques, we list in table 8.6 the exact components of $\vec{\delta}$ at selected points at 10 km altitude, and the components computed from the synthetic data on the surface of a 10°-inclination conical model (within a 0.8°x 0.8° area, with 2' grid), using both the classical approach and the improved techniques. It is obvious that the results from the improved techniques are closer to the exact values than the results from the classical approach, with the exception of the results from collocation at points away from the model's center ($\phi_0 = 45°$, $\lambda_0 = 250°$).

All of our tests clearly indicate that the three techniques which take the effect of the topography into account, offer an improved solution for the computation of the components of $\vec{\delta}$ in space, as compared to the classical approach where the topography is neglected.

Table 8.1: Comparison of Gravity Disturbance Vector Components in Space Computed Rigorously, and From the Classical Approach
(The Direct Integration Method)
(values in mgal; height in meters)

Region Size (Degrees): 8.00 x 8.00
Grid Interval (Minutes): 2.0

Inclination (Degrees): 10.543

LAT	LON	HEIGHT	EXACT: RADIAL	EXACT: HORIZ	COMPUTED: RADIAL	COMPUTED: HORIZ	DIFFERENCES: RADIAL	DIFFERENCES: HORIZ	PERCENTAGE DIF RADIAL	PERCENTAGE DIF HORIZ
45	250 0'	10000.	-36.89	0.0	-22.23	-0.03	-14.66	0.03	39.73	*******
45	250 10'	10000.	-13.51	-9.17	-10.59	-6.13	-2.92	-3.04	21.64	33.16
45	250 20'	10000.	-3.60	-4.02	-3.05	-3.74	-0.54	-1.08	15.10	22.44
45	250 30'	10000.	-1.30	-2.60	-1.11	-2.07	-0.19	-0.53	14.84	20.41
45	250 40'	10000.	-0.59	-1.57	-0.50	-1.26	-0.09	-0.32	15.20	20.06
45	250 50'	10000.	-0.32	-1.04	-0.27	-0.83	-0.05	-0.21	15.38	20.15
45	251 0'	10000.	-0.19	-0.74	-0.16	-0.59	-0.03	-0.15	16.02	19.75

Table 8.2: Comparison of Gravity Disturbance Vector Components in Space Computed Rigorously, and From the Classical Approach
(The Direct Integration Method)
(values in mgal; height in meters)

Region Size (Degrees): 8.00 x 8.00
Grid Interval (Minutes): 1.0

Inclination (Degrees): 10.543

LAT	LON	HEIGHT	EXACT: RADIAL	EXACT: HORIZ	COMPUTED: RADIAL	COMPUTED: HORIZ	DIFFERENCES: RADIAL	DIFFERENCES: HORIZ	PERCENTAGE DIF RADIAL	PERCENTAGE DIF HORIZ
45	250 0'	5000.	-105.36	0.0	-45.50	-0.04	-59.86	0.04	56.82	*******
45	250 2'	5000.	-82.06	-21.19	-42.29	-6.81	-39.77	-14.38	48.47	67.85
45	250 4'	5000.	-55.21	-25.21	-34.63	-11.19	-20.59	-14.02	37.29	55.61
45	250 6'	5000.	-35.67	-23.38	-26.01	-12.90	-9.66	-10.48	27.09	44.82
45	250 8'	5000.	-22.93	-19.64	-18.38	-12.64	-4.55	-6.99	19.83	35.61
45	250 10'	5000.	-14.98	-15.93	-12.34	-11.47	-2.65	-4.46	17.66	28.01
45	250 12'	5000.	-10.10	-12.87	-7.87	-9.91	-2.23	-2.96	22.09	22.99

Table 8.3: Comparison of Gravity Disturbance Vector Components in Space Computed Rigorously, and From the Classical Approach
(The Direct Integration Method)
(values in mgal; height in meters)

Region Size (Degrees): 0.40 x 0.40
Grid Interval (Minutes): 1.0

Inclination (Degrees): 10.543

LAT	LON	HEIGHT	EXACT: RADIAL	EXACT: HORIZ	COMPUTED: RADIAL	COMPUTED: HORIZ	DIFFERENCES: RADIAL	DIFFERENCES: HORIZ	PERCENTAGE DIF RADIAL	PERCENTAGE DIF HORIZ
45	250 0'	10000.	-36.89	0.0	-22.82	-0.04	-14.87	0.04	40.32	*******
45	250 2'	10000.	-34.66	-4.88	-21.22	-2.48	-13.44	-2.40	38.79	49.19
45	250 4'	10000.	-29.48	-8.21	-18.98	-4.48	-10.50	-3.73	35.61	45.44
45	250 6'	10000.	-23.43	-9.66	-15.99	-5.75	-7.45	-3.90	31.78	40.43
45	250 8'	10000.	-17.93	-9.78	-12.86	-6.32	-5.07	-3.46	28.28	35.36
45	250 10'	10000.	-13.51	-9.17	-9.93	-6.32	-3.59	-2.85	26.55	31.10
45	250 12'	10000.	-10.15	-8.24	-7.45	-5.94	-2.69	-2.30	26.55	27.95

Table 8.4: Comparison of Gravity Disturbance Vector Components in Space Computed Rigorously, and From the Classical Approach
(The Direct Integration Method)
(values in mgal; height in meters)

Region Size (Degrees): 0.40 x 0.40
Grid Interval (Minutes): 1.0

Inclination (Degrees): 10.543

LAT	LON	HEIGHT	EXACT: RADIAL	EXACT: HORIZ	COMPUTED: RADIAL	COMPUTED: HORIZ	DIFFERENCES: RADIAL	DIFFERENCES: HORIZ	PERCENTAGE DIF RADIAL	PERCENTAGE DIF HORIZ
45	250 0'	20000.	-12.06	0.0	-8.17	-0.00	-3.89	0.00	32.22	*******
45	250 2'	20000.	-11.84	-0.93	-8.04	-0.61	-3.80	-0.32	32.11	34.48
45	250 4'	20000.	-11.21	-1.76	-7.67	-1.17	-3.55	-0.59	31.63	33.59
45	250 6'	20000.	-10.29	-2.42	-7.09	-1.63	-3.20	-0.79	31.10	32.65
45	250 8'	20000.	-9.19	-2.88	-6.39	-1.97	-2.81	-0.91	30.55	31.43
45	250 10'	20000.	-8.05	-3.15	-5.62	-2.20	-2.43	-0.96	30.15	30.32
45	250 12'	20000.	-6.95	-3.26	-4.86	-2.30	-2.09	-0.96	30.11	29.32

Table 8.5: Comparison of Gravity Disturbance Vector Components in Space Computed Rigorously, and From the Classical Approach (The Direct Integration Method) (values in mgal; height in meters)

Region Size (Degrees): 0.40 x 0.40
Grid Interval (Minutes): 1.0

Inclination (Degrees): 10.543

LAT	LON	HEIGHT	EXACT: RADIAL	EXACT: HORIZ	COMPUTED: RADIAL	COMPUTED: HORIZ	DIFFERENCES: RADIAL	DIFFERENCES: HORIZ	PERCENTAGE DIF RADIAL	PERCENTAGE DIF HORIZ
45	250	0'100000.	-0.63	0.0	-0.42	-0.00	-0.20	0.00	32.58	*******
45	250	2'100000.	-0.63	-0.01	-0.42	-0.01	-0.21	-0.00	32.66	29.01
45	250	4'100000.	-0.63	-0.02	-0.42	-0.02	-0.20	-0.01	32.67	30.15
45	250	6'100000.	-0.62	-0.03	-0.42	-0.02	-0.20	-0.01	32.63	29.14
45	250	8'100000.	-0.62	-0.04	-0.42	-0.03	-0.20	-0.01	32.68	29.86
45	250	10'100000.	-0.61	-0.05	-0.41	-0.04	-0.20	-0.02	32.66	29.64
45	250	12'100000.	-0.61	-0.07	-0.41	-0.05	-0.20	-0.02	32.79	29.83

Table 8.6
Comparison of Gravity Disturbance Vector Components in Space (10 km altitude), Computed from the Improved Techniques and from the Classical Approach
(10°-inclination conical model; 0°.8x0°.8 area; 2' grid; values in mgal; height in meters)

Green's Approach:

LAT	LON	HEIGHT	EXACT: RADIAL	EXACT: HORIZ	COMPUTED: RADIAL	COMPUTED: HORIZ	DIFFERENCES: RADIAL	DIFFERENCES: HORIZ
45	250 0'	10000.	-36.89	0.0	-31.04	-2.49	-5.85	2.49
45	250 2'	10000.	-34.66	-4.88	-28.52	-5.20	-6.14	0.32
45	250 4'	10000.	-29.48	-8.21	-24.25	-7.28	-5.23	-0.93
45	250 6'	10000.	-23.43	-9.66	-19.56	-8.25	-3.87	-1.41
45	250 8'	10000.	-17.93	-9.78	-15.42	-8.36	-2.51	-1.42
45	250 10'	10000.	-13.51	-9.17	-11.94	-7.88	-1.57	-1.28
45	250 12'	10000.	-10.15	-8.24	-9.33	-7.20	-0.82	-1.04

Dirac Approach:

LAT	LON	HEIGHT	EXACT: RADIAL	EXACT: HORIZ	COMPUTED: RADIAL	COMPUTED: HORIZ	DIFFERENCES: RADIAL	DIFFERENCES: HORIZ
45	250 0'	10000.	-36.89	0.0	-35.07	-0.01	-1.82	0.01
45	250 2'	10000.	-34.66	-4.88	-33.11	-4.73	-1.55	-0.15
45	250 4'	10000.	-29.48	-8.21	-28.10	-8.00	-1.39	-0.21
45	250 6'	10000.	-23.43	-9.66	-22.18	-9.49	-1.25	-0.17
45	250 8'	10000.	-17.93	-9.78	-16.74	-9.63	-1.19	-0.15
45	250 10'	10000.	-13.51	-9.17	-12.30	-8.98	-1.21	-0.19
45	250 12'	10000.	-10.15	-8.24	-8.96	-8.01	-1.19	-0.23

Collocation Approach:

LAT	LON	HEIGHT	EXACT: RADIAL	EXACT: HORIZ	COMPUTED: RADIAL	COMPUTED: HORIZ	DIFFERENCES: RADIAL	DIFFERENCES: HORIZ
45	250 0'	10000.	-36.89	0.0	-44.99	-0.02	8.10	0.02
45	250 2'	10000.	-34.66	-4.88	-43.17	-4.10	8.51	-0.78
45	250 4'	10000.	-29.48	-8.21	-38.47	-6.90	8.99	-1.31
45	250 6'	10000.	-23.43	-9.66	-32.69	-8.00	9.26	-1.65
45	250 8'	10000.	-17.93	-9.78	-27.45	-7.76	9.53	-2.01
45	250 10'	10000.	-13.51	-9.17	-23.23	-6.71	9.72	-2.46
45	250 12'	10000.	-10.15	-8.24	-20.13	-5.37	9.99	-2.87

Classical Approach:

LAT	LON	HEIGHT	EXACT: RADIAL	EXACT: HORIZ	COMPUTED: RADIAL	COMPUTED: HORIZ	DIFFERENCES: RADIAL	DIFFERENCES: HORIZ
45	250 0'	10000.	-36.89	0.0	-22.17	-0.04	-14.73	0.04
45	250 2'	10000.	-34.66	-4.88	-21.39	-2.42	-13.28	-2.46
45	250 4'	10000.	-29.48	-8.21	-19.24	-4.36	-10.24	-3.85
45	250 6'	10000.	-23.43	-9.66	-16.40	-5.60	-7.03	-4.06
45	250 8'	10000.	-17.93	-9.78	-13.32	-6.13	-4.61	-3.64
45	250 10'	10000.	-13.51	-9.17	-10.56	-6.15	-2.95	-3.02
45	250 12'	10000.	-10.15	-8.24	-8.22	-5.84	-1.92	-2.40

Chapter 9

SOME TOPICS OF SPECIAL INTEREST RELATED TO THE COMPUTATION OF THE GRAVITY DISTURBANCE VECTOR IN SPACE

During our investigations on the accuracy of the three improved techniques for the computation of the gravity vector in space considering the topography of the earth, some questions related to the applicability of these approaches with real data were raised.

More specifically, the use of the Dirac approach with data having large spacing was questioned, and in section 9.1 below some tests are described that confirm this drawback of the method. In addition, the effect of the truncation, i.e. the neglect of the information from the remote zones is discussed (section 9.2, and 9.3). Despite the fact that the effect of the topography is not considered in our computations for the truncation effects, we think that the results in these two sections will help us in judging the applicability of the Dirac approach with real data, using a higher-degree reference field as opposed to an ellipsoidal one.

9.1 Some Tests with Real Data and the Dirac Approach, for Gravity Anomaly Computations on the Surface of the Earth

In order to test how well the Dirac (iterative) approach converges in a real-world application with point gravity anomalies on the surface of the earth, irregularly distributed, we decided to use the data set described in (Sjöberg, 1978, p.64), and to compare our results with his. This data set consists of 87 point free-air gravity anomalies in the Manitoba area, in Canada, with a mean spacing 0°.5, in an area 2°.5 x 6 and at a mean elevation 400 meters approximately. Note that the RMS value of these gravity anomalies in 14.00 mgal. Table 9.1 contains the location, the elevation, and the gravity anomaly for each one of these points.

From these 87 anomalies, the gravity spikes are iteratively computed on the geosphere, whose depth from the mean sphere R was selected - for test purposes - to be 0, 10, 20, and 30 km. The Gauss-Seidel iterative method of section 5.3.1 was used (equation (5.37)), using (5.38) as the convergence criterion. The RMS difference between the given anomalies, and those computed from the 87 spikes at the same pointsis given in table 9.3. The reason why these RMS differences are not exactly zero, is due to the

fact that the spikes have been computed iteratively, and not directly. In any event, these differences are very small, showing that within three iterations the solution for Δg^S converges.

Table 9.2 is of the same nature as table 9.1, but it contains information about an additional set of 50 anomalies in the same area, distributed within the 87 anomalies of the first set. The RMS value of the 50 anomalies, is 13.5226 mgal. The RMS differences between these anomalies, and those computed from the spikes are also shown in table 9.3. As the reader can see, these RMS differences are of the same magnitude as the RMS value of the 50 anomalies itself. Sjöberg (ibid, p.68) analyzing the same data set with the same method, found similar results, but he did not make any comment about the fact that under the above circumstances, the resulting error of the prediction is 100%!

At first, if we use (5.47) to compute the radius of the smallest sphere which will guarantee the convergence of the iterative solution for $\psi_{min} = 0°.5$, and $h_{max} = 500$ meters, we find that the depth of the geosphere is about 28.5 km. This is in a very good agreement with the optimum depth that Sjöberg found for the same data set in applying the Dirac approach (see his figure 6, page 67), which is approximately 30 km.

One reason for the RMS error to be equal to the RMS value of the predicted quantity, is that the computed quantity is orders of magnitude smaller than its true value (the given surface value). In order to verify this, we computed the gravity anomalies at the surface from the 87 spikes, along a profile between two of the given data points. The coordinates, the elevation, and the computed anomalies at selected points along this profile are given in table 9.4, along with the true values at the end points. We see that the magnitude of the gravity anomaly is dramatically reduced as we go away from either one of the end points. In the middle of the profile, the computed gravity anomaly is practically identical to the given value.

Our interpretation to this - originally surprising - finding is the following. As the gravity anomalies on the geosphere are all zero except at the carrier points, the gravity anomalies on the surface of the earth will also retain the same gravity characteristics of the field that generates them. In other words, the spikes on the geosphere fit only the surface data from which they have been computed, and that cannot be used for the computation of a gravity anomaly away from these points, unless the surface data is very dense to permit an accurate prediction. This also explains the large errors that we found from the simulation test with 5'-grid (table 6.3), as opposed to the errors

Table 9.1

Free-Air Gravity Anomalies in Manitoba, Canada
Sjöberg (1978)

ST #	LATITUDE (DEGREES)	LONGITUDE (DEGREES)	HEIGHT (METERS)	ANOMALY (MGAL)
13676	48.10878	99.18939	501.396	8.12
13675	48.10654	90.39793	465.429	5.72
13668	48.12804	91.19112	421.843	4.32
13661	48.26439	91.47469	431.901	-11.41
15691	48.23920	91.95221	372.161	-16.01
15793	48.52264	90.11258	430.377	-26.16
13650	48.52742	90.55254	470.916	-24.76
13655	48.54848	90.98921	450.799	-8.36
13659	48.47208	91.45769	374.904	-21.45
15688	48.46989	92.10847	362.407	-18.25
10261	48.56660	92.46326	361.797	-18.07
10252	48.60010	92.81689	337.718	-18.97
10248	48.55446	93.62741	346.062	3.74
10245	48.72795	93.91647	352.654	-.20
10643	49.03152	90.02982	473.949	-28.75
15754	49.04839	90.47089	492.252	-11.56
15745	49.02661	91.06570	441.960	-8.25
15702	49.07143	91.61993	439.217	-24.96
13575	49.14218	91.92789	421.843	-19.37
13610	49.50134	90.03463	449.805	5.06
13606	49.59610	90.38807	446.837	-15.16
13604	49.61888	90.92754	437.998	-12.16
15729	49.53860	91.64418	407.213	-17.95
196	49.49666	92.03333	436.778	1.16
15717	49.92172	90.08139	468.173	11.08
15713	49.96526	90.56398	415.137	0.08
15380	49.96666	90.91167	410.261	14.58
10267	49.01868	92.57602	385.267	-17.55
11423	49.02036	92.98222	408.432	21.05
10013	49.53339	92.40990	383.743	6.16
254	49.95332	91.51166	400.812	-22.72
13565	49.92413	91.95653	358.445	-5.62
11409	49.07217	93.54082	352.349	9.74
1554	49.02666	93.91666	356.921	-13.75
12014	49.47910	93.06764	363.626	-32.63
10100	49.52834	93.51404	359.664	-14.54
10111	49.99075	93.49245	348.082	4.17
209	49.03166	94.51999	323.698	-9.55
10157	49.03590	95.21919	323.698	4.95
10163	49.17368	95.47781	344.119	1.62
10161	49.07393	95.96857	330.098	15.24
10227	49.50439	94.00826	344.119	-15.24
10219	49.43992	94.53586	323.088	-13.23
10173	49.48048	95.01280	323.088	-4.64
10170	49.45171	95.51802	343.814	-10.53
10188	49.48811	95.99078	318.211	-4.44
4507	49.05833	96.53999	299.923	4.74
1130	49.57166	96.57333	270.053	1.35
4616	49.58833	96.98000	241.402	0.14
10040	50.04314	92.56009	400.812	-11.24
10964	50.01875	92.93719	395.935	-5.13
10125	50.01784	94.12364	405.079	11.47
10147	50.07710	94.45625	359.054	-1.44
11465	50.29559	95.05542	323.698	9.21
12045	50.05191	95.55070	309.067	11.66
4513	50.00499	96.02499	271.881	2.57
4544	50.04498	96.59000	249.631	-7.54
4552	50.04666	96.51999	248.412	-7.04
5743	50.03166	97.04166	228.295	18.06
16028	50.50333	90.14667	387.401	-15.52
16025	50.57166	90.46832	405.384	1.26
15335	50.46999	91.15166	392.887	-4.72
16048	50.55499	91.42500	396.849	14.87
15344	50.52834	92.05000	356.616	12.27
10050	50.49197	92.57567	357.530	-6.72
10059	50.46123	92.90984	357.835	7.38
10135	50.52052	93.48242	340.461	9.77
12177	50.49446	94.12927	369.417	21.78
12189	50.50020	94.42551	340.157	16.58
12185	50.49776	95.11777	361.188	16.48
11471	50.51193	95.95348	252.679	-11.92
10435	50.58276	95.50301	313.334	7.06
9541	50.53166	96.53833	264.566	1.97
16021	51.02333	90.13666	379.781	-5.32
16016	51.12833	90.45332	373.990	-23.74
15989	51.42500	90.42500	360.273	-33.89
16019	51.42999	90.03166	387.401	-15.39
15323	51.89499	90.14999	350.825	1.52
15310	51.89999	90.93999	365.760	-0.58
16004	51.00833	91.07832	373.990	5.30
16044	51.05000	91.52998	376.123	-22.12
15348	51.06833	92.16666	410.565	-18.53
636	51.06999	92.57166	392.887	3.17
10473	51.16444	92.88702	413.004	-19.14
15986	51.53999	91.08665	378.257	-12.81
15983	51.54832	91.52998	379.781	-11.01
10463	51.56641	92.07666	399.288	-16.12

Table 9.2

Free-Air Gravity Anomalies in Manitoba, Canada
(Test Data Set)
(From: Sjöberg (1978))

ST #	LATITUDE (DEGREES)	LONGITUDE	HEIGHT (METERS)	ANOMALY (MGAL)
99999				
16009	50.59449	91.14833	386.181	9.76
16011	50.74666	90.96165	379.476	10.63
10499	50.79678	92.36719	425.501	8.82
16042	50.95090	91.75833	402.031	-9.20
16012	50.88333	91.01666	378.257	1.71
10052	50.59193	92.61716	428.854	12.66
10047	50.22284	92.84720	358.445	-3.57
10038	50.21497	92.37631	357.835	-3.37
15372	50.49666	91.87166	357.225	12.68
273	50.40833	91.50833	370.027	3.99
15370	50.75499	91.88333	391.973	7.53
16047	50.68333	91.41998	382.219	13.34
10496	50.89524	92.14000	396.543	-2.18
10081	50.21280	93.23963	364.845	7.53
625	50.30666	93.17999	361.493	4.41
16002	51.12833	90.86833	389.390	-21.34
16050	50.29498	91.38998	373.685	-14.68
15331	50.74500	90.75665	390.449	7.83
15334	50.42332	90.71666	391.058	2.09
15056	50.18333	90.68832	404.774	-15.16
15384	50.12999	90.23999	417.576	-3.35
9164	48.91499	90.60001	457.809	-11.23
13576	49.02196	91.96181	425.501	-21.95
15715	49.84846	90.40294	442.265	-2.80
15723	49.74696	90.75410	435.359	-5.18
15675	49.86776	92.09227	382.524	-23.51
10019	49.84630	92.39220	366.674	-18.90
15878	49.92999	91.38333	388.925	-29.92
19203	49.76701	94.87744	359.969	2.11
11455	49.62477	94.02734	373.990	-10.26
10222	49.59979	94.35619	323.088	5.44
5710	49.43166	96.27499	357.225	5.27
5546	49.72333	95.24666	338.328	16.62
10198	49.62842	95.49942	318.211	-1.36
5531	49.71666	94.93666	359.664	10.92
5076	49.71500	94.80666	345.643	14.12
10078	49.90807	93.14622	372.770	-8.51
10104	49.68629	93.87337	379.171	-18.87
10098	49.30328	93.51170	338.023	6.60
5084	49.81332	92.97501	365.092	-10.10
10014	49.62167	92.44067	385.572	18.04
12002	49.49670	92.69481	403.555	11.76
10007	49.22151	92.46306	405.384	-23.49
213	49.14166	92.70332	388.620	-22.67
15725	49.70807	91.09705	435.559	-8.48
15736	49.66466	91.81667	419.405	-24.77
15738	49.24759	91.46384	445.617	-13.99
10249	48.66917	93.27843	337.718	-6.09
13652	48.56082	90.73390	447.751	-23.06
15748	48.83151	90.96706	445.922	-18.72

from a 1'-grid (table 6.4). These results indicate that the Dirac approach should not be used for the interpolation of gravity anomalies on the surface of the earth, unless the data is sufficiently dense to ensure an accurate prediction. Note that the errors in tables 6.5 through 6.8 are much smaller, because of the very find (1') grid being used.

Table 9.3

Comparison of Input with Computed Anomalies, at Various Depths of the Geosphere (Dirac approach). Values in mgal.

Depth $R - R_B$ (km)	# of Iterat.	RMS Diff. (input - computed) 87 points	RMS Diff. (input - computed) 50 points
0	3	$.52 \times 10^{-6}$	13.5266
10	3	$.54 \times 10^{-6}$	13.5266
20	3	$.49 \times 10^{-6}$	13.5266
30	3	$.61 \times 10^{-6}$	13.5266

Note: The iteration is terminated when two successive values for a spike have a 12-digit agreement.

Table 9.4

Computation of the Gravity Anomalies Along a Profile

Station	latitude	longitude		anomaly (mgal)	computed anomaly (mgal)
11423	49°01'13".3	92°58'56".0	408.432	21.05	21.0499996
	49 01 13.4	92 58 56.0	407		21.18
	49 01 12.0	92 58 55.2	405		21.01
	49 01 48.0	92 58 48.0	404		1.10
	49 01 24.0	92 54 00	402.5		0.0065
	49 06 00	92 48 00	401		0.00017
	49 12 00	92 42 00	399		-0.00011
	49 18 00	92 36 00	398		-0.000072
	49 24 00	92 30 00	397		0.000032
	49 30 00	92 24 00	395		0.0081
	49 31 48.	92 24 36.	393		2.45
	49 31 58.8	92 24 32.4	389		5.71
	49 31 59.9	92 24 35.3	286		6.08
10013	49 32 00.2	92 24 35.6	383.743	6.16	6.1600003

9.2 Truncation and Discretization Errors

In the preceding chapters we presented three methods for the computation of the gravity vector in space, from surface data, without neglecting the topography of the earth. The Green's method requires as data mean gravity disturbances on the earth's surface, while the Dirac and the collocation approaches require point gravity anomalies at discrete surface stations. From the practical point of view, none of these methods can operate on a global data set, due to the limitations in computer speed and core. One possible solution to this problem is to use data in a spherical cap - whose center is at the projection of the space point on the surface of the earth -, and to account for the information from the remote zones through a set of potential coefficients. Clearly, if only the data in the cap is used, the resulting truncation error will be smaller (in general), as the size of the cap becomes larger. Therefore, it is very important to know the minimum cap size that yields a certain level of accuracy in computing a particular quantity (the components of $\vec{\delta}$ in our case).

In addition to the truncation effect, the computed quantity is also affected by the fact that we are dealing with discrete data. This type of error is a function of the grid spacing (i.e. the block size) following the Green's approach, or a function of the distance between the discrete data points following the Dirac approach, or collocation. In general, the truncation error is a function of the extent of the area, and the discretization error is a function of the density of the data.

In our simulations, the synthetic data on the surface of the model is assumed to be errorless as being rigorously computed from the disturbing masses. Therefore, the tables in the preceding chapters give the total error, which is caused by the combined effect of:

(a). Truncation and Discretization (Dirac approach).
(b). Truncation and Discretization, missing second-order variations of the topography, and center-point evaluations of the kernels (Green's approach).

For the simulation tests with the Green's approach, we have used relatively small working areas (2°x2° to 8° 8°), the reason being that away from the model's disturbing masses the value of the gravity disturbance diminishes very rapidly (figure 3.2 through 3.5). In other words, the model creates a very local disturbing field and attempts to include more and more data by expanding the size of the working area to 8°x 8° did not improve the results. In addition, grid intervals as small as 0.5' in the inner zone did not result in substantial reduction of the errors of $\vec{\delta}$. These tests

indicate that the errors from the Green's approach are mainly due to the missing second-order variations of the topography, and to the effect of the center-point evaluation of the kernals. These two approximations are the dominant sources of errors in the Green's approach.

For the simulations with the Dirac approach we have used even smaller working areas (0.4°x 0.4° to 2°x 2°). From the results in tables 6.3 and 6.4 we can see that the errors are now dramatically reduced by using five times smaller grid, even if the area extent becomes five times smaller. These results indicate that in our simulations for the Dirac approach, the discretization errors dominate the truncation errors. This is due to the very local characteristics of themodels, and it should not be generalized for an application with real data.

9.3 The Relationship between the Truncation Angle, and the Altitude of the Space Point

It has been found (cf. Hirvonen and Moritz, 1963, p.68), that in applications of the classical approach for the computation of the radial component of $\vec{\delta}$ in space, it is sufficient to extend the integration only as far as 10 times the altitude of the space point, in order to ensure an error smaller than 10%. However, this "rule-of-thumb" is valid only for the Upward Continuation Method (under a planar approximation), and should not be used for the other two techniques (i.e. the Coating Method, and the Direct Integration Method).

From the simulations of chapter 8 it was concluded that the effect of the topography is quite significant, since the errors in $\vec{\delta}$ are reduced by a factor of 2 or more, when the topography is considered in the improved techniques. The question is now, how far from the computation point we should extend the integration using our improved techniques. In other words, what is the relationship between the minimum radius (ψ_0) of the cap inside of which the data is given, and the altitude of the space point (hp), such that the truncation error in $\vec{\delta}$ is below a certain limit (say 100%)?

Clearly, it is out of the scope of the present study to investigate the truncation errors when real data is used. In addition, the effect of the discretization is quite a challenge to be investigated. A procedure for the estimation of the (global RMS) truncation errors in computing the vector $\vec{\xi}$ at a space point (using the Direct Integration classical approach), is described by Shepperd (1979). We decided to use Shepperd's procedure and computer programs, because the topography away from the computation point does not

significantly contribute to the components of $\vec{\delta}$, due to the diminishing magnitude of the terms $\partial S(r, \psi)/\partial \psi$, and $\partial S(r, \psi)/\partial r$ in equations (5.48): Dirac approach, and (8.2): classical approach.

Shepperd's equations for the RMS truncation error of $\vec{\delta}$ at altitude are:

<u>radial</u> error component: $$\varepsilon(\delta g_r) = \left[\sum_{n=0}^{\infty} \left(\frac{\tilde{Q}_n(r,\psi)}{2} \right)^2 \sigma_n^2(\Delta g) \right]^{\frac{1}{2}} \qquad (9.1)$$

<u>horizontal</u> error component: $$\varepsilon(\delta g_h) = \left[\varepsilon(\delta g_\varphi)^2 + \varepsilon(\delta g_\lambda)^2 \right]^{\frac{1}{2}} \qquad (9.2)$$

$$= \left[\sum_{n=1}^{\infty} \frac{q_n^2(r,\psi)}{n(n+1)} \sigma_n^2(\Delta g) \right]^{\frac{1}{2}} ,$$

where $\sigma_n^2(\Delta g)$ are the anomaly degree variances:

$$\sigma_n^2(\Delta g) = c_n = \bar{\gamma}^2 (n-1)^2 \sum_{m=0}^{n} (\bar{C}_{nm}^{*2} + \bar{S}_{nm}^2) \qquad (9.3)$$

$\bar{\gamma}$ is the mean value of the normal gravity (979800 mgal).

$\bar{C}_{nm}^*$, $\bar{S}_{nm}$ are the fully normalized potential coefficients, referred to the same normal field as the gravity anomalies.

and the truncation coefficients for the radial horizontal components of $\vec{\delta}$ are defined as:

$$\tilde{Q}_n(r,\psi_0) = R \int_{\psi_0}^{\pi} \frac{\partial S(r,\psi)}{\partial r} P_n(\cos\psi) \sin\psi \, d\psi \qquad (9.4)$$

$$q_n(r,\psi_0) = \frac{R}{2r} \int_{\psi_0}^{\pi} \frac{S(r,\psi)}{\partial \psi} P_n'(\cos\psi) \sin\psi \, d\psi \qquad (9.5)$$

where:

$$P_n'(x) = -\sqrt{1-x^2} \, \frac{d P_n(x)}{dx}$$

Recursive relationships for the evaluation of these two kinds of truncation coefficients, starting from the Molodenskii's coefficients:

$$Q_n(r,\psi_0) = \int_{\psi_0}^{\pi} S(r,\psi) P_n(\cos\psi) \sin\psi \, d\phi \qquad (9.6)$$

are given in (Shepperd, 1979), along with FORTRAN subroutines for their computation. (These subroutines were converted for double-precision computations).

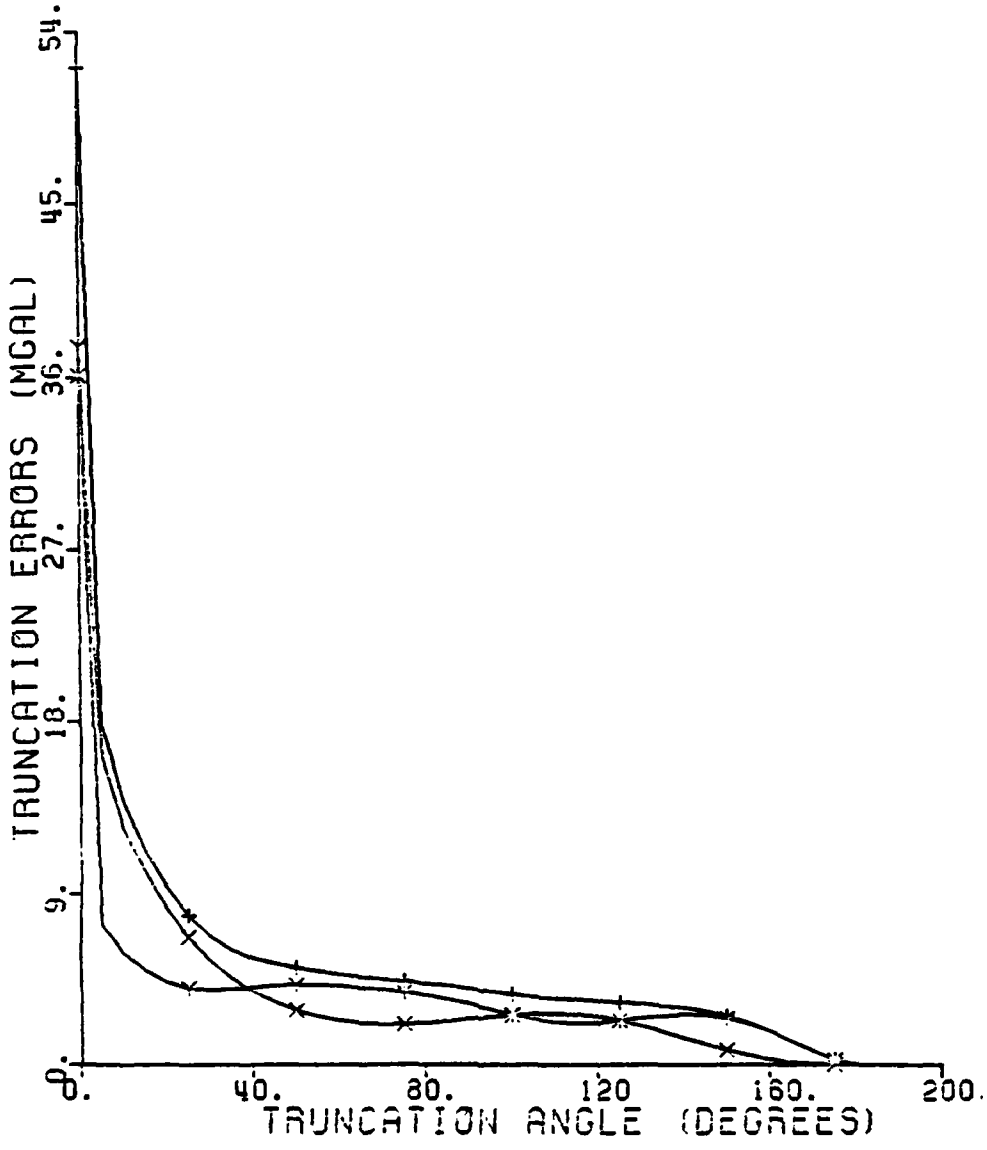

Figure 9.1: Radial (Y), Horizontal (X), and Total (+) Truncation Errors at Altitude h_p = 5000 meters (Maximum degree: 400 , Ellipsoidal Reference Field)

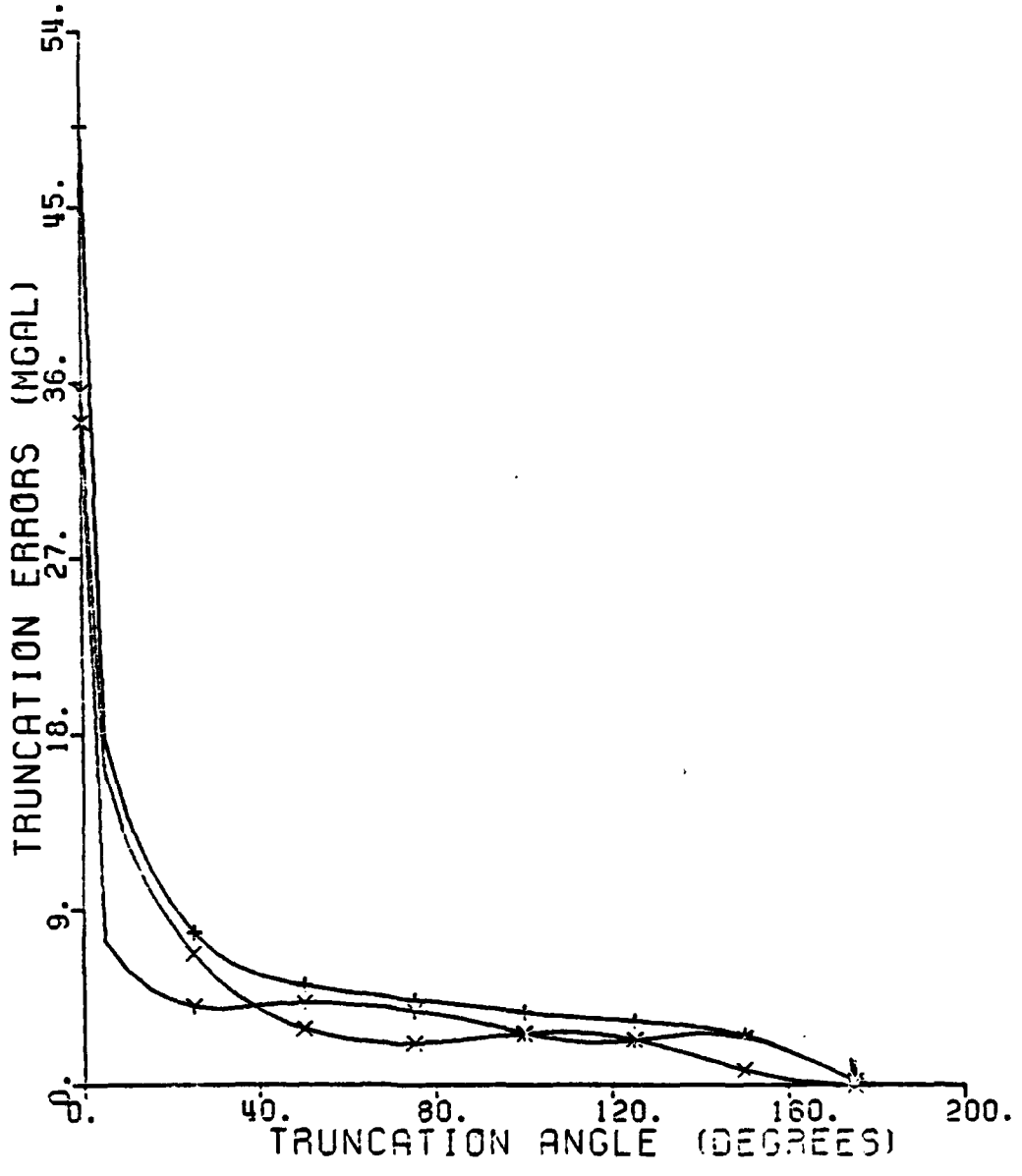

Figure 9.2: Radial (Y), Horizontal (X), and Total (+) Truncation Errors at Altitude $h_p = 10000$ meters (Maximum degree: 400, Ellipsoidal Reference Field)

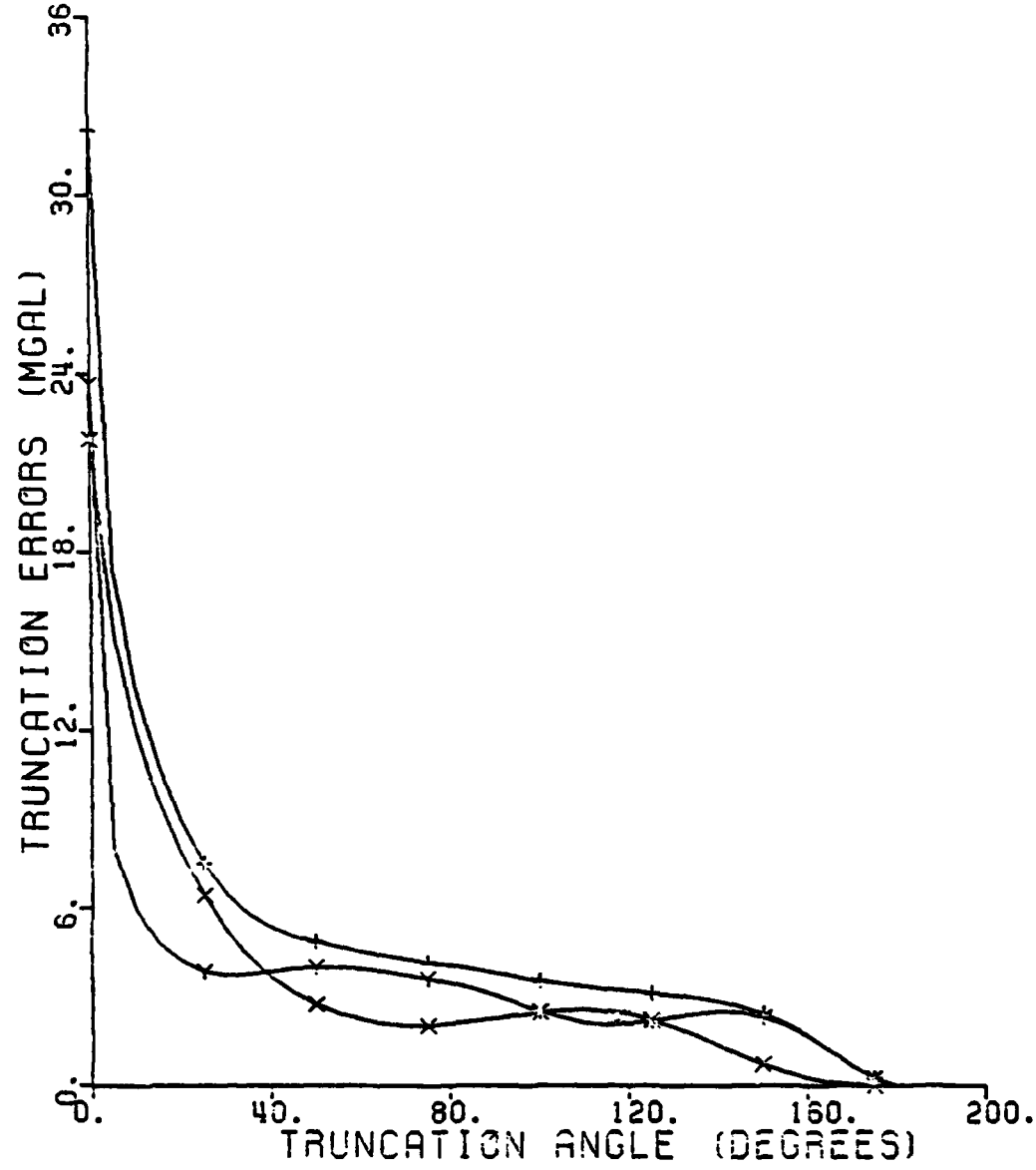

Figure 9.3: Radial (Y), Horizontal (X), and Total (+) Truncation Errors at Altitude $h_p = 100000$ meters (Maximum degree: 400, Ellipsoidal Reference Field)

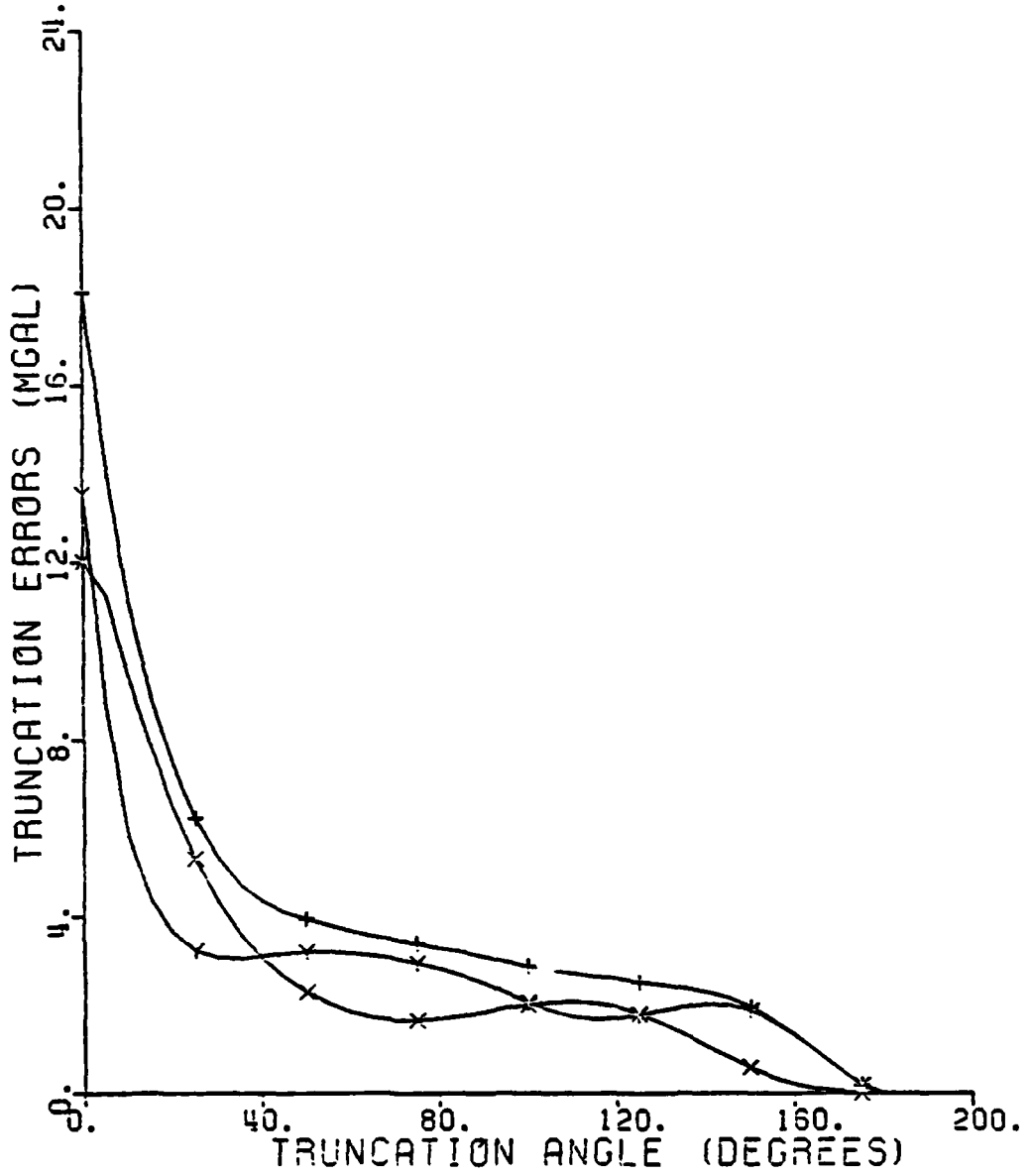

Figure 9.4: Radial (Y), Horizontal (X), and Total (+) Truncation Errors at Altitude h_p = 500000 meters (Maximum degree: 400, Ellipsoidal Reference Field)

For the computation of the anomaly degree variances, we can use the Tscherning-Rapp (1974) model:

$$c_n = \frac{A(n-1)}{(n-2)(n+B)}, \quad n \geq 3$$

$$A = 425.28 \text{ mgal}^2$$

$$B = 24 \qquad (9.7)$$

Using (9.1) and (9.2), the <u>total</u> truncation error at altitude will be:

<u>total</u> error component: $\varepsilon(\delta g) = [\varepsilon(\delta g_r)^2 + \varepsilon(\delta g_h)^2]^{\frac{1}{2}}$ (9.8)

In figures (9.1), (9.2), (9.3), and (9.4) we give the truncation errors for the radial, the horizontal, and the total components of $\vec{\delta}$ at 5 km, 10 km, 100 km, and 500 km altitude respectively, computed from equations (9.1), (9.2), and (9.8). The summations in these equations were carried-out from $n = 2$ to $n_{max} = 400$ with $c_2 = 7.5$ mgal^2 (Tscherning and Rapp, 1974), i.e. assuming an ellipsoidal reference field. This $n_{max} = 400$ was chosen because summations to higher degrees did not yield significantly different results. Note that Shepperd (ibid) performed his computations up to $n_{max} = 20$ only.

The results plotted in these figures indicate that in order to maintain a truncation error smaller than 10% (with rspect to the RMS total magnitude of $\vec{\delta}$ at the same altitude), we should extend the integration over a cap of radius ψ_0 given in table 9.5 (second column) as a funcion of the altitude of the space point.

Table 9.5

Cap Radius (ψ_0) for Truncation Error Smaller than 10% , at Selected Altitudes of the Space Point

	Radius ψ_0 :	
h_p	Ellipsoidal Ref. Field	20th-degree Ref. Field
5 km	50°	3° 25'
10 km	50°	3° 35'
100 km	120°	5° 30'
500 km	155°	30°

It must be pointed-out that the ψ_0 estimates in table 9.5 hold only for the classical approach (chapter 8), and for the Dirac approach (chapter 5), both of which are based on Pizzetti's generalized formula (equations (5.24), and (8.1)). As we can see, by using an ellipsoidal reference field, even for a relatively low altitude (5 km) the integration must be extended within a 50° cap, in order to retain a relative error below the 10% level. In order to verify the correctness of our computations, we computed (from Shepperd's equations) the effect of truncation on δg_r, and $\delta g_{\bar{\phi}} = \delta g_\lambda = \delta g_h/\sqrt{2}$, for a point on the surface of the earth. We used the same anomaly degree variances as in (Hirvonen and Moritz, 1963, p.54):

$$c_2 = 15; \quad c_3 = 43; \quad c_4 = 30; \quad c_5 = c_6 = c_7 = c_8 = 25 \text{ mgal}^2$$

and therefore the summations in equations (9.1) and (9.2) were taken to $n_{max} = 8$. The results are given in table 9.6, where we also list the truncation effects on δg_r (from Hirvonen and Moritz, 1963, table 7.2), computed as:

$$\varepsilon(\delta g_r) = \left[\sum_{n=2}^{n_{max}} Q_n^2 \, c_n\right]^{\frac{1}{2}} \tag{9.9}$$

The truncation effects on $\delta g_{\bar{\phi}}$, and δg_λ in Hirvonen and Moritz (ibid) were incorrectly evaluated (cf. Hagiwara, 1972, p.457). These effects (on ξ and η) should be computed as (ibid, p.461):

$$\varepsilon(\xi) = \frac{1}{2\gamma} \sum_{n=2}^{\infty} Q_n^* \frac{\partial \Delta g_n}{\partial \bar{\phi}}$$

$$\varepsilon(\eta) = \frac{1}{2\gamma \cos\bar{\phi}} \sum_{n=2}^{\infty} Q_n^* \frac{\partial \Delta g_n}{\partial \lambda} \tag{9.10}$$

where

$$Q_n^* = Q_n + \frac{1}{n(n+1)} S(\cos\psi_0) \, P_{n1}(\cos\psi_0) \sin\psi_0 \tag{9.11}$$

and <u>not</u> as in (Hirvonen and Moritz, ibid, p.45):

$$\varepsilon(\xi) = \frac{1}{2\gamma} \sum_{n=2}^{\infty} Q_n \frac{\partial \Delta g_n}{\partial \bar{\phi}}$$

$$\varepsilon(\eta) = \frac{1}{2\gamma \cos\bar{\phi}} \sum_{n=2}^{\infty} Q_n \frac{\partial \Delta g_n}{\partial \lambda}$$

For reasons of symmetry (ibid, p.49) we can take $\varepsilon(\xi) = \varepsilon(\eta)$ and using (9.10) we arrive to the following equations which give the truncation effects on the components $\delta g_{\bar{\phi}}$, δg_λ of $\vec{\delta}$:

$$\varepsilon(\delta g_{\bar{\phi}}) = \varepsilon(\delta g_{\lambda}) = \left(\frac{1}{8} \sum_{n=2}^{\infty} n(n+1)\, Q_n^{*2} c_n\right)^{\frac{1}{2}} \tag{9.12}$$

The results in table 9.6 clearly indicate that the truncation effects on the horizontal components of $\vec{\delta}$ computed from Shepperd's equations are identical to those computed from (9.12) using Hagiwara's Q_n^* coefficients. In addition, the truncation effects $\varepsilon(\delta g_r)$ on the radial component of $\vec{\delta}$ from Shepperd's equation are in a good agreement with the Hirvonen-Moritz (ibid, table 7.2) results.

We have also computed the RMS magnitude of the components of $\vec{\delta}$ using subroutine COVAX (Tscherning, 1976). The quantities that we have actually computed form COVAX, are the variances of $-\frac{1}{r}\frac{\partial T}{\partial r}$ (in Eotvos), ξ, and η (in arcseconds), i.e. the variances of the radial and of the horizontal components of $\vec{\delta}$, at selected altitudes in space. From these variances we have then computed the RMS magnitude of the components of $\vec{\delta}$ as:

$$RMS(\delta g_r) = r(var(-(1/r)\partial T/\partial r))^{\frac{1}{2}} \cdot 10^{-9} \tag{9.13}$$

$$RMS(\delta g_h) = \frac{\bar{\gamma}}{206263.806} (var(\xi) + var(\eta))^{\frac{1}{2}} \tag{9.14}$$

$$RMS(\delta g_{total}) = [RMS(\delta g_r)^2 + RMS(\delta g_h)^2]^{\frac{1}{2}} \tag{9.15}$$

These values must be the same with the truncation error components (9.1), (9.2), and (9.8), for $\psi_0 = 0°$, provided that the same anomaly degree variance model is used (equation (9.7) in our case). The radial, the horizontal, and the total components of $\vec{\delta}$ from COVAX, and from Shepperd's procedure (with $n_{max} = 400$) are given in table 9.7. As we can see, the agreement between the results from the two procedures is very remarkable.

Table 9.6

Comparison of the Truncation Effects on $\vec{\delta}$, Computed from Shepperd's Equations, and from Two Other Sources ($n_{max} = 8$, values in mgal, altitude: 0 meters).

Cap radius	$\varepsilon(\delta g_r)$ (+)	$\varepsilon(\delta g_{\bar{\vartheta}}) = \varepsilon(\delta g_\lambda)$ (++)	Shepperd's Equations $\varepsilon(\delta g_r)$	Shepperd's Equations $\varepsilon(\delta g_{\bar{\varphi}}) = \varepsilon(\delta g_\lambda)$
0°	---	15.00	24.11	15.00
10°	7.5	10.74	7.73	10.74
20°	5.4	7.33	5.89	7.33
30°	4.4	5.14	5.38	5.14
40°	4.2	3.67	5.59	3.67
50°	4.2	2.74	5.79	2.74
60°	4.3	2.29	5.70	2.29
70°	4.1	2.11	5.35	2.11
80°	3.8	2.17	4.84	2.17
90°	3.3	2.33	4.15	2.33
100°	2.7	2.44	3.42	2.45
110°	2.3	2.45	2.93	2.45
120°	2.2	2.22	2.89	2.22
130°	2.4	1.77	3.14	1.77
140°	2.4	1.17	3.28	1.17
150°	2.2	0.61	2.95	0.61
160°	1.6	0.20	2.05	0.21
170°	0.6	0.01	0.74	0.02
180°	0.	0.	0.	0.

(+) from Hirvonen and Moritz, 1963, table 7.2, p.55, using the Molodensky's Q_N coefficients.

(++) from equation (9.12), using Hagiwara's Q_n^* coefficients.

Table 9.7

Comparison of the RMS Components of $\vec{\delta}$ (from COVAX), with the Truncation Errors for $\psi_0 = 0°$ (from Shepperd's equations) at Various Altitudes (values are in mgal)

h_p	Tscherning's COVAX			Shepperd's equations		
	δg_r	δg_h	δg_{total}	δg_r	δg_h	δg_{total}
5 km	38.78	37.35	53.84	37.58	36.07	52.09
10 km	35.76	34.29	49.55	35.53	33.97	49.16
100 km	23.60	22.43	32.56	23.67	21.82	32.20
500 km	13.57	13.91	19.44	13.54	12.01	18.10

The use of a higher degree reference field:

It must be pointed-out that the large cap sizes (ψ_0) given in table 9.5 (column 2), corresponds to the use of an ellipsoidal reference field. Let us now assume that a higher-degree reference field is available, defined by a set of potential coefficients complete to degree and order n_{ref}, e.g. the GEM-9, or the RAPP-180 solution (Rapp, 1980). If such a reference field is used for the computation of the components of $\vec{\delta}$ at a space point, the corresponding truncation effects can be still computed from equations (9.1), (9.2), and (9.8), where the summations are taken from $n_{ref}+1$, up to $n_{max}=400$. For example, if $n_{ref}=20$, we found that in order to maintain the truncation errors below the 10%-level, the cap radii (ψ_0) are much smaller than the radii using an ellipsoidal reference field (table 9.5, 3rd column). Of course, these radii have been computed under the assumption that the reference field (the coefficients) is error-free. Nevertheless, we can conclude that the use of a higher-degree reference field can reduce dramatically the truncation angles, and therefore the computational effort.

SUMMARY, CONCLUSIONS, AND RECOMMENDATIONS

Three approaches have been investigated for the computation of the components of the gravity vector in space from surface data, without neglecting the topography of the earth:

1. A numerical integration approach, based on the application of Green's third identity (chapter 2).
2. The Dirac approach, following the Bjerhammar's discrete solution to the geodetic B.V.P. (chapter 5).
3. The Least-Squares Collocation approach (chapter 7).

In order to avoid the errors which exist in real data, this work has been a simulation study, using as terrain a conical and a spherical model (chapter 3). Seven parameters are needed to define the geometric and the dynamic characteristics of these models, and the two point masses located beneath their surface on their axes, generate the synthetic data for the application of the simulations. The exact gravity disturbance vector components which are computed from the model, are then compared to the corresponding components which are evaluated from each one of the three approaches, in terms of their relative percentage differences (chapters 4, 6, and 7). From the simulations which were performed, the following conclusions can be made.

(a). The errors from the Green's approach become smaller as the altitude of the space point increases. They can be as small as 1% for a very smooth topography (the case of the spherical model), or for a very large but local topographic feature (the case of the 40°-inclination cone, 4.1 km high). The errors can be as large as 25% in certain cases (right above a 20°-inclination cone), but they decrease at space points away from the model. These errors are due to the numerical integration procedure (evaluation of the kernels at the centers of the blocks), and to the neglect of the second - order variations of the topographic surface.

(b). Both, the Dirac and the Collocation approaches, require discrete data on the physical surface of the earth, but they are very time-consuming, especially when a large amount of data is used. An iterative procedure for the analytical continuation of the surface gravity anomalies to the geosphere is described, based on the Gauss-Seidel numerical method. Acceleration techniques which yield a much faster rate of convergence, require an additional series of iterations for the estimation of the eigenvalues of the system of equations,

which has to be solved for the gravity anomalies on the geosphere. The iteration procedure might diverge for very dense data at high elevations. A method for the estimation of the depth of the geosphere is described such that the iteration is guaranteed to converge. The errors in the gravity vector from the Dirac approach now increase as the inclination of the model increases, and as the altitude of the space point increases, but they are still smaller than the errors from the Green's approach using identical models and data.

(c). The collocation approach requires the computation of the covariances between the predicted quantities, and the data. In addition, it is a very time-consuming method, since the inverse of the matrix of the covariances is needed. On an overall basis, the Dirac approach seems to be superior as compared to collocation.

None of the three approaches igrore the topography of the earth as it happens with the classical approach (chapter 9). Comparisons of the improved techniques versus a classical approach (the Direct Integration Method), using identical models and data arrangement, indicated that the errors in ξ from the improved techniques are at least by a factor of 2 smaller than the errors from the classical approach. This clearly indicates the significance of the techniqes described in this paper.

From some tests which were made for gravity anomaly computations on the surface of the earth using real data (section 9.1), it was concluded that the Dirac approach requires very dense data coverage for such a kind of computations (say 1' as in our simulations).

In order to investigate the relationship between the altitude of the space point, and the truncation angle (the radius of the cap within which the data is given, section 9.3), Shepperd's (1979) computer program has been used. It was found that in order to maintain a truncation error in ξ smaller than 10% (with respect to the RMS magnitude of the components of ξ, using an ellipsoidal reference field), we should extend the computations within a 50°-cap, or larger, depending on the altitude of the space point. However, by using a higher-degree reference field (defined by a set of potential coefficients), the truncation angle can be dramatically reduced. The truncation effects discussed in section 9.3 are valid for the Dirac approach, and for the classical approach (the Direct Integration method), both of which are based on the Pizzetti's formula.

From our experience with the simulations performed and described in this study, we would recommend the Green's

approach for the computation of the gravity vector at high altitudes (above 10 km), and the collocation approach for points below the 10 km-level. The Dirac approach is questionable due to the fact that it requires very dense data on the surface of the earth. We would also recommend the use of real data (on the surface of the earth, and in space), for a more realistic comparison between measured and computed components of the gravity vector in space.

References

Barlik, M. "On the Solution of Bjerhammar's Problem in Mountainous Terrain", Translation DM[illegible] 1971.

Bjerhammar, A. "A New Theory of Gravimetric Geodesy", The Royal Institute of Technology, Division of Geodesy, Stockholm, 1963.

Bjerhammar, A. "Discrete Solutions of the Boundary Value Problem in Physical Geodesy", Tellus, Volume XXVII, No. 2, 1975.

Bjerhammar, A. "A Dirac Approach to Physical Geodesy", Zeitschrift Fur Vermessungwesen, No. 2, 1976.

Bjerhammar, A. "A Review of Discrete Methods in Physical Geodesy", in Approximation Methods in Physical Geodesy, Lecture Delivered at The Second International Summer School in the Mountains, Ramsau, Austria, (H. Moritz and H. Sunkel, Editors), Herbert Wichmann Verlag Karlsruhe, 1978.

Carnahan, B. - Luther H.A. - Wilkes, J.C. "Applied Numerical Methods", John Wiley & Sons, Inc. New York, 1969.

Emrick, H.W. "Computation Techniques for Various Gravity Anomaly Correction Terms", United States Air Force Academy, Report No. 73-8, December, 1973.

Forsberg, R. - Tscherning, C.C. "The Use of Height Data in Gravity Field Approximation by Collocation", submitted to JGR, in press, 1981.

Forstner, W. "Studies on the Problem of Bjerhammar", Transactions of the Royal Institute of Technology, No. 24, Stockholm, 1966.

Hagiwara, Y. "Truncation Error Formulas for the Geoidal Height and the Deflection of the Vertical", Bulletin Geodesique, No. 106, 1972.

Heiskanen, W.A. - Moritz, H. "Physical Geodesy". W.H. Freeman, San Francisco, 1967.

Hirvonen, R.A. - Moritz, H. "Practical Computations of Gravity at High Altitudes", Department of Geodetic Science, The Ohio State University, Report No. 27, May 1963.

Hotine, M. "Mathematical Geodesy", ESSA Monograph 2, 1969.

Isaacson, E. - Keller, H. "Analysis of Numerical Methods", John Wiley & Sons, New York, 1966

Junkins, J.L. - Saunders J.T. "Development of Finite Element Model for the Earth's Gravity Field, Phase II - Finite Structure Disturbing Gravity Representations", Technical Report ETL-0097, United States Army Engineer Topographic Laboratories (ETL), Fort Belvoir, Virginia, March, 1977.

Katsambalos, K.E. "Comparison of Some Undulation Prediction Techniques from Altimeter Data", Reports of the Department of Geodetic Science, The Ohio State University, Report No. 303, July, 1980.

Koch, K-R. "Successive Approximation of Solutions of Molodensky's Basic Integral Equation", Department of Geodetic Science, The Ohio State University, Report No. 85, 1967-A.

Koch, K-R. "Determination of the First Derivatives of the Disturbing Potential by Green's Fundamental Formula", Department of Geodetic Science, The Ohio State University, Report No. 90, 1967-B.

Koch, K-R. "Model Computations for Different Solutions of the Geodetic Boundary Value Problem", Department of Geodetic Science, The Ohio State University, Report No. 102, February, 1968-A.

Koch, K-R. "Numerical Examples for Downwarn Continuation of Gravity Anomalies", Reports of the Department of Geodetic Science, The Ohio State University, Report No. 112, July 1968-B.

Lachapelle, G. "Estimation of Disturbing potential Components Using a Combined Integral Formulae and Collocation Approach", Manuscripta Geodetica, Vol. 2, No. 4, 1977.

Molodensky, M.S. - Eremeev, V.F. - Yurkina, M.I., "Methods For Study of the External Gravitational Field and Figure of the Earth", Israel Program for Scientific Translations, Jerusalem, 1962.

Moritz, H. "Studies on the Accuracy of the Computation of Gravity in High Elevations", Department of Geodetic Science, The Ohio State University, Report No. 21, April 1962.

Moritz, H. "The Boundary-Value Problem of Physical Geodesy", Reports of the Department of Geodetic Science, The Ohio State University, Report No. 46, August, 1964.

Moritz, H. "Green's Functions in Physical Geodesy, and the Computation of the External Gravity Field and the Geodetic Boundary-Value Problem", Reports of the Department of Geodetic Science, The Ohio State [illegible] Report No. 49, June, 1965

Moritz, H. "Linear Solutions of the Geodetic Boundary-Value Problem", Reports of the Department of Geodetic Science, The Ohio State University, Report No. 79, December 1966.

Moritz, H. "Advanced Least-Squares Methods", Reports of the Department of Geodetic Science, The Ohio State University, Report No. 175, June, 1972.

Moritz, H. "Precise Gravimetric Geodesy", Reports of the Department of Geodetic Science, The Ohio State University, Report No. 219, December 1974.

Moritz, H. "Advanced Physical Geodesy", Herbert Wichmann Verlag Karlsruhe, W. Germany, 1980.

Moritz, H. - Sünkel, H. (Editors) "Approximation Methods in Geodesy", Herbert Wichmann Verlag Karlsruhe, 1978.

Mueller, I.I. "External Gravity Field of the Earth", in 'Gravity Anomalies: Unserveyed Areas', Geophysical Monograph, No. 9, 1966.

Nakiboglu, S.M. - Lim, T.S. "A Numerical Test of the Initial Value Method for Downward Continuation", Austr. J. Geod. Photo. Surv., No. 30, June, 1979.

Needham, P.E. "The Formation and Evaluation of Detailed Geopotential Models Based on Point Masses", Reports of the Department of Geodetic Science, The Ohio State University Report No. 149, December, 1970.

Orlin, H. "The Three Components of the External Anomalous Gravity Field" Journal of Geophysical Research, Vol.64, No. 12, December 1959.

Paul, M.K. - Nagy, D. "A Study of the Upward Continuation of Gravity Data from a Plane Surface", Studia Geoph. Et Geod., Vol. 16, 1972.

[illegible]trovskaya, M.S. "Upward and Downward Continuation in the Geopotential Determinations", Bulletin Geodesique, Vol. 53, 1979.

Rapp, R.H. "A Fortran Program for the Computation of the Disturbance Components of Gravity", Reports of the Department of Geodetic Science, The Ohio State University, Report No. 76, August 1966.

Rapp, R.H. "Global Anomaly and Undulation Recovery Using Geos-3 Altimeter Data", Reports of the Department of Geodetic Science, The Ohio State University, Report No. 285, May 1979-A.

Rapp, R.H. "Potential Coefficients and Anomaly Degree Variance Modelling Revisited", Reports of the Department of Geodetic Science, The Ohio State University, Report No. 293, September 1979-B.

Rapp, R.H. "A Comparison of Altimeter and Gravimetric Geoids in the Tonga Trench and Indian Ocean Areas", Bulletin Geodesique, Volume 54, No. 2, 1980.

Rapp, R.H. - Agajelu, S.I. "Comparison of Upward Continued Anomalies Computed by the Poisson Integral and by Collocation", Reports of the Department of Geodetic Science, The Ohio State University, Report No. 227, June 1975.

Reit, B-G, "Studies of Gravity in Space According to Bjerhammar", The Royal Institute of Technology, Division of Geodesy, Stockholm, 1966.

Richardson, D.A. - Hopkins, J. "Gravity Disturbance Components Computed at Aircraft Altitude Using the Finite Element Method", DMAAC, St. Louis Air Force Station, Missouri, 63118, December 1978.

Robertson, W.M. "Spherical Geodetic Transformations", Volume 1: Spectral Theory and Optimal Template Design, The Charles Stark Draper Laboratories Inc. Cambridge, Mass. 02139, Report R-1181, September 1978.

Shebalin, J.V. "Flat Earth Upward Continuation", Journal of Geophysical Research, Volume 84, No. 85, 1979.

Shepperd, S.W. "Molodenskii-Type Coefficients with Application to Gravity Disturbance Vector Truncation Errors at Altitude", The Charles Stark Draper Laboratories Inc. Cambridge, Mass. 02139, Report R-1329, 1979.

Sjöberg, L. "On the Discrete Boundary Value Problem of Physical Geodesy, with Harmonic Reductions to an Internal Sphere", The Royal Institute of Technology, Division of Geodesy, Stockholm, 1975.

Sjöberg, L. "A Comparison of Bjerhammar's Method and Collocation in Physical Geodesy", Reports of the Department of Geodetic Science, The Ohio State University, Report No. 273, July 1978.

Sünkel, H. "A Covariance Approximation Procedure", Reports of the Department of Geodetic Science, The Ohio State University, Report No. 286, March 1979.

Sünkel, H. "A General Surface Representation Module Designed For Geodesy", Reports of the Department of Geodetic Science, The Ohio State University, Report No. 292, June 1980.

Tscherning, C.C. "Covariance Expressions for Second and Lower Order Derivatives of the Anomalous Potential", Reports of the Department of Geodetic Science, The Ohio State University, Report No. 225, January, 1976.

Tscherning, C.C. - Forsberg, R. "Prediction of Deflections of the Vertical", paper presented at the Second International Symposium on Problems Related to the Redefination of the North American Geodetic Networks, Arlington, Virginia, 1978.

Tscherning, C.C. - Rapp, R.H. "Closed Covariance Expressions for Gravity Anomalies, Geoid Undulations, and Deflections of the Vertical Implied by Anomaly Degree Variance Models", Reports of the Department of Geodetic Science, The Ohio State University, Report No. 208, May 1974.

Westlake, J.R. A Handbook of Numerical Matrix Inversion and Solution of Linear Equations, John Wiley & Sons, Inc., New York, 1968.

Witte, B. "Die Berechnung Von Schwerestorungen Im Aubenraum Mit Hilfe Des Greenchen Satzes", Zeitschrift Fur Vermessungwesen, No. 4, April, 1969.

Witte, L. De. "Altitude Extension of the Three Anomalous Gravity Components Bulletin Geodesique, No. 93, September 1969.